

CERN-PH-EP-2014-141

Submitted to: Physical Review D

arXiv:1407.0608v2 [hep-ex] 26 Sep 2014

Search for pair-produced third-generation squarks decaying via charm quarks or in compressed supersymmetric scenarios in pp collisions at $\sqrt{s} = 8$ TeV with the ATLAS detector

The ATLAS Collaboration

Abstract

Results of a search for supersymmetry via direct production of third-generation squarks are reported, using 20.3 fb^{-1} of proton-proton collision data at $\sqrt{s} = 8$ TeV recorded by the ATLAS experiment at the LHC in 2012. Two different analysis strategies based on monojet-like and c -tagged event selections are carried out to optimize the sensitivity for direct top squark pair production in the decay channel to a charm quark and the lightest neutralino ($\tilde{t}_1 \rightarrow c + \tilde{\chi}_1^0$) across the top squark–neutralino mass parameter space. No excess above the Standard Model background expectation is observed. The results are interpreted in the context of direct pair production of top squarks and presented in terms of exclusion limits in the $(m_{\tilde{t}_1}, m_{\tilde{\chi}_1^0})$ parameter space. A top squark of mass up to about 240 GeV is excluded at 95% confidence level for arbitrary neutralino masses, within the kinematic boundaries. Top squark masses up to 270 GeV are excluded for a neutralino mass of 200 GeV. In a scenario where the top squark and the lightest neutralino are nearly degenerate in mass, top squark masses up to 260 GeV are excluded. The results from the monojet-like analysis are also interpreted in terms of compressed scenarios for top squark pair production in the decay channel $\tilde{t}_1 \rightarrow b + ff' + \tilde{\chi}_1^0$ and sbottom pair production with $\tilde{b}_1 \rightarrow b + \tilde{\chi}_1^0$, leading to a similar exclusion for nearly mass-degenerate third-generation squarks and the lightest neutralino. The results in this paper significantly extend previous results at colliders.

Search for pair-produced third-generation squarks decaying via charm quarks or in compressed supersymmetric scenarios in pp collisions at $\sqrt{s} = 8$ TeV with the ATLAS detector

The ATLAS Collaboration
(Dated: September 29, 2014)

Results of a search for supersymmetry via direct production of third-generation squarks are reported, using 20.3 fb^{-1} of proton-proton collision data at $\sqrt{s} = 8$ TeV recorded by the ATLAS experiment at the LHC in 2012. Two different analysis strategies based on monojet-like and c -tagged event selections are carried out to optimize the sensitivity for direct top squark pair production in the decay channel to a charm quark and the lightest neutralino ($\tilde{t}_1 \rightarrow c + \tilde{\chi}_1^0$) across the top squark–neutralino mass parameter space. No excess above the Standard Model background expectation is observed. The results are interpreted in the context of direct pair production of top squarks and presented in terms of exclusion limits in the $(m_{\tilde{t}_1}, m_{\tilde{\chi}_1^0})$ parameter space. A top squark of mass up to about 240 GeV is excluded at 95% confidence level for arbitrary neutralino masses, within the kinematic boundaries. Top squark masses up to 270 GeV are excluded for a neutralino mass of 200 GeV. In a scenario where the top squark and the lightest neutralino are nearly degenerate in mass, top squark masses up to 260 GeV are excluded. The results from the monojet-like analysis are also interpreted in terms of compressed scenarios for top squark pair production in the decay channel $\tilde{t}_1 \rightarrow b + ff' + \tilde{\chi}_1^0$ and sbottom pair production with $\tilde{b}_1 \rightarrow b + \tilde{\chi}_1^0$, leading to a similar exclusion for nearly mass-degenerate third-generation squarks and the lightest neutralino. The results in this paper significantly extend previous results at colliders.

PACS numbers: 12.60.Jv, 14.80.Ly, 13.85.Rm

I. INTRODUCTION

Supersymmetry (SUSY) [1–9] is a theoretically favored candidate for physics beyond the Standard Model (SM). It naturally solves the hierarchy problem and provides a possible candidate for dark matter in the universe. SUSY enlarges the SM spectrum of particles by introducing a new supersymmetric partner (sparticle) for each particle in the SM. In particular, a new scalar field is associated with each left- and right-handed quark state, and two squark mass eigenstates \tilde{q}_1 and \tilde{q}_2 result from the mixing of the scalar fields. In some SUSY scenarios, a significant mass difference between the two eigenstates in the bottom squark and top squark sectors can occur, leading to rather light sbottom \tilde{b}_1 and stop \tilde{t}_1 mass states, where sbottom and stop are the SUSY partners of the SM bottom and top quarks, respectively. In addition, naturalness arguments suggest that the third generation squarks should be light with masses below 1 TeV [10, 11]. In a generic supersymmetric extension of the SM that assumes R-parity conservation [12–16], sparticles are produced in pairs and the lightest supersymmetric particle (LSP) is stable. In this paper the LSP is assumed to be the lightest neutralino [17] ($\tilde{\chi}_1^0$).

For a mass difference $\Delta m \equiv m_{\tilde{t}_1} - m_{\tilde{\chi}_1^0} > m_t$ and depending on the SUSY parameters and sparticle mass hierarchy, the dominant decay channels are expected to be $\tilde{t}_1 \rightarrow t + \tilde{\chi}_1^0$ or $\tilde{t}_1 \rightarrow b + \tilde{\chi}_1^\pm$, where the latter decay mode involves charginos ($\tilde{\chi}_1^\pm$) that subsequently can decay into the lightest neutralino via $W^{(*)}$ emission, leading to a four-body decay $\tilde{t}_1 \rightarrow b + ff' + \tilde{\chi}_1^0$, where ff' denotes a pair of fermions (see Fig. 1). If the chargino is heavier than the stop and $m_W + m_b < \Delta m < m_t$, the dominant decay mode is expected to be the three-body $Wb\tilde{\chi}_1^0$ decay. Several searches on 7 TeV data have been carried out in these decay channels in 0-, 1-, and 2-lepton final states [18–21] and have been extended using 8 TeV data [22–

25].

In the scenario for which $\Delta m < m_W + m_b$, the four-body decay mode above competes with the stop decay to a charm quark and the LSP ($\tilde{t}_1 \rightarrow c + \tilde{\chi}_1^0$), which proceeds via a loop decay (see Fig. 1). The corresponding final state is characterized by the presence of two jets from the hadronization of the charm quarks and missing transverse momentum ($\mathbf{p}_T^{\text{miss}}$, denoting its magnitude by E_T^{miss}) from the two undetected LSPs. However, given the relatively small mass difference (Δm), both the transverse momenta of the two charm jets and the E_T^{miss} are low, making it very difficult to extract the signal from the large multijet background. In this study, the event selection makes use of the presence of initial-state radiation (ISR) jets to identify signal events. In this case, the squark-pair system is boosted leading to larger E_T^{miss} . As an example, for a stop with a mass of 200 GeV and Δm of 5 GeV, about 18% of the events have $E_T^{\text{miss}} > 150$ GeV and a jet with $p_T > 150$ GeV. Two different approaches are used to maximize the sensitivity of the analysis across the different Δm regions. A “monojet-like” analysis is carried out, where events with low jet multiplicity and large E_T^{miss} are selected, that is optimized for small Δm ($\Delta m \leq 20$ GeV). For $\Delta m \geq 20$ GeV, the charm jets receive a large enough boost to be detected. In addition to the requirements on the presence of ISR jets, the identification of jets containing the decay products of charm hadrons (c -tagging) is used, leading to a “ c -tagged” analysis that further enhances the sensitivity to the SUSY signal in the region $m_{\tilde{t}_1} > 200$ GeV and $\Delta m \geq 20$ GeV. Results for searches in this channel have been previously reported by collider experiments [26–28]. In addition to the decay channel $\tilde{t}_1 \rightarrow c + \tilde{\chi}_1^0$, the monojet-like results are re-interpreted in terms of the search for stop pair production with $\tilde{t}_1 \rightarrow b + ff' + \tilde{\chi}_1^0$ and small Δm . In such a scenario, the decay products of the top squark are too soft to be identified in the final state, and the signal selection relies on the presence of an ISR jet.

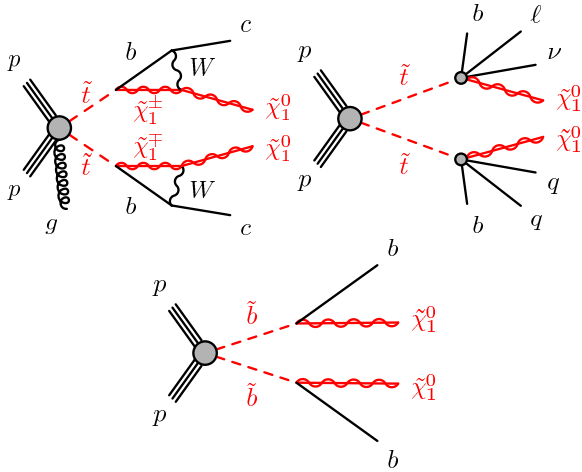


FIG. 1. Diagrams for the pair production of top squarks with the decay modes $\tilde{t}_1 \rightarrow c + \tilde{\chi}_1^0$ or $\tilde{t}_1 \rightarrow b + f f' + \tilde{\chi}_1^0$, and the pair production of sbottom squarks with the decay mode $\tilde{b}_1 \rightarrow b + \tilde{\chi}_1^0$. In one case, the presence of a jet from initial-state radiation is also indicated for illustration purposes.

In the case of sbottom pair production, assuming a SUSY particle mass hierarchy such that the sbottom decays exclusively as $\tilde{b}_1 \rightarrow b + \tilde{\chi}_1^0$ (see Fig. 1), the expected signal for direct sbottom pair production is characterized by the presence of two energetic jets from the hadronization of the bottom quarks and large missing transverse momentum from the two LSPs in the final state. Results on searches in this channel at colliders have been reported [21, 23, 29–31]. In this study, the monojet-like results are also re-interpreted in terms of the search for sbottom pair production with $\tilde{b}_1 \rightarrow b + \tilde{\chi}_1^0$ in a compressed scenario (small sbottom-neutralino mass difference) with two soft b -jets and an energetic ISR jet in the final state.

The paper is organized as follows. The ATLAS detector is described in the next section. Section III provides details of the simulations used in the analysis for background and signal processes. Section IV discusses the reconstruction of jets, leptons and the E_T^{miss} , while Sec. V describes the event selection. The estimation of background contributions and the study of systematic uncertainties are discussed in Secs. VI and VII. The results are presented in Sec. VIII, and are interpreted in terms of the search for stop and sbottom pair production. Finally, Sec. IX is devoted to the conclusions.

II. EXPERIMENTAL SETUP

The ATLAS detector [32] covers almost the whole solid angle around the collision point with layers of tracking detectors, calorimeters and muon chambers. The ATLAS inner detector (ID) has full coverage [33] in ϕ and covers the pseudorapidity range $|\eta| < 2.5$. It consists of a silicon pixel detector, a silicon microstrip detector, and a straw tube tracker that also measures transition radiation for particle identification, all im-

mersed in a 2 T axial magnetic field produced by a solenoid.

High-granularity liquid-argon (LAr) electromagnetic sampling calorimeters, with excellent energy and position resolution, cover the pseudorapidity range $|\eta| < 3.2$. The hadronic calorimetry in the range $|\eta| < 1.7$ is provided by a scintillator-tile calorimeter, consisting of a large barrel and two smaller extended barrel cylinders, one on either side of the central barrel. In the endcaps ($|\eta| > 1.5$), LAr hadronic calorimeters match the outer $|\eta|$ limits of the endcap electromagnetic calorimeters. The LAr forward calorimeters provide both the electromagnetic and hadronic energy measurements, and extend the coverage to $|\eta| < 4.9$.

The muon spectrometer measures the deflection of muon tracks in the large superconducting air-core toroid magnets in the pseudorapidity range $|\eta| < 2.7$, using separate trigger and high-precision tracking chambers. Over most of the η -range, a precise measurement of the track coordinates in the principal bending direction of the magnetic field is provided by monitored drift tubes. At large pseudorapidities, cathode strip chambers with higher granularity are used in the innermost plane over $2.0 < |\eta| < 2.7$. The muon trigger system covers the pseudorapidity range $|\eta| < 2.4$.

III. MONTE CARLO SIMULATION

Monte Carlo (MC) simulated event samples are used to assist in computing detector acceptance and reconstruction efficiencies, determine signal and background contributions, and estimate systematic uncertainties on the final results.

Samples of simulated W +jets and Z +jets events are generated using SHERPA-1.4.1 [34], including LO matrix elements for up to 5 partons in the final state and using massive b/c -quarks, with CT10 [35] parton distribution functions (PDF) and its own model for hadronization. Similar samples are generated using the ALPGEN-v2.14 [36] generator and are employed to assess the corresponding modeling uncertainties. The MC predictions are initially normalized to next-to-next-to-leading-order (NNLO) predictions according to DYNNLO [37, 38] using MSTW2008 NNLO PDF sets [39].

The production of top quark pairs ($t\bar{t}$) is simulated using the POWHEG-r2129 [40] MC generator. ALPGEN and MC@NLO-4.06 [41] MC simulated samples are used to assess $t\bar{t}$ modeling uncertainties. Single top production samples are generated with POWHEG for the s - and Wt -channel and MC@NLO is used to determine systematic uncertainties, while AcerMC-v3.8 [42] is used for single top production in the t -channel. Finally, samples of $t\bar{t}$ production associated with additional vector bosons ($t\bar{t} + W$ and $t\bar{t} + Z$ processes) are generated with MADGRAPH-5.1.4.8 [43]. In the case of POWHEG and MADGRAPH, parton showers are implemented using PYTHIA-6.426 [44], while HERWIG-6.5.20 [45] interfaced to JIMMY [46] is used for the ALPGEN and MC@NLO generators. A top quark mass of 172.5 GeV and the CTEQ6L1 PDFs are used. The Perugia 2011C [47] and AUET2B [48] tunes for the underlying event are used for the $t\bar{t}$, single top and $t\bar{t} + W/Z$ processes, respectively. The

cross section prediction at NNLO+NNLL (next-to-next-to-leading-logarithm) accuracy, as determined by Top++2.0 [49], is used in the normalization of the $t\bar{t}$ [50] sample. An approximate NLO+NNLL prediction is used for the Wt [51] process and NLO cross sections are considered for $t\bar{t} + W$ and $t\bar{t} + Z$ processes.

Diboson samples (WW , WZ and ZZ production) are generated using SHERPA, using massive b/c -quarks, with CT10 PDFs, and are normalized to NLO predictions [52]. Additional samples are generated with HERWIG to assess uncertainties. Finally, Higgs boson production including ZH , WH and $t\bar{t}H$ processes is generated using PYTHIA-8.165 [53] with CTEQ6L1 PDFs.

Stop pair production with $\tilde{t}_1 \rightarrow c + \tilde{\chi}_1^0$ is modeled with MADGRAPH with one additional jet from the matrix element. The showering is done with PYTHIA-6 and using the AUET2B tune for the underlying event, which involves CTEQ6L1 PDFs. Samples are produced with stop masses between 100 GeV and 400 GeV and $\tilde{\chi}_1^0$ masses between 70 GeV and 390 GeV. The Δm step size increases with Δm from 2 GeV to 30 GeV and the maximum Δm considered is 82 GeV. The region $\Delta m < 2$ GeV is not considered since in this regime the stop can become long-lived leading to the signature studied in Ref. [54]. Similarly, MC simulated samples are produced separately for $\tilde{t}_1 \rightarrow b + ff' + \tilde{\chi}_1^0$ and $\tilde{b}_1 \rightarrow b + \tilde{\chi}_1^0$ processes across the stop-neutralino and sbottom-neutralino mass planes. In the case of the $\tilde{t}_1 \rightarrow b + ff' + \tilde{\chi}_1^0$ process, samples are produced with stop masses in the range between 100 GeV and 300 GeV and Δm that varies between 10 GeV and 80 GeV. For sbottom pair production with $\tilde{b}_1 \rightarrow b + \tilde{\chi}_1^0$, samples are produced with sbottom masses in the range between 100 GeV and 350 GeV and $\tilde{\chi}_1^0$ masses in the range between 1 GeV and 340 GeV, with a sbottom-neutralino mass difference that varies between 10 GeV and 50 GeV. Signal cross sections are calculated to NLO in the strong coupling constant, adding the resummation of soft gluon emission at next-to-leading-logarithmic (NLO+NLL) accuracy [55–57]. The nominal cross section and the uncertainty are taken from an envelope of cross section predictions using different PDF sets and factorization and renormalization scales, as described in Ref. [58].

Differing pileup (multiple proton-proton interactions in the same or neighboring bunch-crossings) conditions as a function of the instantaneous luminosity are taken into account by overlaying simulated minimum-bias events generated with PYTHIA-8 onto the hard-scattering process and re-weighting them according to the distribution of the mean number of interactions observed. The MC generated samples are processed either with a full ATLAS detector simulation [59] based on GEANT4 [60] or a fast simulation based on the parameterization of the response of the electromagnetic and hadronic showers in the ATLAS calorimeters [61] and a simulation of the trigger system. The results based on fast simulation are validated against fully simulated samples. The simulated events are reconstructed and analyzed with the same analysis chain as for the data, using the same trigger and event selection criteria discussed in Section V.

IV. RECONSTRUCTION OF PHYSICS OBJECTS

Jets are reconstructed from energy deposits in the calorimeters using the anti- k_r jet algorithm [62] with the distance parameter (in η - ϕ space) $\Delta R = \sqrt{(\Delta\eta)^2 + (\Delta\phi)^2}$ set to 0.4. The measured jet transverse momentum (p_T) is corrected for detector effects, including the non-compensating character of the calorimeter, by weighting energy deposits arising from electromagnetic and hadronic showers differently. In addition, jets are corrected for contributions from pileup, as described in Ref. [63]. Jets with corrected $p_T > 20$ GeV and $|\eta| < 2.8$ are considered in the analysis. In order to remove jets originating from pileup collisions, central jets ($|\eta| < 2.4$) with $p_T < 50$ GeV and with charged-particle tracks associated to them must have a jet vertex fraction (JVF) above 0.5, where the JVF is defined as the ratio of the sum of transverse momentum of matched tracks that originate from the primary vertex to the sum of transverse momentum of all tracks associated with the jet.

The presence of leptons (muons or electrons) in the final state is used in the analysis to define control samples and to reject background contributions in the signal regions (see Secs. V and VI). Muon candidates are formed by combining information from the muon spectrometer and inner tracking detectors as described in Ref. [64] and are required to have $p_T > 10$ GeV, $|\eta| < 2.4$ and $\Delta R > 0.4$ with respect to any jet with $p_T > 20$ GeV. The latter requirement is increased to 30 GeV in the case of the monojet-like analysis. This increases the efficiency for the selection of real muons from W boson decays. It also avoids biases in the muon selection due to the presence of low p_T jets with large pileup contributions, affecting the $W(\rightarrow \mu\nu)$ +jets events, as determined by simulations. This is particularly relevant for the monojet-like analysis since, as described in Sec. VI, $W(\rightarrow \mu\nu)$ +jets control samples in data are used to constrain the irreducible $Z(\rightarrow \nu\bar{\nu})$ +jets background contribution in the signal regions. In addition, muons are required to be isolated: the sum of the transverse momenta of the tracks not associated with the muon in a cone of radius $\Delta R = 0.2$ around the muon direction is required to be less than 1.8 GeV.

Electron candidates are initially required to have $p_T > 10$ GeV and $|\eta| < 2.47$, and to pass the *medium* electron shower shape and track selection criteria described in Ref. [65] and reoptimized for 2012 data. Overlaps between identified electrons and jets in the final state are resolved. Jets are discarded if their separation ΔR from an identified electron is less than 0.2. The electrons separated by ΔR between 0.2 and 0.4 from any remaining jet are removed. In the monojet-like analysis, electrons are selected with $p_T > 20$ GeV in both the control and signal regions. The use of the same p_T threshold in control and signal regions minimizes the impact from lepton reconstruction and identification uncertainties on the final results. The 20 GeV p_T requirement together with the monojet-like selection also applied to define the control regions brings the background from jets misidentified as electrons to negligible levels without the need for electron isolation requirements. As detailed in Sec. V and Sec. VI, slightly different requirements on the lepton p_T are applied in the c -

tagged analysis to define signal regions and background control samples. In this case, the electrons are required to have $p_T > 10$ GeV and $p_T > 20$ GeV for signal and control samples, respectively, and to be isolated: the total track momentum not associated with the electron in a cone of radius 0.2 around the electron candidate is required to be less than 10% of the electron p_T . In the c -tagged analysis, the use of a tighter electron veto in the signal regions, compared to that in the monojet-like analysis, contributes to the reduction of the sizable background from top-quark-related processes.

E_T^{miss} is reconstructed using all energy deposits in the calorimeter up to a pseudorapidity $|\eta| < 4.9$ and without including information from identified muons in the final state. Clusters associated with either electrons or photons with $p_T > 10$ GeV and those associated with jets with $p_T > 20$ GeV make use of the corresponding calibrations for these objects. Softer jets and clusters not associated with these objects are calibrated using both calorimeter and tracking information [66].

Jets are tagged as containing the decay products of charm hadrons (c -tagging) via a dedicated algorithm using multivariate techniques. It combines information from the impact parameters of displaced tracks and topological properties of secondary and tertiary decay vertices reconstructed within the jet. The algorithm provides three probabilities: one targeted for light-flavor quarks and gluon jets (P_u), one for charm jets (P_c) and one for b -quark jets (P_b). From these probabilities, anti- b and anti- u discriminators are calculated:

$$\text{anti} - b \equiv \log \left(\frac{P_c}{P_b} \right) \quad \text{and} \quad \text{anti} - u \equiv \log \left(\frac{P_c}{P_u} \right), \quad (1)$$

and used for the selected jets in the final state. Figure 2 shows the distributions of the anti- b and anti- u discriminators for the first- and the third-leading jets (sorted in decreasing jet p_T), respectively. The data are compared to MC simulations for the different SM processes, separated by jet flavor [67], and the data-driven multijet background prediction (see Sec. VIC), and include the signal preselection defined in Sec. V without applying the tagging requirements. Good agreement is observed between data and simulations. Two operating points specific to c -tagging are used. The *medium* operating point ($\log(P_c/P_b) > -0.9$, $\log(P_c/P_u) > 0.95$) has a c -tagging efficiency of $\approx 20\%$, and a rejection factor of ≈ 8 for b -jets, ≈ 200 for light-flavor jets, and ≈ 10 for τ jets. The *loose* operating point ($\log(P_c/P_b) > -0.9$) has a c -tagging efficiency of $\approx 95\%$, with a factor of 2.5 rejection of b -jets but without any significant rejection for light-flavor or τ jets. The efficiencies and rejections are quoted for jets with $30 \text{ GeV} < p_T < 200 \text{ GeV}$ and $|\eta| < 2.5$ in simulated $t\bar{t}$ events, and reach a plateau at high jet p_T .

The c -tagging efficiency is calibrated using data with the method described in Ref. [68] for 7 TeV collisions. This method makes use of a jet sample enriched in charm-quark-initiated jets containing a D^{*+} meson identified in the $D^0(\rightarrow K^- \pi^+) \pi^+$ decay mode [69]. The same calibration method applied to the 8 TeV data leads to reduced uncertainties. The standard calibration techniques are used for the b -jet [70, 71] and light-jet [72] rejections: a data-to-simulation multiplica-

tive scale factor of about 0.9, with a very moderate jet p_T dependence, is applied to the simulated heavy-flavor tagging efficiencies in the MC samples. The total uncertainty for the c -tagging efficiency varies between 20% at low p_T and 9% at high p_T and includes: uncertainties on the heavy-flavor content of the charm-quark jet enriched sample and on the b -tagging scale factors; uncertainties on the D^{*+} mass fit; uncertainties on the jet energy scale and resolution; and uncertainties on the extrapolation of the results to inclusive charm-quark jets. Similarly, data-to-simulation multiplicative scale factors of order 1.5 are applied to the simulated efficiency for tagging light-jets (mistags). They are determined with a precision in the range between 20% and 40% depending on jet p_T and η .

V. EVENT SELECTION

The data sample considered in this paper was collected with tracking detectors, calorimeters, muon chambers, and magnets fully operational, and corresponds to a total integrated luminosity of 20.3 fb^{-1} . The uncertainty on the integrated luminosity is 2.8%, and it is estimated, following the same methodology detailed in Ref. [73], from a preliminary calibration of the luminosity scale derived from beam-separation scans performed in November 2012. The data were selected online using a trigger logic that selects events with E_T^{miss} above 80 GeV, as computed at the final stage of the three-level trigger system of ATLAS [74]. With respect to the final analysis requirements, the trigger selection is fully efficient for $E_T^{\text{miss}} > 150 \text{ GeV}$, as determined using a data sample with muons in the final state. Table I summarizes the different event selection criteria applied in the signal regions. The following preselection criteria are applied.

- Events are required to have a reconstructed primary vertex consistent with the beamspot envelope and having at least five associated tracks; when more than one such vertex is found, the vertex with the largest summed p_T^2 of the associated tracks is chosen.
- Events are required to have $E_T^{\text{miss}} > 150 \text{ GeV}$ and at least one jet with $p_T > 150 \text{ GeV}$ and $|\eta| < 2.8$ ($|\eta| < 2.5$) in the final state for the monojet-like (c -tagged) selection.
- Events are rejected if they contain any jet with $p_T > 20 \text{ GeV}$ and $|\eta| < 4.5$ that presents a charged fraction [75], electromagnetic fraction in the calorimeter, or sampling fraction inconsistent with the requirement that they originate from a proton-proton collision [76]. Additional requirements based on the timing and the pulse shape of the cells in the calorimeter are applied to suppress coherent noise and electronic noise bursts in the calorimeter producing anomalous energy deposits [77], which have a negligible effect on the signal efficiency.
- Events with isolated muons with $p_T > 10 \text{ GeV}$ are vetoed. Similarly, events with electrons with $p_T >$

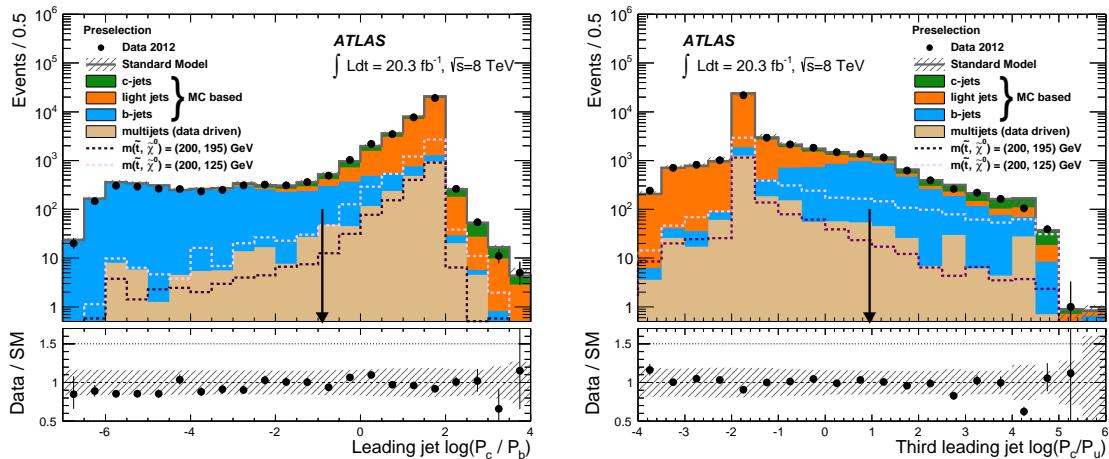


FIG. 2. Distribution of the discriminator against b -jets, $\log(P_c/P_b)$, for the first-leading jet and against light-jets, $\log(P_c/P_u)$, for the third-leading jet. The data are compared to MC simulations for the different SM processes, separated by jet flavor, and include the signal preselection defined in Sec. V without applying the tagging requirements, which are indicated by the arrows. The bottom panels show the ratio between data and MC predictions. The error bands in the ratios include the statistical and experimental uncertainties in the predictions. For illustration purposes, the distributions of two different SUSY scenarios for stop pair production with the decay mode $\tilde{t}_1 \rightarrow c + \tilde{\chi}_1^0$ are included. In the SUSY signal, the first-leading jet mostly originates from ISR and the third-leading jet is expected to contain a large fraction of c -jets.

20 GeV ($p_T > 10$ GeV) are vetoed in the monojet-like (c -tagged) selection.

A. Monojet-like selection

The monojet-like analysis targets the region in which the stop and the lightest neutralino are nearly degenerate in mass so that the jets from the charm-quark fragmentation (c -jets) are too soft to be identified. Stop pair production events are then characterized by large E_T^{miss} and a small number of jets, and can be identified via the presence of an energetic jet from initial-state radiation. A maximum of three jets with $p_T > 30$ GeV and $|\eta| < 2.8$ in the event are allowed. An additional requirement on the azimuthal separation of $\Delta\phi(\text{jet}, \mathbf{p}_T^{\text{miss}}) > 0.4$ between the missing transverse momentum direction and that of each of the selected jets is imposed. This requirement reduces the multijet background contribution where the large E_T^{miss} originates mainly from jet energy mismeasurement. Three separate signal regions (here denoted by M1, M2 and M3) are defined with increasing lower thresholds on the leading jet p_T and E_T^{miss} , as the result of an optimization performed across the stop–neutralino mass plane with increasing \tilde{t} and $\tilde{\chi}_1^0$ masses. For the M1 selection, events are required to have $E_T^{\text{miss}} > 220$ GeV and leading jet $p_T > 280$ GeV. For the M2 (M3) selection, the thresholds are increased to $E_T^{\text{miss}} > 340$ GeV ($E_T^{\text{miss}} > 450$ GeV) and leading jet $p_T > 340$ GeV ($p_T > 450$ GeV).

B. c -tagged selection

The kinematics of the charm jets from the stop decays depend mainly on Δm . As Δm decreases, the p_T of the charm jets

become softer and it is more likely that other jets from initial state radiation have a higher transverse momentum than the charm jets. As a consequence, the stop signal is expected to have relatively large jet multiplicities and a c -tagged jet can be found among any of the subleading jets. An optimization of the c -tagged selection criteria is performed across the \tilde{t} and $\tilde{\chi}_1^0$ mass plane to maximize the sensitivity to a SUSY signal. In the c -tagged analysis, the events are required to have at least four jets with $p_T > 30$ GeV, $|\eta| < 2.5$ and $\Delta\phi(\text{jet}, \mathbf{p}_T^{\text{miss}}) > 0.4$. A veto against b -jets is applied to the selected jets in the event by using a loose c -tag requirement. In addition, at least one of the three subleading jets is required to be c -tagged using the medium criteria. The leading jet is required to have $p_T > 290$ GeV and two separate signal regions, here denoted by C1 and C2, are defined with $E_T^{\text{miss}} > 250$ GeV and $E_T^{\text{miss}} > 350$ GeV, respectively. The tighter requirement on E_T^{miss} for the C2 signal region targets models with larger stop and neutralino masses.

VI. BACKGROUND ESTIMATION

The expected SM background is dominated by $Z(\rightarrow \nu\bar{\nu})+\text{jets}$, $t\bar{t}$ and $W(\rightarrow \ell\nu)+\text{jets}$ ($\ell = e, \mu, \tau$) production, and includes small contributions from $Z/\gamma^*(\rightarrow \ell^+\ell^-)+\text{jets}$, single top, $t\bar{t} + V$, diboson (WW, WZ, ZZ) and multijet processes. In the monojet-like analysis, the $Z(\rightarrow \nu\bar{\nu})+\text{jets}$ processes constitute more than 50% – 60% of the total background, followed by a 30% – 40% contribution from $W(\rightarrow \ell\nu)+\text{jets}$ processes. In the c -tagged selection, the background contributions from $Z(\rightarrow \nu\bar{\nu})+\text{jets}$, $W(\rightarrow \ell\nu)+\text{jets}$, and top-quark related processes are similar, and each constitutes about 25% to 30% of the total background.

The $W/Z+\text{jets}$ backgrounds are estimated using MC event

TABLE I. Event selection criteria applied for monojet-like (M1–M3) and c -tagged (C1,C2) analyses, as described in Sec. V.

Selection criteria			
Preselection			
Primary vertex			
$E_T^{\text{miss}} > 150$ GeV			
At least one jet with $p_T > 150$ GeV and $ \eta < 2.8$			
Jet quality requirements			
Lepton vetoes			
Monojet-like selection			
At most three jets with $p_T > 30$ GeV and $ \eta < 2.8$			
$\Delta\phi(\text{jet}, \mathbf{p}_T^{\text{miss}}) > 0.4$			
Signal region	M1	M2	M3
Minimum leading jet p_T (GeV)	280	340	450
Minimum E_T^{miss} (GeV)	220	340	450
c -tagged selection			
At least four jets with $p_T > 30$ GeV and $ \eta < 2.5$			
$\Delta\phi(\text{jet}, \mathbf{p}_T^{\text{miss}}) > 0.4$			
All four jets must pass loose tag requirements (b -jet vetoes)			
At least one medium charm tag in the three subleading jets			
Signal region	C1	C2	
Minimum leading jet p_T (GeV)	290	290	
Minimum E_T^{miss} (GeV)	250	350	

samples normalized using data in control regions. The simulated W/Z +jets events are re-weighted to data as a function of the generated p_T of the vector boson, following a procedure similar to that in Ref. [78] based on the comparison of data and simulation in an event sample enriched in Z +jets events, which is found to improve the agreement between data and simulation. The weights applied to the simulation result from the comparison of the reconstructed boson p_T distribution in data and SHERPA MC simulation in W +jets and Z +jets control samples where the jet and E_T^{miss} preselection requirements (see Table I) have been applied. The weights are defined in several bins in boson p_T . Due to the limited number of data events at large boson p_T , an inclusive last bin with boson $p_T > 400$ GeV is used. The uncertainties of the re-weighting procedure are taken into account in the final results.

The top-quark background contribution to the monojet-like analysis is very small and is determined using MC simulated samples. In the case of the c -tagged analysis, the top-quark background is sizable, as it is enhanced by the jet multiplicity and c -tag requirements, and is estimated using MC simulated samples normalized in a top-quark-enriched control region. The simulated $t\bar{t}$ events are re-weighted based on the measurement in the data [79], indicating that the differential cross section as a function of the p_T of the $t\bar{t}$ system is softer than that predicted by the MC simulation.

The normalization factors for W/Z +jets and $t\bar{t}$ background contributions are extracted simultaneously using a global fit to all control regions and include systematic uncertainties, to

properly take into account correlations. The remaining SM backgrounds from $t\bar{t} + W/Z$, single top, diboson and Higgs processes are determined using Monte Carlo simulated samples, while the multijet background contribution is extracted from data. Finally, the potential contributions from beam-related background and cosmic rays are estimated in data using jet timing information and are found to be negligible.

In the following subsections, details on the definition of W/Z +jets and $t\bar{t}$ control regions and on the data-driven determination of the multijet background are given. This is followed by a description of the background fits and the validation of the resulting background estimations.

A. W/Z +jets background

In the monojet-like analysis, control samples in data, orthogonal to the signal regions, with identified electrons or muons in the final state and with the same requirements on the jet p_T , subleading jet vetoes, and E_T^{miss} , are used to determine the W/Z +jets electroweak background contributions from data. A $W(\rightarrow \mu\nu)$ +jets control sample is defined using events with a muon with $p_T > 10$ GeV and W transverse mass [80] in the range $30 \text{ GeV} < m_T < 100 \text{ GeV}$. Similarly, a $Z/\gamma^*(\rightarrow \mu^+\mu^-)$ +jets control sample is selected, requiring the presence of two muons with invariant mass in the range $66 \text{ GeV} < m_{\mu\mu} < 116 \text{ GeV}$. The E_T^{miss} -based online trigger used in the analysis does not include muon informa-

tion in the E_T^{miss} calculation. This allows the $W(\rightarrow \mu\nu)$ +jets and $Z/\gamma^*(\rightarrow \mu^+\mu^-)$ +jets control samples to be collected with the same trigger as for the signal regions. Finally, a $W(\rightarrow e\nu)$ +jets dominated control sample is defined with an electron candidate with $p_T > 20$ GeV. The E_T^{miss} calculation includes the contribution of the energy cluster from the identified electron in the calorimeter, since $W(\rightarrow e\nu)$ +jets processes contribute to the background in the signal regions when the electron is not identified. In the $W(\rightarrow \mu\nu)$ +jets and $Z/\gamma^*(\rightarrow \mu^+\mu^-)$ +jets control regions, the E_T^{miss} does not include muon momentum contributions, motivated by the fact that these control regions are used to estimate the irreducible $Z(\rightarrow \nu\bar{\nu})$ +jets background in the signal regions.

The definition of the control regions in the c -tagged analysis follows closely that of the monojet-like approach with differences motivated by the background composition and the contribution from heavy-flavor jets. A tighter cut of $81 \text{ GeV} < m_{\mu\mu} < 101 \text{ GeV}$ is used to define the $Z/\gamma^*(\rightarrow \mu^+\mu^-)$ +jets control sample, as required to further reject $t\bar{t}$ contamination. This is complemented with a corresponding $Z/\gamma^*(\rightarrow e^+e^-)$ +jets control sample, with the same mass requirements, for which the energy clusters associated with the identified electrons are then removed from the calorimeter. The $Z/\gamma^*(\rightarrow e^+e^-)$ +jets control sample is collected using a trigger that selects events with an electron in the final state. As in the monojet-like case, in the $W(\rightarrow e\nu)$ +jets control region the E_T^{miss} calculation includes the contribution from the identified electron. The electron also contributes to the number of jets in the final state, since the presence of a misidentified electron in the signal region can potentially affect the c -tagging results. The c -tagging and the heavy-flavor composition are two of the major uncertainties (of the order of 10% – 30%) in the c -tagged selection and the same tagging criteria as used in the signal selection are therefore applied to the $W(\rightarrow \mu\nu)$ +jets, $W(\rightarrow e\nu)$ +jets, $Z/\gamma^*(\rightarrow \mu^+\mu^-)$ +jets and $Z/\gamma^*(\rightarrow e^+e^-)$ +jets control regions. Since this reduces significantly the selection efficiency related to these control regions, the kinematic selections on the leading jet p_T and E_T^{miss} are both reduced to 150 GeV, where the trigger selection still remains fully efficient. This introduces the need for a MC-based extrapolation of the normalization factors, as determined using data at relatively low leading jet p_T and E_T^{miss} , to the signal regions. This extrapolation is tested in dedicated validation regions as described in Sec. [VIE](#).

Monte Carlo–based transfer factors, determined from the SHERPA simulation and including the boson p_T re-weighting explained above, are defined for each of the signal selections to estimate the different electroweak background contributions in the signal regions. As an example, in the case of the dominant $Z(\rightarrow \nu\bar{\nu})$ +jets background process in the monojet-like selection, its contribution to a given signal region $N_{\text{signal}}^{Z(\rightarrow \nu\bar{\nu})}$ is determined using the $W(\rightarrow \mu\nu)$ +jets control sample in data according to

$$N_{\text{signal}}^{Z(\rightarrow \nu\bar{\nu})} = (N_{W(\rightarrow \mu\nu),\text{control}}^{\text{data}} - N_{W(\rightarrow \mu\nu),\text{control}}^{\text{non-}W}) \times \frac{N_{\text{signal}}^{\text{MC}(Z(\rightarrow \nu\bar{\nu}))}}{N_{W(\rightarrow \mu\nu),\text{control}}^{\text{MC}}}, \quad (2)$$

where $N_{\text{signal}}^{\text{MC}(Z(\rightarrow \nu\bar{\nu}))}$ denotes the background predicted by the MC simulation in the signal region, and $N_{W(\rightarrow \mu\nu),\text{control}}^{\text{data}}$, $N_{W(\rightarrow \mu\nu),\text{control}}^{\text{MC}}$, and $N_{W(\rightarrow \mu\nu),\text{control}}^{\text{non-}W}$ denote, in the control region, the number of $W(\rightarrow \mu\nu)$ +jets candidates in data and MC simulation, and the non- $W(\rightarrow \mu\nu)$ background contribution, respectively. The $N_{W(\rightarrow \mu\nu),\text{control}}^{\text{non-}W}$ term refers mainly to top-quark and diboson processes, but also includes contributions from other W/Z +jets processes. The transfer factors for each process (e.g, the last term in Eq. (2)) are defined as the ratio of simulated events for the process in the signal region over the total number of simulated events in the control region.

In the monojet-like analysis, the $W(\rightarrow \mu\nu)$ +jets control sample is used to define transfer factors for $W(\rightarrow \mu\nu)$ +jets and $Z(\rightarrow \nu\bar{\nu})$ +jets processes. As discussed in Secs. [VID](#) and [VII](#), the use of the $W(\rightarrow \mu\nu)$ +jets control sample to constrain the normalization of the $Z(\rightarrow \nu\bar{\nu})$ +jets process translates into a reduced uncertainty on the estimation of the main irreducible background contribution, due to a partial cancellation of systematic uncertainties and the statistical power of the $W(\rightarrow \mu\nu)$ +jets control sample in data, about seven times larger than the $Z/\gamma^*(\rightarrow \mu^+\mu^-)$ +jets control sample. The $W(\rightarrow e\nu)$ +jets control sample is used to constrain $W(\rightarrow e\nu)$ +jets, $W(\rightarrow \tau\nu)$ +jets, $Z/\gamma^*(\rightarrow \tau^+\tau^-)$ +jets, and $Z/\gamma^*(\rightarrow e^+e^-)$ +jets contributions. Finally, the $Z/\gamma^*(\rightarrow \mu^+\mu^-)$ +jets control sample is used to constrain the $Z/\gamma^*(\rightarrow \mu^+\mu^-)$ +jets background contribution.

The c -tagged analysis follows a similar approach to determine the normalization factors for each of the W/Z +jets background contributions. However, in this case the $Z(\rightarrow \nu\bar{\nu})$ +jets, $Z/\gamma^*(\rightarrow e^+e^-)$ +jets and $Z/\gamma^*(\rightarrow \mu^+\mu^-)$ +jets normalization factors are extracted from the combined $Z/\gamma^*(\rightarrow \ell^+\ell^-)$ +jets ($\ell = e, \mu$) control sample, motivated by the fact that these processes involve identical heavy-flavor production mechanisms. Simulation studies indicate a very similar heavy-flavor composition in control and signal regions.

Figure [3](#) shows, for the M1 monojet-like kinematic selection and in the different control regions, the distributions of the E_T^{miss} and the leading-jet p_T in data and MC simulations. The MC predictions include data-driven normalization factors as a result of the use of transfer factors from control to signal regions discussed above. Similarly, the distributions for events in the W/Z +jets control regions of the c -tagged selection are shown in Fig. [4](#). Altogether, the MC simulation provides a good description of the shape of the measured distributions for both the monojet-like and c -tagged selections in the different control regions.

B. Top quark background

The background contribution from top-quark-related production processes to the monojet-like selection is small and is entirely determined from MC simulations. In the case of the c -tagged analysis, single top and $t\bar{t} + W/Z$ processes are directly taken from MC simulations and the $t\bar{t}$ MC predictions are normalized to the data in a separate control region.

The $t\bar{t}$ background contribution is dominated by events with hadronic τ -lepton decays and ISR jets in the final state. A $t\bar{t}$ control sample is selected with two opposite-charge leptons (ee , $\mu\mu$, or $e\mu$ configurations) in the final state, the same selection criteria for jet multiplicity and c -tagging as in the signal region, and relaxed $E_T^{\text{miss}} > 150$ GeV and leading jet $p_T > 150$ GeV requirements. In order to reduce the potential $Z/\gamma^* (\rightarrow e^+e^-)$ +jets and $Z/\gamma^* (\rightarrow \mu^+\mu^-)$ +jets contamination in the $t\bar{t}$ control sample, ee and $\mu\mu$ events with a dilepton invariant mass within 15 GeV of the nominal Z boson mass are rejected. Figure 5 compares the distributions for data and simulation in the $t\bar{t}$ control region. The MC simulation provides a good description of the shape of the measured distributions.

C. Multijets background

The multijet background with large E_T^{miss} mainly originates from the misreconstruction of the energy of a jet in the calorimeter and to a lesser extent is due to the presence of neutrinos in the final state from heavy-flavor decays. In this analysis, the multijet background is determined from data, using a *jet smearing* method as described in Ref. [81], which relies on the assumption that the E_T^{miss} of multijet events is dominated by fluctuations in the jet response in the detector that can be measured in the data. Different response functions are used for untagged and heavy-flavor tagged jets. For the M1 monojet-like and C1 c -tagged analyses, the multijet background constitutes about 1% of the total background, and is negligible for the other signal regions.

D. Background fits

The use of control regions to constrain the normalization of the dominant background contributions from $Z(\rightarrow \nu\bar{\nu})$ +jets, W +jets, (and $t\bar{t}$ in the case of the c -tagged analysis) reduces significantly the relatively large theoretical and experimental systematic uncertainties, of the order of 20%–30%, associated with purely MC-based background predictions in the signal regions. A complete study of systematic uncertainties is carried out in the monojet-like and c -tagged analyses, as detailed in Sec. VII. To determine the final uncertainty on the total background, all systematic uncertainties are treated as nuisance parameters with Gaussian shapes in a fit based on the profile likelihood method [82], that takes into account correlations among systematic variations. The fit takes also into account cross contamination between different background sources in the control regions.

A simultaneous likelihood fit to the $W(\rightarrow \mu\nu)$ +jets, $W(\rightarrow e\nu)$ +jets, $Z/\gamma^*(\rightarrow \ell^+\ell^-)$ +jets and $t\bar{t}$ control regions (the latter only in the case of the c -tagged analysis) is performed separately for each analysis to normalize and constrain the corresponding background estimates in the signal regions. The results of the background-only fits in the control regions are presented in Tables II–IV for the monojet-like selections, and in Table V for the c -tagged analysis. As the tables indicate, the W/Z +jets background predictions receive multiplicative

normalization factors that vary in the range between 1.1 and 0.9 for the monojet-like analysis, depending on the process and the kinematic selection, and between 0.8 and 0.9 for the c -tagged analyses. In the c -tagged analysis, the $t\bar{t}$ background predictions are normalized with a scale factor 1.1 for both the C1 and C2 selections.

E. Validation of the background determination

In the monojet-like analysis, the control regions are defined using the same requirements for E_T^{miss} , leading jet p_T , event topologies, and jet vetoes as in the signal regions, such that no extrapolation in E_T^{miss} and jet p_T is needed from control to signal regions. The agreement between data and background predictions is confirmed in a low- p_T validation region defined using the same monojet-like selection criteria with E_T^{miss} and leading jet p_T limited to the range 150–220 GeV.

In the case of the c -tagged analysis, for which the control regions are defined with lower thresholds on the leading jet p_T and E_T^{miss} compared to those of the signal regions, the $W(\rightarrow \mu\nu)$ +jets, $W(\rightarrow e\nu)$ +jets, $Z/\gamma^*(\rightarrow \ell^+\ell^-)$ +jet and $t\bar{t}$ yields fitted in the control regions are then validated in dedicated validation regions (here denoted by V1–V5). The definition of the validation regions is presented in Table VI and is such that there is no overlap of events with the control and signal regions. The validation regions V1–V4 differ from the signal regions only on the thresholds imposed on the E_T^{miss} and leading jet p_T . In the case of V5, the same requirements as one of the signal regions on E_T^{miss} and leading jet p_T are imposed but the number of jets is limited to be exactly three. Similar to the transfer factors from control to signal regions, transfer factors from the control to the validation regions are also defined based on MC simulation. The same experimental systematic uncertainties are evaluated and taken into account in the extrapolation. These transfer factors are subject to the modeling uncertainties of the simulation, which are also applied in the validation regions. Hence, the extrapolation to the validation regions is identical to that of the signal regions. Table VII presents the comparison between data and the scaled MC predictions in the validation regions and Fig. 6 presents the E_T^{miss} and leading jet p_T distributions for V3 to V5 regions. Good agreement, within uncertainties, is observed between data and predictions demonstrating a good understanding of the background yields.

VII. SYSTEMATIC UNCERTAINTIES AND BACKGROUND FITS

In this section the impact of each source of systematic uncertainty on the total background prediction in the signal regions, as determined via the global fits explained in Sec. VID, is discussed separately for monojet-like and c -tagged selections. Finally, the experimental and theoretical uncertainties on the SUSY signal yields are discussed.

TABLE II. Data and background predictions in the control regions before and after the fit is performed for the M1 selection. The background predictions include both the statistical and systematic uncertainties. The individual uncertainties are correlated, and do not necessarily add in quadrature to the total background uncertainty.

M1 control regions	$W(\rightarrow e\nu)$	$W(\rightarrow \mu\nu)$	$Z/\gamma^*(\rightarrow \mu^+\mu^-)$
Observed events (20.3 fb ⁻¹)	9271	14786	2100
SM prediction (post-fit)	9270 ± 110	14780 ± 150	2100 ± 50
Fitted $W(\rightarrow e\nu)$	6580 ± 130	0.4 ± 0.2	–
Fitted $W(\rightarrow \mu\nu)$	39 ± 5	12110 ± 200	2.4 ± 0.2
Fitted $W(\rightarrow \tau\nu)$	1640 ± 40	1130 ± 30	0.6 ± 0.1
Fitted $Z/\gamma^*(\rightarrow e^+e^-)$	0.04 ^{+0.07} _{-0.04}	–	–
Fitted $Z/\gamma^*(\rightarrow \mu^+\mu^-)$	3.6 ± 0.5	290 ± 20	2010 ± 50
Fitted $Z/\gamma^*(\rightarrow \tau^+\tau^-)$	116 ± 3	43 ± 3	2.9 ± 0.3
Fitted $Z(\rightarrow \nu\bar{\nu})$	17 ± 3	4.2 ± 0.4	–
Expected $t\bar{t}$, single top, $t\bar{t}+V$	600 ± 80	880 ± 90	32 ± 9
Expected dibosons	280 ± 90	330 ± 110	58 ± 21
MC exp. SM events	9354	15531	2140
Fit input $W(\rightarrow e\nu)$	6644	0.4	–
Fit input $W(\rightarrow \mu\nu)$	41	12839	2.5
Fit input $W(\rightarrow \tau\nu)$	1650	1142	0.6
Fit input $Z/\gamma^*(\rightarrow e^+e^-)$	0.04	–	–
Fit input $Z/\gamma^*(\rightarrow \mu^+\mu^-)$	3.7	291	2044
Fit input $Z/\gamma^*(\rightarrow \tau^+\tau^-)$	117	44	3.0
Fit input $Z(\rightarrow \nu\bar{\nu})$	18	4.5	–
Fit input $t\bar{t}$, single top, $t\bar{t}+V$	600	880	32
Fit input dibosons	280	330	58

A. Monojet-like analysis

Uncertainties on the absolute jet and E_T^{miss} energy scale and resolution [63] translate into an uncertainty on the total background that varies between 1.1% for M1 and 1.3% for M3. Uncertainties related to jet quality requirements and pileup description and corrections to the jet p_T and E_T^{miss} introduce a 0.2% to 0.3% uncertainty on the background predictions. Uncertainties on the simulated lepton identification and reconstruction efficiencies, energy/momentum scale and resolution translate into a 1.2% and 0.9% uncertainty in the total background for M1 and M3 selections, respectively.

Variations of the renormalization/factorization and parton-shower matching scales and PDFs in the SHERPA W/Z +jets background samples translate into a 1% to 0.4% uncertainty in the total background. Variations within uncertainties in the re-weighting procedure for the simulated W and Z p_T distributions introduce less than a 0.2% uncertainty on the total background estimates.

Model uncertainties, related to potential differences between W +jets and Z +jets final states, affecting the normalization of the dominant $Z(\rightarrow \nu\bar{\nu})$ +jets and the small $Z/\gamma^*(\rightarrow \tau^+\tau^-)$ +jets and $Z/\gamma^*(\rightarrow e^+e^-)$ +jets background contributions, as determined in $W(\rightarrow \mu\nu)$ +jets and $W(\rightarrow e\nu)$ +jets

control regions, are studied in detail. This includes uncertainties related to PDFs and renormalization/factorization scale settings, the parton shower parameters and the hadronization model used in the MC simulations, and the dependence on the lepton reconstruction and acceptance. As a result, an additional 3% uncertainty on the $Z(\rightarrow \nu\bar{\nu})$ +jets, $Z/\gamma^*(\rightarrow \tau^+\tau^-)$ +jets and $Z/\gamma^*(\rightarrow e^+e^-)$ +jets contributions is included for all the selections. Separate studies using parton-level predictions for W/Z +jet production, as implemented in MCFM-6.8 [83], indicate that NLO strong corrections affect the $W(\rightarrow \mu\nu)$ +jets to $Z(\rightarrow \nu\bar{\nu})$ +jets ratio by less than 1% in the E_T^{miss} and leading jet p_T kinematic range considered. In addition, the effect from NLO electroweak corrections on the W +jets to Z +jets ratio is taken into account [84–86]. Dedicated parton-level calculations are performed with the same E_T^{miss} and leading jet p_T requirements as in the M1 to M3 signal regions. The studies suggest an effect on the W +jets to Z +jets ratio that varies between about 2% for M1 and 3% for M2 and M3, although the calculations suffer from large uncertainties, mainly due to the limited knowledge of the photon PDFs inside the proton. In this analysis, these results are conservatively adopted as an additional uncertainty on the $Z(\rightarrow \nu\bar{\nu})$ +jets, $Z/\gamma^*(\rightarrow \tau^+\tau^-)$ +jets and $Z/\gamma^*(\rightarrow e^+e^-)$ +jets contributions. Altogether, this translates into an uncertainty on the total background that varies from 1.9% and 2.1% for

TABLE III. Data and background predictions in the control regions before and after the fit is performed for the M2 selection. The background predictions include both the statistical and systematic uncertainties. The individual uncertainties are correlated, and do not necessarily add in quadrature to the total background uncertainty.

M2 control regions	$W(\rightarrow e\nu)$	$W(\rightarrow \mu\nu)$	$Z/\gamma^*(\rightarrow \mu^+\mu^-)$
Observed events (20.3 fb ⁻¹)	1835	4285	650
SM prediction (post-fit)	1840 ± 45	4280 ± 70	650 ± 26
Fitted $W(\rightarrow e\nu)$	1260 ± 43	–	–
Fitted $W(\rightarrow \mu\nu)$	10 ± 2	3500 ± 90	0.8 ± 0.2
Fitted $W(\rightarrow \tau\nu)$	350 ± 13	330 ± 15	0.28 ± 0.03
Fitted $Z/\gamma^*(\rightarrow e^+e^-)$	0.03 ^{+0.05} _{-0.03}	–	–
Fitted $Z/\gamma^*(\rightarrow \mu^+\mu^-)$	1.2 ± 0.2	71 ± 4	620 ± 27
Fitted $Z/\gamma^*(\rightarrow \tau^+\tau^-)$	17 ± 1	8.5 ± 0.6	1.0 ± 0.1
Fitted $Z(\rightarrow \nu\bar{\nu})$	4.6 ± 0.7	0.8 ± 0.1	–
Expected $t\bar{t}$, single top, $t\bar{t}+V$	120 ± 20	240 ± 35	8 ± 2
Expected dibosons	80 ± 30	130 ± 53	21 ± 7
SM prediction (pre-fit)	1873	4513	621
Fit input $W(\rightarrow e\nu)$	1287	–	–
Fit input $W(\rightarrow \mu\nu)$	11	3725	0.8
Fit input $W(\rightarrow \tau\nu)$	352	342	0.3
Fit input $Z/\gamma^*(\rightarrow e^+e^-)$	0.04	–	–
Fit input $Z/\gamma^*(\rightarrow \mu^+\mu^-)$	1.2	67	590
Fit input $Z/\gamma^*(\rightarrow \tau^+\tau^-)$	17	8.7	1.0
Fit input $Z(\rightarrow \nu\bar{\nu})$	4.9	0.8	–
Fit input $t\bar{t}$, single top, $t\bar{t}+V$	120	240	8
Fit input dibosons	80	130	21

the M1 and M2 selections, respectively, to about 2.6% for the M3 selection.

Theoretical uncertainties on the predicted background yields for top-quark-related processes include: uncertainties on the absolute $t\bar{t}$, single top and $t\bar{t} + Z/W$ cross sections; uncertainties on the MC generators and the modeling of parton showers employed (see Sec. III); variations in the set of parameters that govern the parton showers and the amount of initial- and final-state soft gluon radiation; and uncertainties due to the choice of renormalization and factorization scales and PDFs. This introduces an uncertainty on the total background prediction that varies between 1.6% and 1.0% for the M1 and M3 selections, respectively. Uncertainties on the diboson contribution are estimated in a similar way and translate into an uncertainty on the total background in the range between 0.7% and 1.3%. A conservative 100% uncertainty on the multijet background estimation is adopted, leading to a 1% uncertainty on the total background for the M1 selection. Finally, statistical uncertainties related to the data control regions and simulation samples lead to an additional uncertainty on the final background estimates in the signal regions that vary between 1.2% for M1 and 1.4% for M3 selections. Other uncertainties related to the trigger efficiency and the determination of the total integrated luminosity [73] are also included, which cancel out in the case of the domi-

nant background contributions that are determined using data-driven methods, leading to a less than 0.3% uncertainty on the total background.

B. c -tagged analysis

In the c -tagged analysis, the jet energy scale uncertainty translates into a 0.3% to 2.2% uncertainty in the final background estimate. Uncertainties related to the *loose* and *medium* c -tag introduce a 2.8% and 2.5% uncertainty on the background yield for the C1 and C2 selections, respectively. Uncertainties related to the jet energy resolution, soft contributions to E_T^{miss} , modeling of multiple pp interactions, trigger and lepton reconstruction and identification (momentum and energy scales, resolutions and efficiencies) translate into about a 1.2% (1.4%) uncertainty for the C1 (C2) selection. Variations of the renormalization/factorization and parton-shower matching scales and PDFs in the SHERPA W/Z +jets background samples translate into a 3.0% and 3.3% uncertainty in the total background for the C1 and C2 selections, respectively. Uncertainties in the re-weighting of the simulated W and Z p_T distributions, affecting the extrapolation of the MC normalization factors from the control to the signal regions, introduce a less than 0.6% uncertainty in the final background

TABLE IV. Data and background predictions in the control regions before and after the fit is performed for the M3 selection. The background predictions include both the statistical and systematic uncertainties. The individual uncertainties are correlated, and do not necessarily add in quadrature to the total background uncertainty.

M3 control regions	$W(\rightarrow e\nu)$	$W(\rightarrow \mu\nu)$	$Z/\gamma^*(\rightarrow \mu^+\mu^-)$
Observed (20.3 fb^{-1})	417	946	131
SM prediction (post-fit)	420 ± 20	950 ± 30	130 ± 12
Fitted $W(\rightarrow e\nu)$	270 ± 17	–	–
Fitted $W(\rightarrow \mu\nu)$	2.2 ± 0.4	750 ± 37	0.3 ± 0.1
Fitted $W(\rightarrow \tau\nu)$	84 ± 6	79 ± 6	0.02 ± 0.01
Fitted $Z/\gamma^*(\rightarrow e^+e^-)$	–	–	–
Fitted $Z/\gamma^*(\rightarrow \mu^+\mu^-)$	0.7 ± 0.1	13 ± 1	120 ± 12
Fitted $Z/\gamma^*(\rightarrow \tau^+\tau^-)$	4.7 ± 0.4	1.8 ± 0.3	0.28 ± 0.03
Fitted $Z(\rightarrow \nu\bar{\nu})$	1.2 ± 0.2	0.08 ± 0.02	–
Expected $t\bar{t}$, single top, $t\bar{t}+V$	31 ± 5	65 ± 10	1 ± 1
Expected dibosons	22 ± 8	40 ± 17	5 ± 3
SM prediction (pre-fit)	416	1023	132
Fit input $W(\rightarrow e\nu)$	271	–	–
Fit input $W(\rightarrow \mu\nu)$	2.4	824	0.3
Fit input $W(\rightarrow \tau\nu)$	83	79	0.02
Fit input $Z/\gamma^*(\rightarrow e^+e^-)$	–	–	–
Fit input $Z/\gamma^*(\rightarrow \mu^+\mu^-)$	0.7	13	125
Fit input $Z/\gamma^*(\rightarrow \tau^+\tau^-)$	4.6	1.8	0.3
Fit input $Z(\rightarrow \nu\bar{\nu})$	1.3	0.10	–
Fit input $t\bar{t}$, single top, $t\bar{t}+V$	31	65	1
Fit input dibosons	22	40	5

estimates. In the c -tagged analysis, the Z +jets and W +jets background is enriched in heavy-flavor jets produced in association with the vector boson and the same heavy-flavor processes are present in the signal region and the V +jets control regions. Theoretical uncertainties on the background predictions for top-related processes and diboson contributions are computed following the same prescriptions as in the monojet-like analysis and constitute the dominant sources of systematic uncertainty. In the case of top-related processes, this translates into an uncertainty on the total background prediction of 5.2% and 5.0% for C1 and C2 selections, respectively. Similarly, the uncertainties on the diboson contributions lead to an uncertainty on the total background of 5.5% (11.5%) for the C1 (C2) selection. The limited number of SM MC events and data events in the control regions lead to an additional uncertainty of 3.0% (4.4%) for the C1 (C2) signal region. Finally, a conservative 100% uncertainty on the multijet background contribution in the control and signal regions is also adopted, which translates into a 0.4% and 0.9% uncertainty on the total background for the C1 and C2 selections, respectively.

C. Signal systematic uncertainties

Different sources of systematic uncertainty on the predicted SUSY signals are considered. Experimental uncertainties related to the jet and E_T^{miss} reconstruction, energy scales and resolutions introduce uncertainties in the signal yields in the range 3% to 7% and 10% to 27% for the monojet-like and c -tagged analyses, respectively, depending on the stop and neutralino masses considered. In the c -tagged analysis, uncertainties on the simulated c -tagging efficiencies for *loose* and *medium* tags introduce 9% to 16% uncertainties in the signal yields. In addition, a 2.8% uncertainty on the integrated luminosity is included. Uncertainties affecting the signal acceptance times efficiency ($A \times \varepsilon$) related to the generation of the SUSY samples are determined using additional samples with modified parameters. This includes uncertainties on the modeling of the initial- and final-state gluon radiation, the choice of renormalization/factorization scales, and the parton-shower matching scale settings. Altogether this translates into an uncertainty on the signal yields that tends to increase with decreasing Δm and varies between 8% and 12% in the monojet-like analyses, and between 17% and 38% in the c -tagged selections, depending on the stop and neutralino masses. Finally, uncertainties on the predicted SUSY signal cross sections include PDF uncertainties, variations on

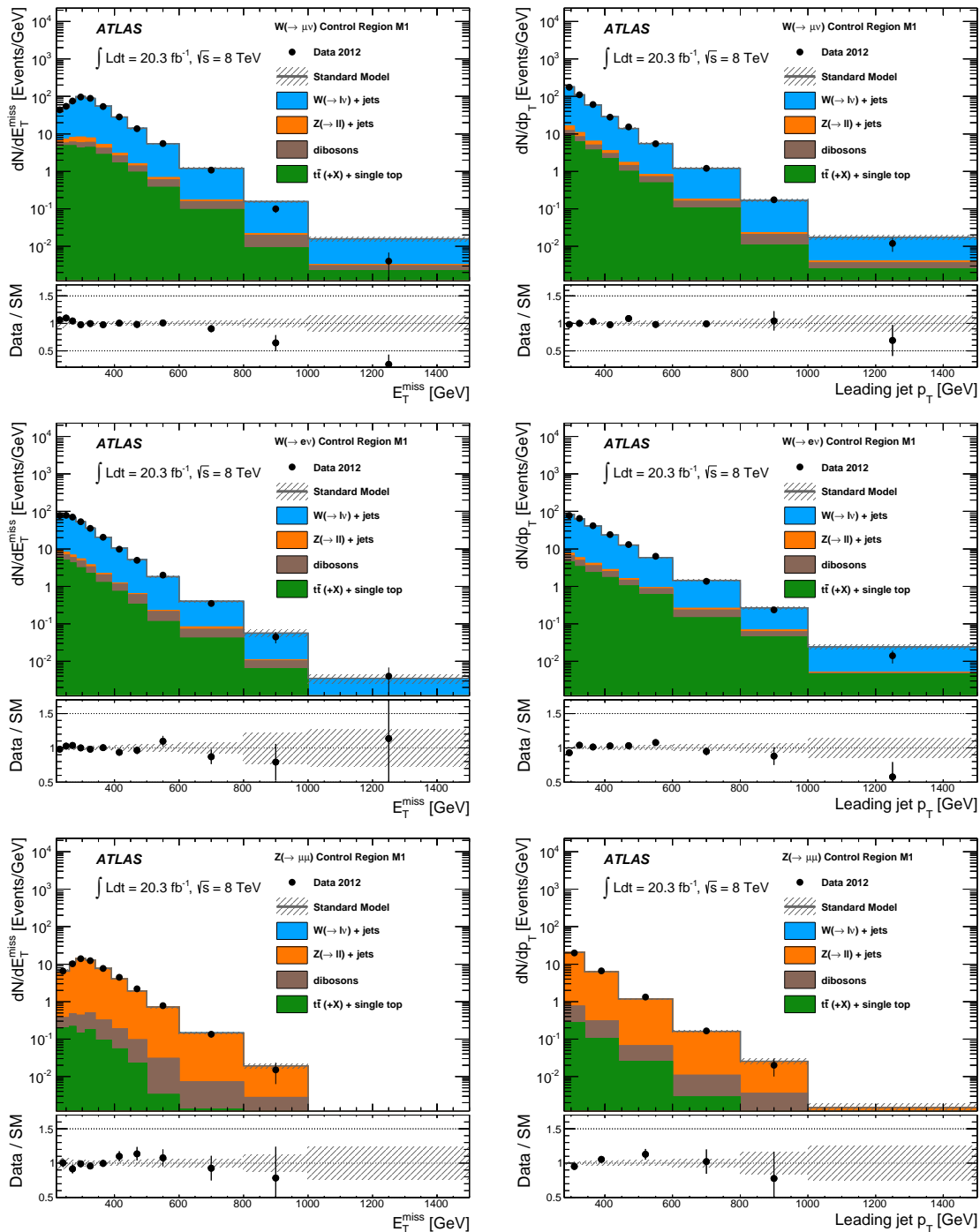


FIG. 3. The measured E_T^{miss} and leading jet p_T distributions in the $W(\rightarrow \mu\nu)+\text{jets}$ (top), $W(\rightarrow e\nu)+\text{jets}$ (middle), and $Z/\gamma^*(\rightarrow \mu^+\mu^-)+\text{jets}$ (bottom) control regions, for the M1 selection, compared to the background predictions. The latter include the global normalization factors extracted from the fit. The error bands in the ratios include the statistical and experimental uncertainties on the background predictions.

the $\alpha_s(M_Z)$ value employed, as well as variations of the renormalization and factorization scales by factors of two and one-half. Altogether, this results in a total theoretical uncertainty on the cross section that varies between 14% and 16% for stop masses in the range between 100 GeV and 400 GeV.

VIII. RESULTS AND INTERPRETATION

The data and the expected background predictions for the monojet-like and c -tagged analyses are summarized in Table VIII. Good agreement is observed between the data and

TABLE V. Data and background predictions in the W/Z +jets and $t\bar{t}$ control regions before and after the fit is performed for the c -tagged selection. The background predictions include both the statistical and systematic uncertainties. The individual uncertainties are correlated, and do not necessarily add in quadrature to the total background uncertainty.

c -tagged control regions	$W(\rightarrow \mu\nu)$	$W(\rightarrow e\nu)$	$Z \rightarrow \ell\ell$	$t\bar{t}$
Observed events (20.3 fb $^{-1}$)	1783	785	113	140
SM prediction (post-fit)	1780 \pm 42	790 \pm 28	110 \pm 11	140 \pm 12
Fitted $W(\rightarrow e\nu)$	–	260 \pm 49	0.08 \pm 0.02	0.19 \pm 0.05
Fitted $W(\rightarrow \mu\nu)$	480 \pm 110	0.1 \pm 0.1	0.01 \pm 0.01	0.6 \pm 0.1
Fitted $W(\rightarrow \tau\nu)$	70 \pm 14	29 \pm 6	–	0.06 \pm 0.02
Fitted $Z(\rightarrow \nu\bar{\nu})$	–	0.35 \pm 0.05	–	–
Fitted $Z/\gamma^*(\rightarrow e^+e^-)$	–	–	49 \pm 6	–
Fitted $Z/\gamma^*(\rightarrow \mu^+\mu^-)$	22 \pm 3	–	45 \pm 5	6.4 \pm 0.8
Fitted $Z/\gamma^*(\rightarrow \tau^+\tau^-)$	16 \pm 3	3.7 \pm 0.7	–	1.9 \pm 0.4
Fitted $t\bar{t}$	1000 \pm 110	400 \pm 43	7.1 \pm 0.8	120 \pm 12
Expected $t\bar{t} + V$	9 \pm 1	4.5 \pm 0.5	1.0 \pm 0.1	1.8 \pm 0.2
Expected single top	95 \pm 18	49 \pm 9	0.35 \pm 0.08	7 \pm 1
Expected dibosons	76 \pm 15	35 \pm 8	11 \pm 2	5 \pm 1
Expected Higgs	1.1 \pm 0.2	0.5 \pm 0.1	0.06 \pm 0.01	0.14 \pm 0.02
SM prediction (pre-fit)	1830	790	127	132
Fit input $W(\rightarrow e\nu)$	–	290	0.08	0.20
Fit input $W(\rightarrow \mu\nu)$	588	0.1	0.02	0.7
Fit input $W(\rightarrow \tau\nu)$	79	32	–	0.10
Fit input $Z(\rightarrow \nu\bar{\nu})$	–	0.40	–	–
Fit input $Z/\gamma^*(\rightarrow e^+e^-)$	–	–	56	–
Fit input $Z/\gamma^*(\rightarrow \mu^+\mu^-)$	25	–	52	7.4
Fit input $Z/\gamma^*(\rightarrow \tau^+\tau^-)$	17	4.1	–	2.2
Fit input $t\bar{t}$	940	374	6.7	108
Fit input $t\bar{t} + V$	9	4.5	1.0	1.8
Fit input single top	95	49	0.35	7
Fit input dibosons	76	35	11	5
Fit input Higgs	1.1	0.5	0.06	0.14

TABLE VI. Definition of the validation regions for the c -tagged selection.

	V1	V2	V3	V4	V5
Preselection					
Tagging	One medium c -tag among jets 2–4(2–3) for V1–V4(V5) Three (two) loose c -tags, acting as b -veto, for other 3(2) jets for V1–V4(V5)				
N_e	0	0	0	0	0
N_μ	0	0	0	0	0
N_{jet}	≥ 4	≥ 4	≥ 4	≥ 4	= 3
$E_{\text{T}}^{\text{miss}}$ (GeV)	$\in [150, 250]$	$\in [200, 250]$	$\in [150, 250]$	> 150	> 250
Leading jet p_{T} (GeV)	$\in [150, 250]$	$\in [200, 290]$	> 150	$\in [150, 290]$	> 290

the SM predictions in each case. The SM predictions for the monojet-like selections are determined with a total uncer-

tainty of 2.9%, 3.2%, and 4.6% for the M1, M2, M3 signal regions, respectively, which include correlations between un-

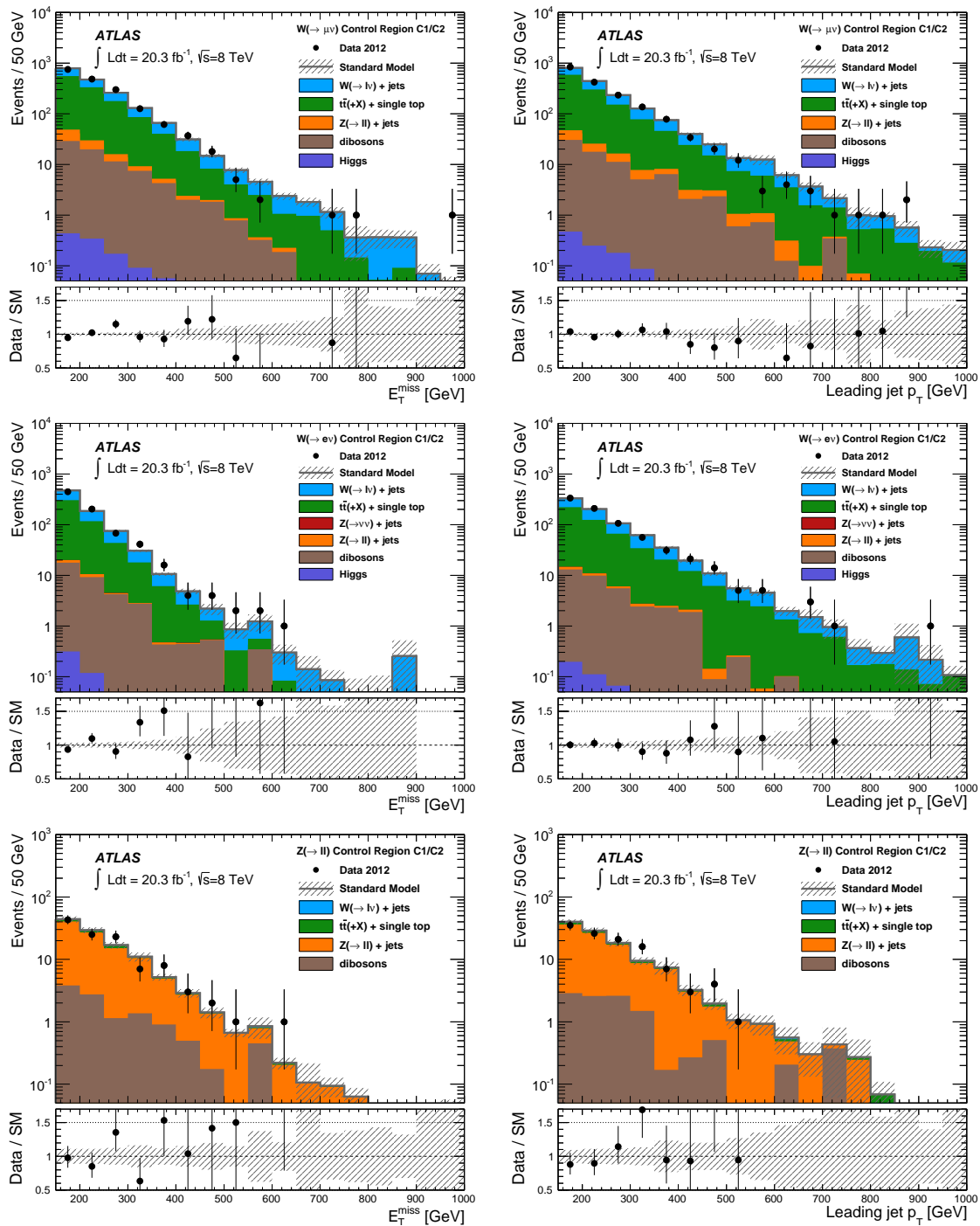


FIG. 4. The measured E_T^{miss} and leading jet p_T distributions in the $W(\rightarrow \mu\nu)+\text{jets}$ (top), $W(\rightarrow e\nu)+\text{jets}$ (middle), and $Z/\gamma^*(\rightarrow \ell^+\ell^-)+\text{jets}$ (bottom) control regions, for the c -tagged selection, compared to the background predictions. The latter include the global normalization factors extracted from the fit. The error bands in the ratios include the statistical and experimental uncertainties on the background predictions.

certainties on the individual background contributions. Similarly, the SM predictions for the c -tagged analyses are determined with a total uncertainty of 10% for C1 and 14% for C2 selections. Figure 7 shows the measured leading jet p_T and E_T^{miss} distributions for the monojet-like selections compared

to the background predictions. Similarly, Fig. 8 presents the leading jet p_T , E_T^{miss} and jet multiplicity distributions for the c -tagged selections. For illustration purposes, the distribution of two different SUSY scenarios for stop pair production in the $\tilde{\tau}_1 \rightarrow c + \tilde{\chi}_1^0$ decay channel with stop masses of 200 GeV

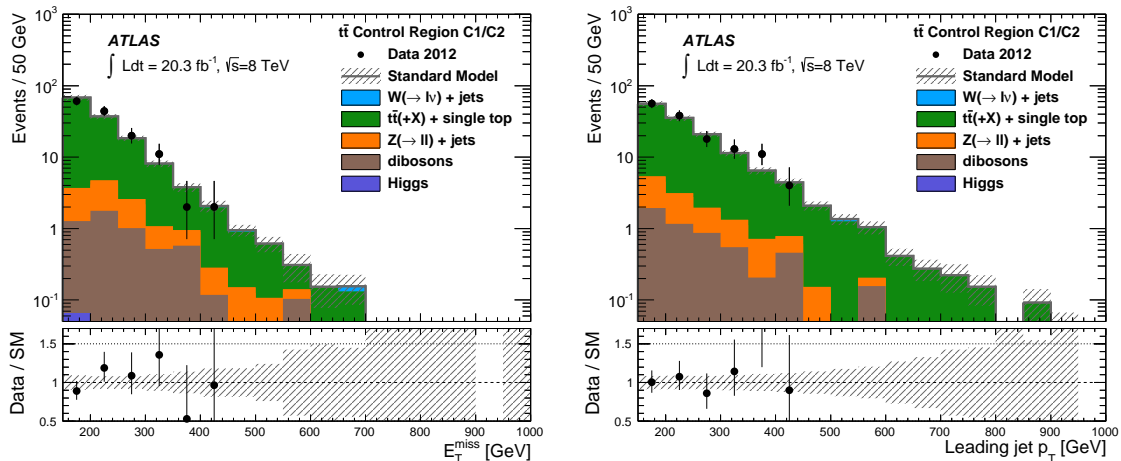


FIG. 5. The measured E_T^{miss} and leading jet p_T distributions in the $t\bar{t}$ control region, for the c -tagged selection, compared to the background predictions. The latter include the global normalization factors extracted from the fit. The error bands in the ratios include the statistical and experimental uncertainties on the background predictions.

TABLE VII. Observed events and SM background predictions from the control regions for the V1 to V5 validation regions. The errors shown are the statistical plus systematic uncertainties. The individual uncertainties are correlated, and do not necessarily add in quadrature to the total background uncertainty.

c -tagged validation regions	V1	V2	V3	V4	V5
Observed events (20.3 fb^{-1})	1534	257	2233	2157	215
Fit prediction	1530 ± 90	260 ± 20	2300 ± 190	2200 ± 190	200 ± 50
$W(\rightarrow e\nu)$	70 ± 13	12 ± 2	100 ± 20	100 ± 18	9 ± 3
$W(\rightarrow \mu\nu)$	60 ± 14	10 ± 2	90 ± 20	90 ± 19	10 ± 3
$W(\rightarrow \tau\nu)$	330 ± 60	64 ± 12	470 ± 86	460 ± 82	50 ± 19
$Z(\rightarrow \nu\bar{\nu})$	260 ± 44	52 ± 12	360 ± 56	410 ± 95	80 ± 20
$Z/\gamma^*(\rightarrow e^+e^-)$	—	—	—	—	—
$Z/\gamma^*(\rightarrow \mu^+\mu^-)$	1.1 ± 0.1	0.14 ± 0.02	1.6 ± 0.2	1.5 ± 0.2	0.11 ± 0.03
$Z/\gamma^*(\rightarrow \tau^+\tau^-)$	8 ± 1	0.9 ± 0.2	12 ± 2	10 ± 2	0.5 ± 0.2
$t\bar{t}$	630 ± 90	92 ± 14	830 ± 160	830 ± 170	20 ± 5
$t\bar{t} + V$	6.3 ± 0.7	1.3 ± 0.1	10 ± 1	10 ± 1	0.16 ± 0.05
Single top	60 ± 12	9 ± 2	80 ± 17	80 ± 16	8 ± 1
Dibosons	60 ± 14	14 ± 3	100 ± 22	100 ± 23	18 ± 3
Higgs	0.7 ± 0.1	0.15 ± 0.03	1.1 ± 0.2	1.1 ± 0.2	0.09 ± 0.02
Multijets	40 ± 19	0.8 ± 0.8	200 ± 99	70 ± 36	—

and neutralino masses of 125 GeV and 195 GeV are included.

The agreement between the data and the SM predictions for the total number of events in the different signal regions is translated into 95% confidence level (CL) upper limits on the visible cross section, $\sigma \times A \times \epsilon$, using the CL_s modified frequentist approach [87], considering the systematic uncertainties on the SM backgrounds and assuming there is no signal contamination in the control regions. The upper limits are derived from pseudo-experiments and from an asymptotic approximation [82], which gives similar results. For the monojet-like analysis, values of $\sigma \times A \times \epsilon$ in the range be-

tween 96 fb and 9.6 fb are excluded at 95% CL. In the case of the c -tagged analysis, visible cross sections above 1.76 fb and 0.95 fb, for the C1 and the C2 selections, respectively, are excluded at 95% CL, as shown in Table IX.

A. Stop pair production with $\tilde{t}_1 \rightarrow c + \tilde{\chi}_1^0$

The results are then translated into exclusion limits on the pair production of top squarks with $\tilde{t}_1 \rightarrow c + \tilde{\chi}_1^0$ (BR=100%) as a function of the stop mass for different neutralino masses.

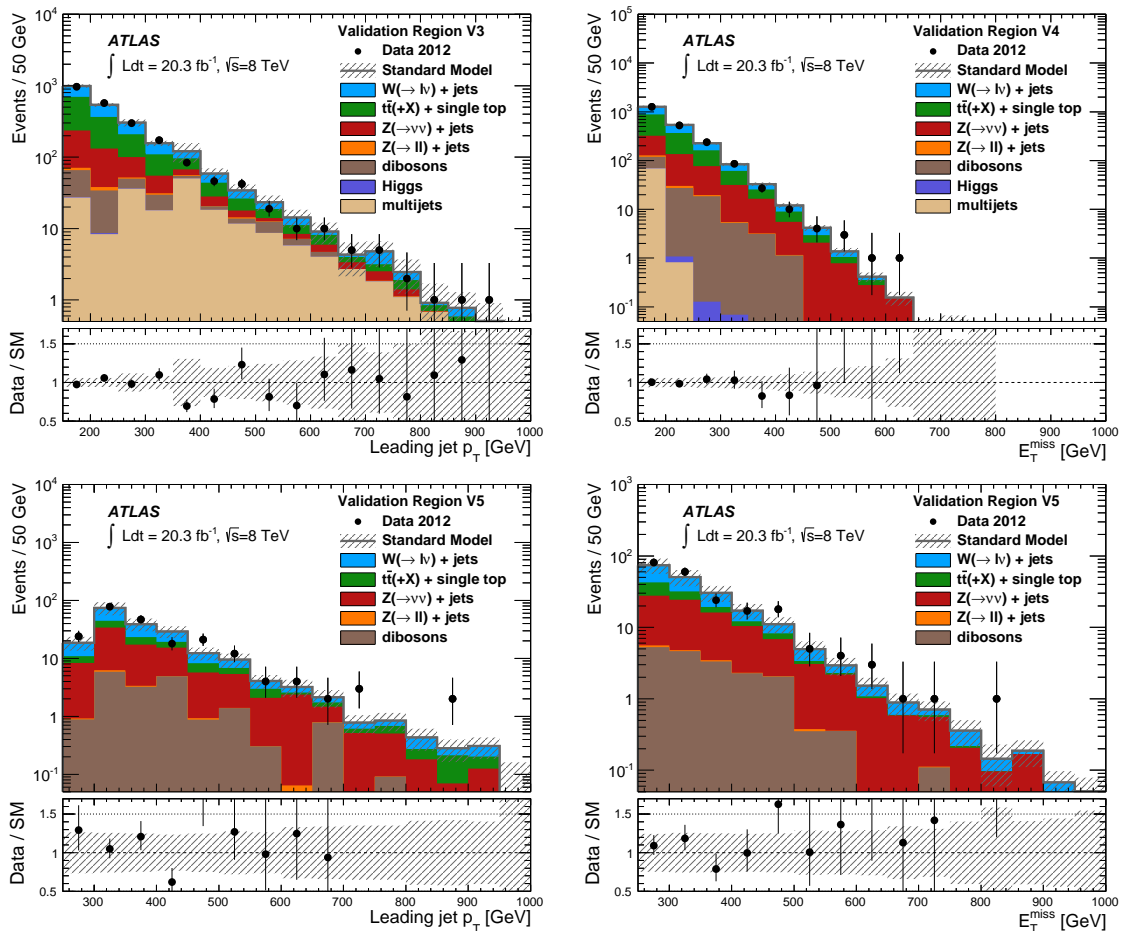


FIG. 6. Measured leading jet p_T and E_T^{miss} distributions for the V3–V4 (top) and V5 (bottom) selections compared to the SM predictions. The error bands in the ratios include both the statistical and systematic uncertainties on the background predictions.

TABLE VIII. Data and SM background prediction in the signal region for the monojet-like and c -tagged selections. For the SM predictions both the statistical and systematic uncertainties are included. In each case the individual uncertainties can be correlated, and do not necessarily add in quadrature to the total background uncertainty.

Signal Region	M1	M2	M3	C1	C2
Observed events (20.3 fb^{-1})	33054	8606	1776	208	71
SM prediction	33450 ± 960	8620 ± 270	1770 ± 81	210 ± 21	75 ± 11
$W(\rightarrow l\nu)$	3300 ± 140	700 ± 43	130 ± 12	11 ± 2	3.0 ± 0.7
$W(\rightarrow \mu\nu)$	3000 ± 100	700 ± 29	133 ± 8	8 ± 2	3.0 ± 0.7
$W(\rightarrow \tau\nu)$	7800 ± 290	1690 ± 74	320 ± 24	42 ± 9	14 ± 3
$Z/\gamma^*(\rightarrow e^+e^-)$	–	–	–	–	–
$Z/\gamma^*(\rightarrow \mu^+\mu^-)$	170 ± 27	53 ± 9	13 ± 3	0.07 ± 0.01	0.04 ± 0.01
$Z/\gamma^*(\rightarrow \tau^+\tau^-)$	95 ± 6	17 ± 1	1.8 ± 0.3	0.7 ± 0.1	0.15 ± 0.03
$Z(\rightarrow \nu\bar{\nu})$	17400 ± 720	5100 ± 240	1090 ± 72	62 ± 9	27 ± 3
$t\bar{t}$, single top, $t\bar{t}+V$	780 ± 73	150 ± 19	27 ± 4	63 ± 13	18 ± 4
Dibosons	650 ± 99	220 ± 40	60 ± 14	21 ± 13	10 ± 9
Higgs	–	–	–	0.16 ± 0.03	0.07 ± 0.01
Multijets	300 ± 300	30 ± 30	4 ± 4	2 ± 2	0.1 ± 0.1

Expected and observed 95% CL exclusion limits are set using the CL_s approach, for which a simultaneous fit to the sig-

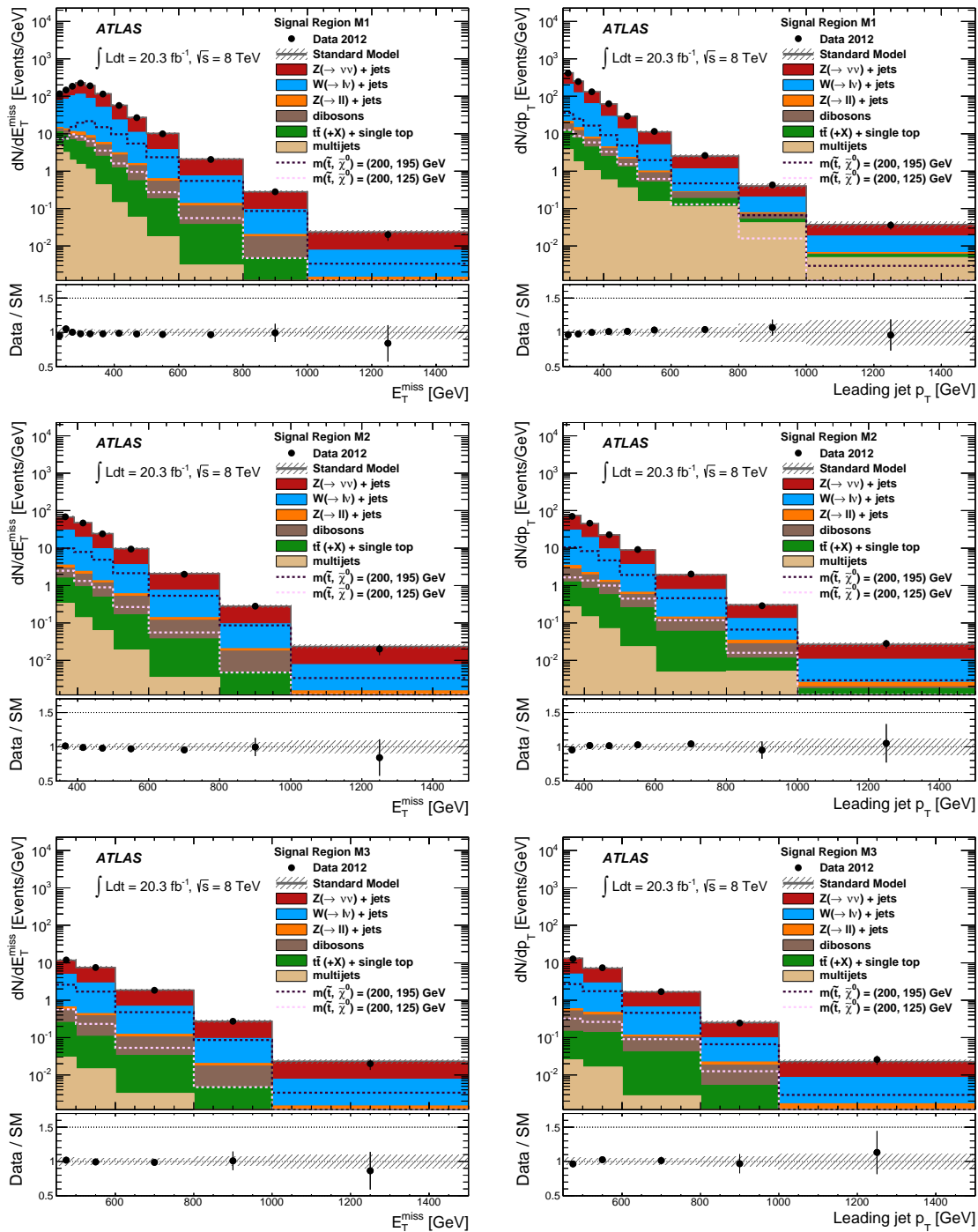


FIG. 7. Measured E_T^{miss} and leading jet p_T distributions for the M1 (top), M2 (middle), and M3 (bottom) selections compared to the SM predictions. For illustration purposes, the distribution of two different SUSY scenarios are included. The error bands in the ratios include both the statistical and systematic uncertainties on the background predictions.

nal and control regions is performed including statistical and systematic uncertainties. Uncertainties on the signal acceptance times efficiency, the background predictions, and the luminosity are considered, and correlations between systematic uncertainties on signal and background predictions are taken

into account. The fit accounts for any potential contamination of signal events in the control regions which a priori has been estimated to be very small. In addition, observed limits are computed using $\pm 1\sigma$ variations on the theoretical predictions for the SUSY cross sections. For each SUSY point consid-

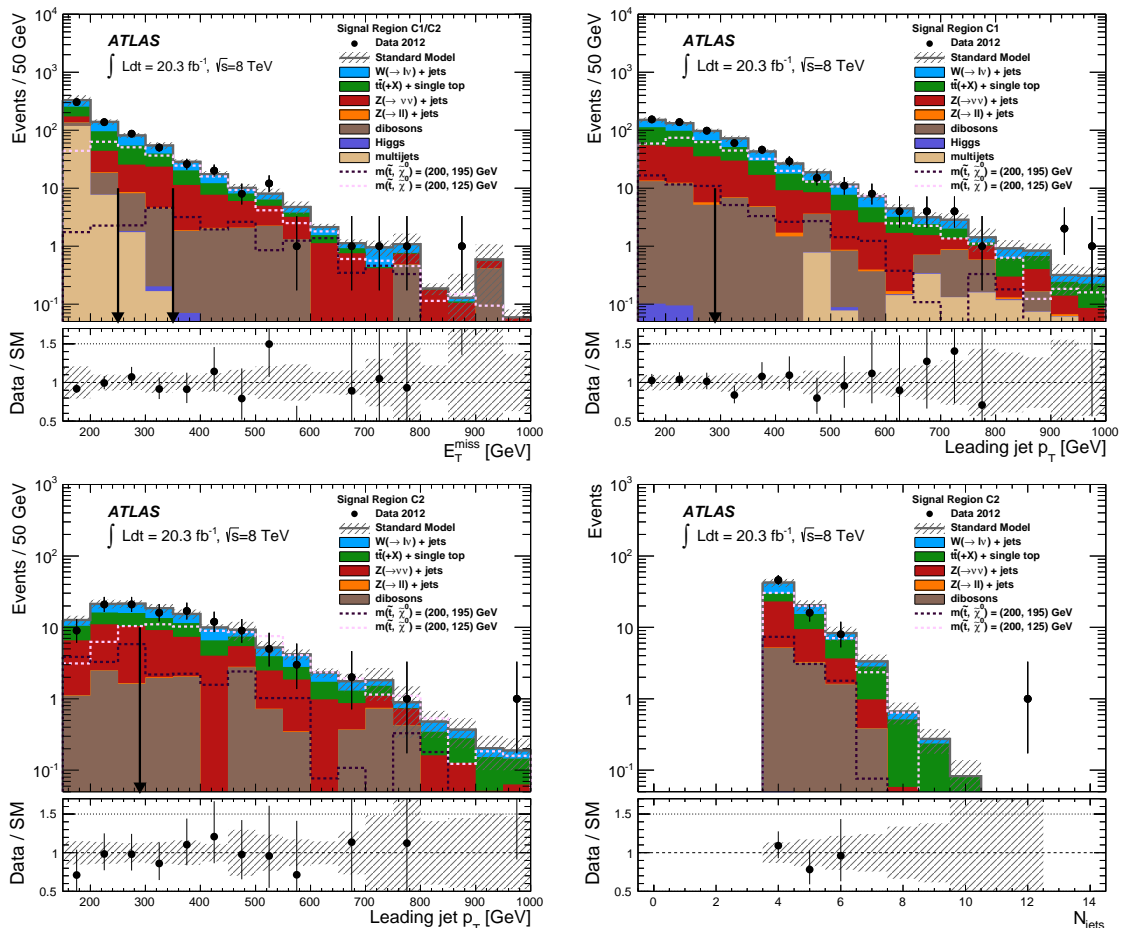


FIG. 8. (top) Measured E_T^{miss} and leading jet p_T distributions for the C1 selection before the cut in the variable shown (as indicated by the vertical arrows) is applied. In the case of the E_T^{miss} distribution, the cuts corresponding to C1 and C2 selections are both indicated. (bottom) Measured leading jet p_T and jet multiplicity for the C2 selection. The data are compared to the SM predictions. For illustration purposes, the distribution of two different SUSY scenarios are included. The error bands in the ratios include both the statistical and systematic uncertainties on the background predictions.

TABLE IX. Left to right: 95% CL upper limits on the visible cross section ($\langle\sigma\rangle_{\text{obs}}^{95}$) and on the number of signal events (S_{obs}^{95}). The third column (S_{exp}^{95}) shows the 95% CL upper limit on the number of signal events, given the expected number (and $\pm 1\sigma$ on the expectation) of background events. The CL_B value, i.e. the confidence level observed for the background-only hypothesis, and the p_0 values, which represents the probability of the background alone to fluctuate to the observed numbers of events or higher, are also reported. The p_0 -values are truncated at 0.5 if the number of observed events is below the number of expected events. The limits derived using an asymptotic approximation instead of pseudo-experiments are given in parentheses.

Signal region	$\langle\sigma\rangle_{\text{obs}}^{95}$ [fb]	S_{obs}^{95}	S_{exp}^{95}	CL_B	p_0
M1	96.2 (95.4)	1951 (1935)	1960_{-320}^{+840} (1950_{-290}^{+850})	0.49	0.50
M2	28.4 (28.7)	575 (581)	590_{-120}^{+210} (600_{-120}^{+200})	0.48	0.50
M3	9.6 (9.6)	195 (195)	190_{-53}^{+69} (190_{-54}^{+69})	0.51	0.49
C1	1.76 (1.75)	35.8 (35.5)	37_{-10}^{+9} (37_{-11}^{+10})	0.45	0.50
C2	0.95 (0.93)	19.3 (18.9)	22_{-6}^{+8} (22_{-6}^{+9})	0.35	0.50

ered, observed and expected limits are computed separately for the different monojet-like and c -tagged analyses, and the

one with the best expected limit is adopted as the nominal result. Finally, the 95% CL observed limits corresponding to the -1σ variations on the SUSY theoretical cross sections are then quoted.

Figure 9 shows the results separately for the monojet-like and c -tagged analyses, illustrating their complementary regions of sensitivity. As anticipated, the monojet-like selections drive the exclusion limits at very low Δm for which the M2 and M3 signal regions enhance the sensitivity to large stop and neutralino masses. The c -tagged results determine the exclusion limits in the rest of the plane. Figure 10 presents the combined results. Masses for the stop up to 240 GeV are excluded at 95% CL for arbitrary neutralino masses, within the kinematic boundaries. For neutralino masses of about 200 GeV, stop masses below 270 GeV are excluded at 95% CL. In the compressed scenario with the stop and neutralino nearly degenerate in mass, the exclusion extends up to stop masses of 260 GeV. The region with $\Delta m < 2$ GeV is not considered in the exclusion since in this regime the stop could become long-lived. These results significantly extend previous exclusion limits [27, 28] on the stop and neutralino masses in this channel.

B. Stop and sbottom pair production with $\tilde{t}_1 \rightarrow b + ff' + \tilde{\chi}_1^0$ and $\tilde{b}_1 \rightarrow b + \tilde{\chi}_1^0$

The monojet-like results are also interpreted in terms of exclusion limits on the stop pair production in the four-body decay mode $\tilde{t}_1 \rightarrow b + ff' + \tilde{\chi}_1^0$ (BR=100%) and the sbottom pair production with $\tilde{b}_1 \rightarrow b + \tilde{\chi}_1^0$ (BR=100%), using the same CL_s approach as explained above. As already mentioned, this is particularly relevant in a mass-degenerate scenario in which the decay products of the squarks are too soft to be identified in the final state, and the signal selection relies on the presence of an ISR jet. Figure 11 shows the expected and observed 95% CL exclusion limits as a function of the stop and neutralino masses for the $\tilde{t}_1 \rightarrow b + ff' + \tilde{\chi}_1^0$ decay channel. For $\Delta m \sim m_b$, stop masses up to 255 GeV are excluded at 95% CL. Top squarks with mass of about 150 GeV and 200 GeV are excluded for $m_b < \Delta m < 50$ GeV and $m_b < \Delta m < 35$ GeV, respectively.

Finally, Fig. 12 presents the expected and observed 95% CL exclusion limits as a function of the sbottom and neutralino masses for the $\tilde{b}_1 \rightarrow b + \tilde{\chi}_1^0$ decay channel, compared to previous results. In the scenario with $m_{\tilde{b}_1} - m_{\tilde{\chi}_1^0} \sim m_b$, this analysis extends the 95% CL exclusion limits up to a sbottom mass of 255 GeV.

IX. CONCLUSIONS

In summary, this paper presents results of a search for stop pair production in the decay channel $\tilde{t}_1 \rightarrow c + \tilde{\chi}_1^0$ using 20.3 fb $^{-1}$ of proton-proton collision data at $\sqrt{s} = 8$ TeV recorded with the ATLAS experiment at the LHC. Two different analysis strategies based on monojet-like and c -tagged

event selections are carried out that optimize the sensitivity across the stop–neutralino mass plane. Good agreement is observed between the data and the SM predictions. The results are translated into 95% CL exclusion limits on the stop and neutralino masses. A stop mass of about 240 GeV is excluded at 95% confidence level for $m_{\tilde{t}_1} - m_{\tilde{\chi}_1^0} < 85$ GeV, as the maximum mass difference in which the decay mode $\tilde{t}_1 \rightarrow c + \tilde{\chi}_1^0$ dominates. Stop masses up to 270 GeV are excluded for a neutralino mass of 200 GeV. In a scenario with the stop and the lightest neutralino nearly degenerate in mass, stop masses up to 260 GeV are excluded. The results from the monojet-like analysis are also re-interpreted in terms of stop pair production in the four-body decay channel $\tilde{t}_1 \rightarrow b + ff' + \tilde{\chi}_1^0$ and sbottom pair production with $\tilde{b}_1 \rightarrow b + \tilde{\chi}_1^0$, leading to a similar exclusion for the mass-degenerate scenario. The results in this paper significantly extend previous results [23, 26–30] at colliders.

ACKNOWLEDGMENTS

We thank CERN for the very successful operation of the LHC, as well as the support staff from our institutions without whom ATLAS could not be operated efficiently.

We acknowledge the support of ANPCyT, Argentina; YerPhI, Armenia; ARC, Australia; BMWF and FWF, Austria; ANAS, Azerbaijan; SSTC, Belarus; CNPq and FAPESP, Brazil; NSERC, NRC and CFI, Canada; CERN; CONICYT, Chile; CAS, MOST and NSFC, China; COLCIENCIAS, Colombia; MSMT CR, MPO CR and VSC CR, Czech Republic; DNRF, DNSRC and Lundbeck Foundation, Denmark; EPLANET, ERC and NSRF, European Union; IN2P3-CNRS, CEA-DSM/IRFU, France; GNSF, Georgia; BMBF, DFG, HGF, MPG and AvH Foundation, Germany; GSRT and NSRF, Greece; ISF, MINERVA, GIF, I-CORE and Benoziyo Center, Israel; INFN, Italy; MEXT and JSPS, Japan; CNRST, Morocco; FOM and NWO, Netherlands; BRF and RCN, Norway; MNiSW and NCN, Poland; GRICES and FCT, Portugal; MNE/IFA, Romania; MES of Russia and ROSATOM, Russian Federation; JINR; MSTD, Serbia; MSSR, Slovakia; ARRS and MIZŠ, Slovenia; DST/NRF, South Africa; MINECO, Spain; SRC and Wallenberg Foundation, Sweden; SER, SNSF and Cantons of Bern and Geneva, Switzerland; NSC, Taiwan; TAEK, Turkey; STFC, the Royal Society and Leverhulme Trust, United Kingdom; DOE and NSF, United States of America.

The crucial computing support from all WLCG partners is acknowledged gratefully, in particular from CERN and the ATLAS Tier-1 facilities at TRIUMF (Canada), NDGF (Denmark, Norway, Sweden), CC-IN2P3 (France), KIT/GridKA (Germany), INFN-CNAF (Italy), NL-T1 (Netherlands), PIC (Spain), ASGC (Taiwan), RAL (UK) and BNL (USA) and in the Tier-2 facilities worldwide.

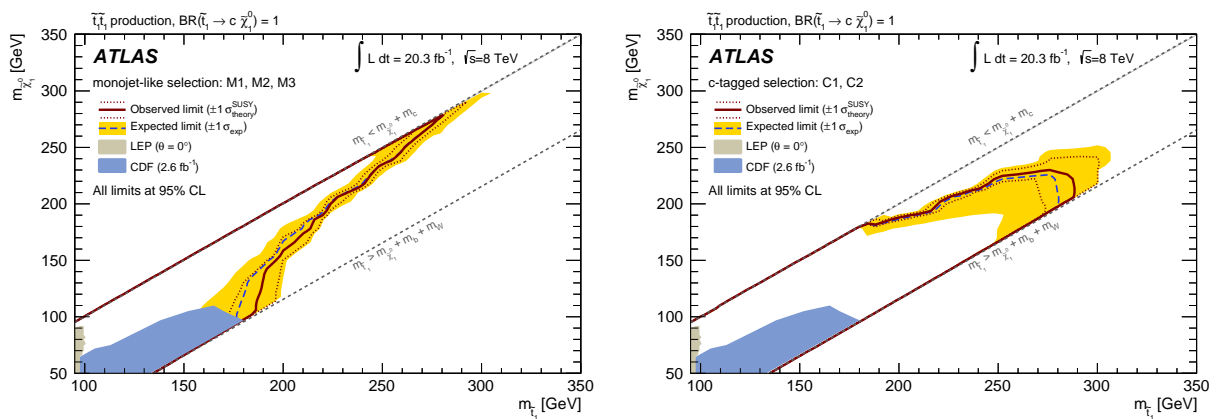


FIG. 9. Exclusion plane at 95% CL as a function of stop and neutralino masses for the decay channel $\tilde{t}_1 \rightarrow c + \tilde{\chi}_1^0$ (BR=100%) as determined separately for the monojet-like (left) and the c -tagged (right) selections. The observed (red line) and expected (blue line) upper limits from this analysis are compared to previous results from Tevatron experiments [27, 28], and from LEP [26] experiments at CERN with squark mixing angle $\theta = 0^\circ$. The dotted lines around the observed limit indicate the range of observed limits corresponding to $\pm 1\sigma$ variations on the NLO SUSY cross-section predictions. The shaded area around the expected limit indicates the expected $\pm 1\sigma$ ranges of limits in the absence of a signal. A band for $\Delta m < 2$ GeV indicates the region in the phase space for which the stop can become long-lived.

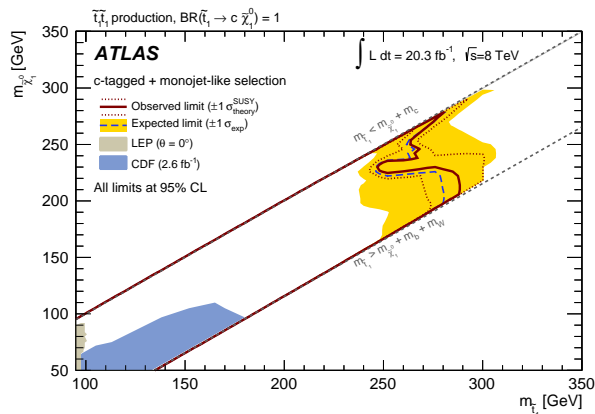


FIG. 10. Exclusion plane at 95% CL as a function of stop and neutralino masses for the decay channel $\tilde{t}_1 \rightarrow c + \tilde{\chi}_1^0$ (BR=100%). The observed (red line) and expected (blue line) upper limits from this analysis are compared to previous results from Tevatron experiments [27, 28], and from LEP [26] experiments at CERN with squark mixing angle $\theta = 0^\circ$. The dotted lines around the observed limit indicate the range of observed limits corresponding to $\pm 1\sigma$ variations on the NLO SUSY cross-section predictions. The shaded area around the expected limit indicates the expected $\pm 1\sigma$ ranges of limits in the absence of a signal. A band for $\Delta m < 2$ GeV indicates the region in the phase space for which the stop can become long-lived.

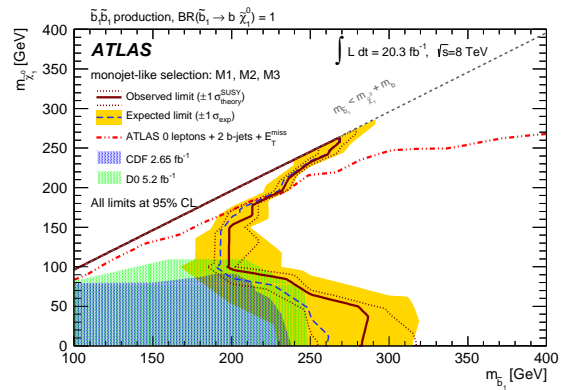


FIG. 12. Exclusion plane at 95% CL as a function of sbottom and neutralino masses for the decay channel $\tilde{b}_1 \rightarrow b + \tilde{\chi}_1^0$ (BR=100%). The observed (red line) and expected (blue line) upper limits from this analysis are compared to previous results from CDF [29], D0 [30], and ATLAS [23]. For the latter, the area below the dashed-dotted line is excluded. The dotted lines around the observed limit indicate the range of observed limits corresponding to $\pm 1\sigma$ variations on the NLO SUSY cross-section predictions. The shaded area around the expected limit indicates the expected $\pm 1\sigma$ ranges of limits in the absence of a signal. A band for $m_{\tilde{b}_1} - m_{\tilde{\chi}_1^0} - m_b < 2$ GeV indicates the region in the phase space for which the sbottom can become long-lived.

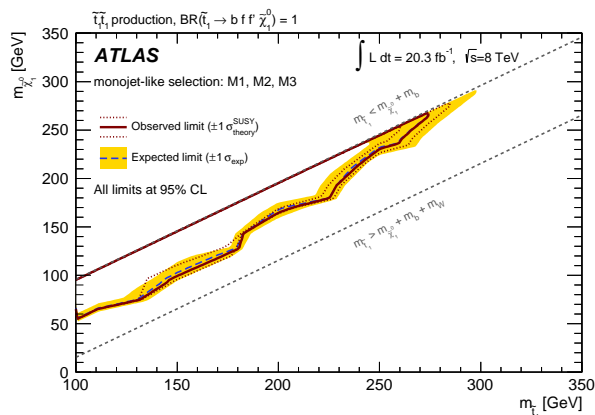


FIG. 11. Exclusion plane at 95% CL as a function of stop and neutralino masses for the decay channel $\tilde{t}_1 \rightarrow b + f f' + \tilde{\chi}_1^0$ (BR=100%). The dotted lines around the observed limit indicate the range of observed limits corresponding to $\pm 1\sigma$ variations on the NLO SUSY cross-section predictions. The shaded area around the expected limit indicates the expected $\pm 1\sigma$ ranges of limits in the absence of a signal. A band for $m_{\tilde{t}_1} - m_{\tilde{\chi}_1^0} - m_b < 2$ GeV indicates the region in the phase space for which the stop can become long-lived.

- [1] H. Miyazawa, *Prog. Theor. Phys.* **36** (6), 1266 (1966).
- [2] P. Ramond, *Phys. Rev.* **D3**, 2415 (1971).
- [3] Y. A. Golfand and E. P. Likhtman, *JETP Lett.* **13**, 323 (1971), [*Pisma Zh.Eksp.Teor.Fiz.* 13:452-455,1971].
- [4] A. Neveu and J. H. Schwarz, *Nucl. Phys.* **B31**, 86 (1971).
- [5] A. Neveu and J. H. Schwarz, *Phys. Rev.* **D4**, 1109 (1971).
- [6] J. Gervais and B. Sakita, *Nucl. Phys.* **B34**, 632 (1971).
- [7] D. V. Volkov and V. P. Akulov, *Phys. Lett.* **B46**, 109 (1973).
- [8] J. Wess and B. Zumino, *Phys. Lett.* **B49**, 52 (1974).
- [9] J. Wess and B. Zumino, *Nucl. Phys.* **B70**, 39 (1974).
- [10] R. Barbieri and G. Giudice, *Nucl. Phys.* **B306**, 63 (1988).
- [11] B. de Carlos and J. Casas, *Phys. Lett.* **B309**, 320 (1993), [arXiv:hep-ph/9303291 \[hep-ph\]](#).
- [12] P. Fayet, *Phys. Lett.* **B64**, 159 (1976).
- [13] P. Fayet, *Phys. Lett.* **B69**, 489 (1977).
- [14] G. R. Farrar and P. Fayet, *Phys. Lett.* **B76**, 575 (1978).
- [15] P. Fayet, *Phys. Lett.* **B84**, 416 (1979).
- [16] S. Dimopoulos and H. Georgi, *Nucl. Phys.* **B193**, 150 (1981).
- [17] Neutralinos ($\tilde{\chi}_j^0$, $j=1-4$ in the order of increasing mass) and charginos ($\tilde{\chi}_j^\pm$, $j=1,2$) are SUSY mass eigenstates formed from the mixing of the SUSY partners of the charged and neutral Higgs and electroweak gauge bosons.
- [18] ATLAS Collaboration, *Phys. Rev. Lett.* **109**, 211802 (2012), [arXiv:1208.1447 \[hep-ex\]](#).
- [19] ATLAS Collaboration, *Phys. Rev. Lett.* **109**, 211803 (2012), [arXiv:1208.2590 \[hep-ex\]](#).
- [20] ATLAS Collaboration, *JHEP* **1211**, 094 (2012), [arXiv:1209.4186 \[hep-ex\]](#).
- [21] CMS Collaboration, [arXiv:1405.3961 \[hep-ex\]](#).
- [22] ATLAS Collaboration, *JHEP* **1406**, 124 (2014), [arXiv:1403.4853 \[hep-ex\]](#).
- [23] ATLAS Collaboration, *JHEP* **1310**, 189 (2013), [arXiv:1308.2631 \[hep-ex\]](#).
- [24] CMS Collaboration, *Eur. Phys. J.* **C73**, 2677 (2013), [arXiv:1308.1586 \[hep-ex\]](#).
- [25] ATLAS Collaboration, [arXiv:1406.1122 \[hep-ex\]](#).
- [26] ALEPH, DELPHI, L3 and OPAL and the LEP SUSY Working Group, Notes LEPSUSYWG/01-03.1 and 04-01.1, <http://lepsusy.web.cern.ch/lepsusy/Welcome.html>.
- [27] T. Aaltonen *et al.* (CDF Collaboration), *JHEP* **1210**, 158 (2012), [arXiv:1203.4171 \[hep-ex\]](#).
- [28] V. Abazov *et al.* (D0 Collaboration), *Phys. Lett.* **B665**, 1 (2008), [arXiv:0803.2263 \[hep-ex\]](#).
- [29] T. Aaltonen *et al.* (CDF Collaboration), *Phys. Rev. Lett.* **105**, 081802 (2010), [arXiv:1005.3600 \[hep-ex\]](#).
- [30] V. M. Abazov *et al.* (D0 Collaboration), *Phys. Lett.* **B693**, 95 (2010), [arXiv:1005.2222 \[hep-ex\]](#).
- [31] ATLAS Collaboration, *Phys. Rev. Lett.* **108**, 181802 (2012), [arXiv:1112.3832 \[hep-ex\]](#).
- [32] ATLAS Collaboration, *JINST* **3**, S08003 (2008).
- [33] ATLAS uses a right-handed coordinate system with its origin at the nominal interaction point (IP) in the center of the detector and the z -axis along the beam pipe. The x -axis points from the IP to the center of the LHC ring, and the y -axis points upward. The azimuthal angle ϕ is measured around the beam axis, and the polar angle θ is measured with respect to the z -axis. We define transverse energy $E_T = E \sin\theta$, transverse momentum $p_T = p \sin\theta$, and pseudorapidity $\eta = -\ln(\tan(\theta/2))$.
- [34] T. Gleisberg *et al.*, *JHEP* **02**, 007 (2009), [arXiv:0811.4622 \[hep-ph\]](#).
- [35] H.-L. Lai *et al.*, *Phys. Rev.* **D82**, 074024 (2010), [arXiv:1007.2241 \[hep-ph\]](#).
- [36] M. L. Mangano, M. Moretti, F. Piccinini, R. Pittau, and A. Polosa, *JHEP* **07**, 001 (2003), [arXiv:hep-ph/0206293](#).
- [37] S. Catani and M. Grazzini, *Phys. Rev. Lett.* **98**, 222002 (2007).
- [38] S. Catani *et al.*, *Phys. Rev. Lett.* **103**, 082001 (2009).
- [39] A. Martin *et al.*, *Eur. Phys. J. C* **63**, 189 (2009), [arXiv:hep-ph/0901.0002](#).
- [40] S. Frixione, P. Nason, and G. Ridolfi, *JHEP* **0709**, 126 (2007), [arXiv:hep-ph/0707.3088](#).
- [41] S. Frixione and B. R. Webber, *JHEP* **0206**, 029 (2002), [arXiv:hep-ph/0204244 \[hep-ph\]](#).
- [42] B. P. Kersevan and E. Richter-Was, *Comput.Phys.Commun.* **149**, 142 (2003), [arXiv:hep-ph/0201302 \[hep-ph\]](#).
- [43] J. Alwall *et al.*, *JHEP* **09**, 028 (2007), [arXiv:0706.2334 \[hep-ph\]](#).
- [44] T. Sjostrand, S. Mrenna, and P. Z. Skands, *JHEP* **0605**, 026 (2006), [arXiv:hep-ph/0603175 \[hep-ph\]](#).
- [45] G. Corcella *et al.*, *JHEP* **01**, 010 (2001), [arXiv:hep-ph/0011363](#).
- [46] J. Butterworth, J. R. Forshaw, and M. Seymour, *Z.Phys.* **C72**, 637 (1996), [arXiv:hep-ph/9601371 \[hep-ph\]](#).
- [47] P. Z. Skands, *Phys. Rev.* **D82**, 074018 (2010), [arXiv:1005.3457 \[hep-ph\]](#).
- [48] ATLAS Collaboration, ATLAS-PHYS-PUB-2011-009, (2011). <http://cds.cern.ch/record/1363300>.
- [49] M. Czakon and A. Mitov, [arXiv:1112.5675 \[hep-ph\]](#).
- [50] M. Czakon, P. Fiedler, and A. Mitov, *Phys. Rev. Lett.* **110**, 252004 (2013), [arXiv:1303.6254 \[hep-ph\]](#).
- [51] N. Kidonakis, *Phys. Rev.* **D82**, 054018 (2010), [arXiv:1005.4451 \[hep-ph\]](#).
- [52] J. M. Campbell, R. K. Ellis, and C. Williams, *JHEP* **1107**, 018 (2011), [arXiv:1105.0020 \[hep-ph\]](#).
- [53] T. Sjostrand, S. Mrenna, and P. Z. Skands, *Comput.Phys.Commun.* **178**, 852 (2008), [arXiv:0710.3820 \[hep-ph\]](#).
- [54] M. Johansen, J. Edsjo, S. Hellman, and D. Milstead, *JHEP* **1008**, 005 (2010), [arXiv:1003.4540 \[hep-ph\]](#).
- [55] W. Beenakker, M. Kramer, T. Plehn, M. Spira, and P. M. Zerwas, *Nucl. Phys.* **B515**, 3 (1998), [hep-ph/9710451](#).
- [56] W. Beenakker, S. Brensing, M. Kramer, A. Kulesza, E. Laenen, and I. Niessen, *JHEP* **1008**, 098 (2010), [arXiv:1006.4771 \[hep-ph\]](#).
- [57] W. Beenakker *et al.*, *Int.J.Mod.Phys.* **A26**, 2637 (2011), [arXiv:1105.1110 \[hep-ph\]](#).
- [58] M. Kramer *et al.*, (2012), [arXiv:1206.2892 \[hep-ph\]](#).
- [59] ATLAS Collaboration, *Eur. Phys. J.* **C70**, 823 (2010) [arXiv:1005.4568 \[hep-ex\]](#).
- [60] S. Agostinelli *et al.* (GEANT4), *Nucl. Instrum. Meth.* **A506**, 250 (2003).
- [61] ATLAS Collaboration, ATLAS-PHYS-PUB-2010-013, (2010). <http://cds.cern.ch/record/1300517>.
- [62] M. Cacciari, G. P. Salam, and G. Soyez, *JHEP* **04**, 063 (2008), [arXiv:0802.1189 \[hep-ph\]](#).
- [63] ATLAS Collaboration, *Eur. Phys. J.* **C73**, 2304 (2013), [arXiv:1112.6426 \[hep-ex\]](#).
- [64] ATLAS Collaboration, [arXiv:1404.4562 \[hep-ex\]](#).
- [65] ATLAS Collaboration, [arXiv:1404.2240 \[hep-ex\]](#).
- [66] ATLAS Collaboration, *Eur. Phys. J.* **C72**, 1844 (2012), [arXiv:1108.5602 \[hep-ex\]](#).
- [67] The jet flavor in the MC samples is determined by associating jets to partons in η - ϕ space.

- [68] ATLAS Collaboration, ATLAS-CONF-2012-039 (2012). <http://cds.cern.ch/record/1435193>.
- [69] Charge conjugate states are included.
- [70] ATLAS Collaboration, ATLAS-CONF-2012-043 (2012). <http://cds.cern.ch/record/1435197>.
- [71] ATLAS Collaboration, ATLAS-CONF-2012-097 (2012). <http://cds.cern.ch/record/1460443>.
- [72] ATLAS Collaboration, ATLAS-CONF-2012-040 (2012). <http://cds.cern.ch/record/1435194>.
- [73] ATLAS Collaboration, *Eur. Phys. J.* **C73**, 2518 (2013), [arXiv:1302.4393 \[hep-ex\]](https://arxiv.org/abs/1302.4393).
- [74] ATLAS Collaboration, *Eur. Phys. J.* **C72**, 1849 (2012), [arXiv:1110.1530 \[hep-ex\]](https://arxiv.org/abs/1110.1530).
- [75] The charged fraction is defined as $f_{\text{ch}} = \sum p_{\text{T}}^{\text{track,jet}} / p_{\text{T}}^{\text{jet}}$, where $\sum p_{\text{T}}^{\text{track,jet}}$ is the scalar sum of the transverse momenta of tracks associated with the primary vertex within a cone of radius $\Delta R = 0.4$ around the jet axis, and $p_{\text{T}}^{\text{jet}}$ is the jet transverse momentum as determined from calorimetric measurements.
- [76] ATLAS Collaboration, *JINST* **8**, P07004 (2013), [arXiv:1303.0223 \[hep-ex\]](https://arxiv.org/abs/1303.0223).
- [77] ATLAS Collaboration, ATLAS-CONF-2012-020 (2012). <http://cdsweb.cern.ch/record/1430034>.
- [78] ATLAS Collaboration, *Phys. Rev.* **D86**, 092002 (2012), [arXiv:1208.4688 \[hep-ex\]](https://arxiv.org/abs/1208.4688).
- [79] ATLAS Collaboration, *Eur. Phys. J.* **C73**, 2261 (2013), [arXiv:1207.5644 \[hep-ex\]](https://arxiv.org/abs/1207.5644).
- [80] The transverse mass m_{T} is defined by the lepton (ℓ) and neutrino (ν) p_{T} and direction as $m_{\text{T}} = \sqrt{2p_{\text{T}}^{\ell} p_{\text{T}}^{\nu} (1 - \cos(\phi^{\ell} - \phi^{\nu}))}$, where the (x, y) components of the neutrino momentum are taken to be the same as the corresponding $\mathbf{p}_{\text{T}}^{\text{miss}}$ components.
- [81] ATLAS Collaboration, *Phys. Rev.* **D87**, 012008 (2013), [arXiv:1208.0949 \[hep-ex\]](https://arxiv.org/abs/1208.0949).
- [82] G. Cowan, K. Cranmer, E. Gross, and O. Vitells, *Eur. Phys. J.* **C71**, 1554 (2011), [arXiv:1007.1727 \[physics.data-an\]](https://arxiv.org/abs/1007.1727).
- [83] J. M. Campbell and R. K. Ellis, *Phys. Rev.* **D65**, 113007 (2002), [arXiv:hep-ph/0202176 \[hep-ph\]](https://arxiv.org/abs/hep-ph/0202176).
- [84] A. Denner, S. Dittmaier, T. Kasprzik, and A. Mueck, *Eur. Phys. J.* **C73**, 2297 (2013), [arXiv:1211.5078 \[hep-ph\]](https://arxiv.org/abs/1211.5078).
- [85] A. Denner, S. Dittmaier, T. Kasprzik, and A. Mueck, *JHEP* **1106**, 069 (2011), [arXiv:1103.0914 \[hep-ph\]](https://arxiv.org/abs/1103.0914).
- [86] A. Denner, S. Dittmaier, T. Kasprzik, and A. Mueck, *JHEP* **0908**, 075 (2009), [arXiv:0906.1656 \[hep-ph\]](https://arxiv.org/abs/0906.1656).
- [87] A. L. Read, *J. Phys. G* **G28**, 2693 (2002).

The ATLAS Collaboration

G. Aad⁸⁴, B. Abbott¹¹², J. Abdallah¹⁵², S. Abdel Khalek¹¹⁶, O. Abidinov¹¹, R. Aben¹⁰⁶, B. Abi¹¹³, M. Abolins⁸⁹, O.S. AbouZeid¹⁵⁹, H. Abramowicz¹⁵⁴, H. Abreu¹⁵³, R. Abreu³⁰, Y. Abulaiti^{147a,147b}, B.S. Acharya^{165a,165b,a}, L. Adamczyk^{38a}, D.L. Adams²⁵, J. Adelman¹⁷⁷, S. Adomeit⁹⁹, T. Adye¹³⁰, T. Agatonovic-Jovin^{13a}, J.A. Aguilar-Saavedra^{125a,125f}, M. Agustoni¹⁷, S.P. Ahlen²², F. Ahmadov^{64,b}, G. Aielli^{134a,134b}, H. Akerstedt^{147a,147b}, T.P.A. Åkesson⁸⁰, G. Akimoto¹⁵⁶, A.V. Akimov⁹⁵, G.L. Alberghi^{20a,20b}, J. Albert¹⁷⁰, S. Albrand⁵⁵, M.J. Alconada Verzini⁷⁰, M. Aleksa³⁰, I.N. Aleksandrov⁶⁴, C. Alexa^{26a}, G. Alexander¹⁵⁴, G. Alexandre⁴⁹, T. Alexopoulos¹⁰, M. Alhroob^{165a,165c}, G. Alimonti^{90a}, L. Alio⁸⁴, J. Alison³¹, B.M.M. Allbrooke¹⁸, L.J. Allison⁷¹, P.P. Allport⁷³, J. Almond⁸³, A. Aloisio^{103a,103b}, A. Alonso³⁶, F. Alonso⁷⁰, C. Alpigiani⁷⁵, A. Altheimer³⁵, B. Alvarez Gonzalez⁸⁹, M.G. Alviggi^{103a,103b}, K. Amako⁶⁵, Y. Amaral Coutinho^{24a}, C. Amelung²³, D. Amidei⁸⁸, S.P. Amor Dos Santos^{125a,125c}, A. Amorim^{125a,125b}, S. Amoroso⁴⁸, N. Amram¹⁵⁴, G. Amundsen²³, C. Anastopoulos¹⁴⁰, L.S. Ancu⁴⁹, N. Andari³⁰, T. Andeen³⁵, C.F. Anders^{58b}, G. Anders³⁰, K.J. Anderson³¹, A. Andreazza^{90a,90b}, V. Andrei^{58a}, X.S. Anduaga⁷⁰, S. Angelidakis⁹, I. Angelozzi¹⁰⁶, P. Anger⁴⁴, A. Angerami³⁵, F. Anghinolfi³⁰, A.V. Anisenkov¹⁰⁸, N. Anjos^{125a}, A. Annovi⁴⁷, A. Antonaki⁹, M. Antonelli⁴⁷, A. Antonov⁹⁷, J. Antos^{145b}, F. Anulli^{133a}, M. Aoki⁶⁵, L. Aperio Bella¹⁸, R. Apolle^{119,c}, G. Arabidze⁸⁹, I. Aracena¹⁴⁴, Y. Arai⁶⁵, J.P. Araque^{125a}, A.T.H. Arce⁴⁵, J-F. Arguin⁹⁴, S. Argyropoulos⁴², M. Arik^{19a}, A.J. Armbruster³⁰, O. Arnaez³⁰, V. Arnal⁸¹, H. Arnold⁴⁸, M. Arratia²⁸, O. Arslan²¹, A. Artamonov⁹⁶, G. Artoni²³, S. Asai¹⁵⁶, N. Asbah⁴², A. Ashkenazi¹⁵⁴, B. Åsman^{147a,147b}, L. Asquith⁶, K. Assamagan²⁵, R. Astalos^{145a}, M. Atkinson¹⁶⁶, N.B. Atlay¹⁴², B. Auerbach⁶, K. Augsten¹²⁷, M. Auresseau^{146b}, G. Avolio³⁰, G. Azuelos^{94,d}, Y. Azuma¹⁵⁶, M.A. Baak³⁰, A. Baas^{58a}, C. Bacci^{135a,135b}, H. Bachacou¹³⁷, K. Bachas¹⁵⁵, M. Backes³⁰, M. Backhaus³⁰, J. Backus Mayes¹⁴⁴, E. Badescu^{26a}, P. Bagiacchi^{133a,133b}, P. Bagnaia^{133a,133b}, Y. Bai^{33a}, T. Bain³⁵, J.T. Baines¹³⁰, O.K. Baker¹⁷⁷, P. Balek¹²⁸, F. Balli¹³⁷, E. Banas³⁹, Sw. Banerjee¹⁷⁴, A.A.E. Bannoura¹⁷⁶, V. Bansal¹⁷⁰, H.S. Bansil¹⁸, L. Barak¹⁷³, S.P. Baranov⁹⁵, E.L. Barberio⁸⁷, D. Barberis^{50a,50b}, M. Barbero⁸⁴, T. Barillari¹⁰⁰, M. Barisonzi¹⁷⁶, T. Barklow¹⁴⁴, N. Barlow²⁸, B.M. Barnett¹³⁰, R.M. Barnett¹⁵, Z. Barnovska⁵, A. Baroncelli^{135a}, G. Barone⁴⁹, A.J. Barr¹¹⁹, F. Barreiro⁸¹, J. Barreiro Guimarães da Costa⁵⁷, R. Bartoldus¹⁴⁴, A.E. Barton⁷¹, P. Bartos^{145a}, V. Bartsch¹⁵⁰, A. Bassalat¹¹⁶, A. Basye¹⁶⁶, R.L. Bates⁵³, J.R. Batley²⁸, M. Battaglia¹³⁸, M. Battistin³⁰, F. Bauer¹³⁷, H.S. Bawa^{144,e}, M.D. Beattie⁷¹, T. Beau⁷⁹, P.H. Beauchemin¹⁶², R. Beccherle^{123a,123b}, P. Bechtel²¹, H.P. Beck¹⁷, K. Becker¹⁷⁶, S. Becker⁹⁹, M. Beckingham¹⁷¹, C. Becot¹¹⁶, A.J. Beddall^{19c}, A. Beddall^{19c}, S. Bedikian¹⁷⁷, V.A. Bednyakov⁶⁴, C.P. Bee¹⁴⁹, L.J. Beemster¹⁰⁶, T.A. Beermann¹⁷⁶, M. Begel²⁵, K. Behr¹¹⁹, C. Belanger-Champagne⁸⁶, P.J. Bell⁴⁹, W.H. Bell⁴⁹, G. Bella¹⁵⁴, L. Bellagamba^{20a}, A. Bellerive²⁹, M. Bellomo⁸⁵, K. Belotskiy⁹⁷, O. Beltramello³⁰, O. Benary¹⁵⁴, D. Benchechroun^{136a}, K. Bendtz^{147a,147b}, N. Benekos¹⁶⁶, Y. Benhammou¹⁵⁴, E. Benhar Nocchioli⁴⁹, J.A. Benitez Garcia^{160b}, D.P. Benjamin⁴⁵, J.R. Bensinger²³, K. Benslama¹³¹, S. Bentvelsen¹⁰⁶, D. Berge¹⁰⁶, E. Bergeas Kuutmann¹⁶, N. Berger⁵, F. Berghaus¹⁷⁰, J. Beringer¹⁵, C. Bernard²², P. Bernat⁷⁷, C. Bernius⁷⁸, F.U. Bernlochner¹⁷⁰, T. Berry⁷⁶, P. Berta¹²⁸, C. Bertella⁸⁴, G. Bertoli^{147a,147b}, F. Bertolucci^{123a,123b}, C. Bertsche¹¹², D. Bertsche¹¹², M.I. Besana^{90a}, G.J. Besjes¹⁰⁵, O. Bessidskaia^{147a,147b}, M. Bessner⁴², N. Besson¹³⁷, C. Betancourt⁴⁸, S. Bethke¹⁰⁰, W. Bhimji⁴⁶, R.M. Bianchi¹²⁴, L. Bianchini²³, M. Bianco³⁰, O. Biebel⁹⁹, S.P. Bieniek⁷⁷, K. Bierwagen⁵⁴, J. Biesiada¹⁵, M. Biglietti^{135a}, J. Bilbao De Mendizabal⁴⁹, H. Bilokon⁴⁷, M. Bindi⁵⁴, S. Binet¹¹⁶, A. Bingul^{19c}, C. Bini^{133a,133b}, C.W. Black¹⁵¹, J.E. Black¹⁴⁴, K.M. Black²², D. Blackburn¹³⁹, R.E. Blair⁶, J.-B. Blanchard¹³⁷, T. Blazek^{145a}, I. Bloch⁴², C. Blocker²³, W. Blum^{82,*}, U. Blumenschein⁵⁴, G.J. Bobbink¹⁰⁶, V.S. Bobrovnikov¹⁰⁸, S.S. Bocchetta⁸⁰, A. Bocci⁴⁵, C. Bock⁹⁹, C.R. Boddy¹¹⁹, M. Boehler⁴⁸, T.T. Boek¹⁷⁶, J.A. Bogaerts³⁰, A.G. Bogdanov¹⁰⁸, A. Bogouch^{91,*}, C. Bohm^{147a}, J. Bohm¹²⁶, V. Boisvert⁷⁶, T. Bold^{38a}, V. Boldea^{26a}, A.S. Boldyrev⁹⁸, M. Bomben⁷⁹, M. Bona⁷⁵, M. Boonekamp¹³⁷, A. Borisov¹²⁹, G. Borisso⁷¹, M. Borri⁸³, S. Borroni⁴², J. Bortfeldt⁹⁹, V. Bortolotto^{135a,135b}, K. Bos¹⁰⁶, D. Boscherini^{20a}, M. Bosman¹², H. Boterenbrood¹⁰⁶, J. Boudreau¹²⁴, J. Bouffard², E.V. Bouhova-Thacker⁷¹, D. Boumediene³⁴, C. Bourdarios¹¹⁶, N. Bousson¹¹³, S. Boutouil^{136d}, A. Boveia³¹, J. Boyd³⁰, I.R. Boyko⁶⁴, J. Bracinik¹⁸, A. Brandt⁸, G. Brandt¹⁵, O. Brandt^{58a}, U. Bratzler¹⁵⁷, B. Brau⁸⁵, J.E. Brau¹¹⁵, H.M. Braun^{176,*}, S.F. Brazzale^{165a,165c}, B. Brelier¹⁵⁹, K. Brendlinger¹²¹, A.J. Brennan⁸⁷, R. Brenner¹⁶⁷, S. Bressler¹⁷³, K. Bristow^{146c}, T.M. Bristow⁴⁶, D. Britton⁵³, F.M. Brochu²⁸, I. Brock²¹, R. Brock⁸⁹, C. Bromberg⁸⁹, J. Bronner¹⁰⁰, G. Brooijmans³⁵, T. Brooks⁷⁶, W.K. Brooks^{32b}, J. Brosamer¹⁵, E. Brost¹¹⁵, J. Brown⁵⁵, P.A. Bruckman de Renstrom³⁹, D. Bruncko^{145b}, R. Bruneliere⁴⁸, S. Brunet⁶⁰, A. Bruni^{20a}, G. Bruni^{20a}, M. Bruschi^{20a}, L. Bryngemark⁸⁰, T. Buanes¹⁴, Q. Buat¹⁴³, F. Bucci⁴⁹, P. Buchholz¹⁴², R.M. Buckingham¹¹⁹, A.G. Buckley⁵³, S.I. Buda^{26a}, I.A. Budagov⁶⁴, F. Buehrer⁴⁸, L. Bugge¹¹⁸, M.K. Bugge¹¹⁸, O. Bulekov⁹⁷, A.C. Bundock⁷³, H. Burckhart³⁰, S. Burdin⁷³, B. Burghgrave¹⁰⁷, S. Burke¹³⁰, I. Burmeister⁴³, E. Busato³⁴, D. Büscher⁴⁸, V. Büscher⁸², P. Bussey⁵³, C.P. Buszello¹⁶⁷, B. Butler⁵⁷, J.M. Butler²², A.I. Butt³, C.M. Buttar⁵³, J.M. Butterworth⁷⁷, P. Butti¹⁰⁶, W. Buttinger²⁸, A. Buzatu⁵³, M. Byszewski¹⁰, S. Cabrera Urbán¹⁶⁸, D. Caforio^{20a,20b}, O. Cakir^{4a}, P. Calafiura¹⁵, A. Calandri¹³⁷, G. Calderini⁷⁹, P. Calfayan⁹⁹, R. Calkins¹⁰⁷, L.P. Caloba^{24a}, D. Calvet³⁴, S. Calvet³⁴, R. Camacho Toro⁴⁹, S. Camarda⁴², D. Cameron¹¹⁸, L.M. Caminada¹⁵, R. Caminal Armadans¹², S. Campana³⁰, M. Campanelli⁷⁷, A. Campoverde¹⁴⁹, V. Canale^{103a,103b}, A. Canepa^{160a}, M. Cano Bret⁷⁵, J. Cantero⁸¹, R. Cantrill^{125a}, T. Cao⁴⁰, M.D.M. Capeans Garrido³⁰, I. Caprini^{26a}, M. Caprini^{26a}, M. Capua^{37a,37b}, R. Caputo⁸², R. Cardarelli^{134a}, T. Carli³⁰, G. Carlino^{103a}, L. Carminati^{90a,90b}, S. Caron¹⁰⁵, E. Carquin^{32a}, G.D. Carrillo-Montoya^{146c}, J.R. Carter²⁸, J. Carvalho^{125a,125c}, D. Casadei⁷⁷, M.P. Casado¹², M. Casolino¹², E. Castaneda-Miranda^{146b}, A. Castelli¹⁰⁶, V. Castillo Gimenez¹⁶⁸, N.F. Castro^{125a}, P. Catastini⁵⁷, A. Catinaccio³⁰, J.R. Catmore¹¹⁸, A. Cattai³⁰, G. Cattani^{134a,134b}, S. Caughron⁸⁹, V. Cavaliere¹⁶⁶, D. Cavalli^{90a},

M. Cavalli-Sforza¹², V. Cavasinni^{123a,123b}, F. Ceradini^{135a,135b}, B. Cerio⁴⁵, K. Cerny¹²⁸, A.S. Cerqueira^{24b}, A. Cerri¹⁵⁰, L. Cerrito⁷⁵, F. Cerutti¹⁵, M. Cerv³⁰, A. Cervelli¹⁷, S.A. Cetin^{19b}, A. Chafaq^{136a}, D. Chakraborty¹⁰⁷, I. Chalupkova¹²⁸, P. Chang¹⁶⁶, B. Chapleau⁸⁶, J.D. Chapman²⁸, D. Charfeddine¹¹⁶, D.G. Charlton¹⁸, C.C. Chau¹⁵⁹, C.A. Chavez Barajas¹⁵⁰, S. Cheatham⁸⁶, A. Chegwidan⁸⁹, S. Chekanov⁶, S.V. Chekulaev^{160a}, G.A. Chelkov^{64,f}, M.A. Chelstowska⁸⁸, C. Chen⁶³, H. Chen²⁵, K. Chen¹⁴⁹, L. Chen^{33d,g}, S. Chen^{33c}, X. Chen^{146c}, Y. Chen⁶⁶, Y. Chen³⁵, H.C. Cheng⁸⁸, Y. Cheng³¹, A. Cheplakov⁶⁴, R. Cherkaoui El Moursli^{136e}, V. Chernyatin^{25,*}, E. Cheu⁷, L. Chevalier¹³⁷, V. Chiarella⁴⁷, G. Chieffari^{103a,103b}, J.T. Childers⁶, A. Chilingarov⁷¹, G. Chiodini^{72a}, A.S. Chisholm¹⁸, R.T. Chislett⁷⁷, A. Chitan^{26a}, M.V. Chizhov⁶⁴, S. Chouridou⁹, B.K.B. Chow⁹⁹, D. Chromek-Burckhart³⁰, M.L. Chu¹⁵², J. Chudoba¹²⁶, J.J. Chwastowski³⁹, L. Chytka¹¹⁴, G. Ciapetti^{133a,133b}, A.K. Ciftci^{4a}, R. Ciftci^{4a}, D. Cinca⁵³, V. Cindro⁷⁴, A. Ciocio¹⁵, P. Cirkovic^{13b}, Z.H. Citron¹⁷³, M. Citterio^{90a}, M. Ciubancan^{26a}, A. Clark⁴⁹, P.J. Clark⁴⁶, R.N. Clarke¹⁵, W. Cleland¹²⁴, J.C. Clemens⁸⁴, C. Clement^{147a,147b}, Y. Coadou⁸⁴, M. Cobal^{165a,165c}, A. Coccaro¹³⁹, J. Cochran⁶³, L. Coffey²³, J.G. Cogan¹⁴⁴, J. Coggeshall¹⁶⁶, B. Cole³⁵, S. Cole¹⁰⁷, A.P. Colijn¹⁰⁶, J. Collot⁵⁵, T. Colombo^{58c}, G. Colon⁸⁵, G. Compostella¹⁰⁰, P. Conde Muiño^{125a,125b}, E. Coniavitis⁴⁸, M.C. Conidi¹², S.H. Connell^{146b}, I.A. Connelly⁷⁶, S.M. Consonni^{90a,90b}, V. Consorti⁴⁸, S. Constantinescu^{26a}, C. Conta^{120a,120b}, G. Conti⁵⁷, F. Conventi^{103a,h}, M. Cooke¹⁵, B.D. Cooper⁷⁷, A.M. Cooper-Sarkar¹¹⁹, N.J. Cooper-Smith⁷⁶, K. Copic¹⁵, T. Cornelissen¹⁷⁶, M. Corradi^{20a}, F. Corriveau^{86,i}, A. Corso-Radu¹⁶⁴, A. Cortes-Gonzalez¹², G. Cortiana¹⁰⁰, G. Costa^{90a}, M.J. Costa¹⁶⁸, D. Costanzo¹⁴⁰, D. Côté⁸, G. Cottin²⁸, G. Cowan⁷⁶, B.E. Cox⁸³, K. Cranmer¹⁰⁹, G. Cree²⁹, S. Crépe-Renaudin⁵⁵, F. Crescioli⁷⁹, W.A. Cribbs^{147a,147b}, M. Crispin Ortuzar¹¹⁹, M. Cristinziani²¹, V. Croft¹⁰⁵, G. Crosetti^{37a,37b}, C.-M. Cuciuc^{26a}, T. Cuhadar Donszelmann¹⁴⁰, J. Cummings¹⁷⁷, M. Curatolo⁴⁷, C. Cuthbert¹⁵¹, H. Czirr¹⁴², P. Czodrowski³, Z. Czyczula¹⁷⁷, S. D'Auria⁵³, M. D'Onofrio⁷³, M.J. Da Cunha Sargedas De Sousa^{125a,125b}, C. Da Via⁸³, W. Dabrowski^{38a}, A. Dafinca¹¹⁹, T. Dai⁸⁸, O. Dale¹⁴, F. Dallaire⁹⁴, C. Dallapiccola⁸⁵, M. Dam³⁶, A.C. Daniels¹⁸, M. Dano Hoffmann¹³⁷, V. Dao⁴⁸, G. Darbo^{50a}, S. Darmora⁸, J.A. Dassoulas⁴², A. Dattagupta⁶⁰, W. Davey²¹, C. David¹⁷⁰, T. Davidek¹²⁸, E. Davies^{119,c}, M. Davies¹⁵⁴, O. Davignon⁷⁹, A.R. Davison⁷⁷, P. Davison⁷⁷, Y. Davygora^{58a}, E. Dawe¹⁴³, I. Dawson¹⁴⁰, R.K. Daya-Ishmukhametova⁸⁵, K. De⁸, R. de Asmundis^{103a}, S. De Castro^{20a,20b}, S. De Cecco⁷⁹, N. De Groot¹⁰⁵, P. de Jong¹⁰⁶, H. De la Torre⁸¹, F. De Lorenzi⁶³, L. De Nooij¹⁰⁶, D. De Pedis^{133a}, A. De Salvo^{133a}, U. De Sanctis^{165a,165b}, A. De Santo¹⁵⁰, J.B. De Vivie De Regie¹¹⁶, W.J. Dearnaley⁷¹, R. Debbes²⁵, C. Debenedetti¹³⁸, B. Dechenaux⁵⁵, D.V. Dedovich⁶⁴, I. Deigaard¹⁰⁶, J. Del Peso⁸¹, T. Del Prete^{123a,123b}, F. Deliot¹³⁷, C.M. Delitzsch⁴⁹, M. Deliyergiyev⁷⁴, A. Dell'Acqua³⁰, L. Dell'Asta²², M. Dell'Orso^{123a,123b}, M. Della Pietra^{103a,h}, D. della Volpe⁴⁹, M. Delmastro⁵, P.A. Delsart⁵⁵, C. Deluca¹⁰⁶, S. Demers¹⁷⁷, M. Demichev⁶⁴, A. Demilly⁷⁹, S.P. Denisov¹²⁹, D. Derendarz³⁹, J.E. Derkaoui^{136d}, F. Derue⁷⁹, P. Dervan⁷³, K. Desch²¹, C. Deterre⁴², P.O. Deviveiros¹⁰⁶, A. Dewhurst¹³⁰, S. Dhaliwal¹⁰⁶, A. Di Ciaccio^{134a,134b}, L. Di Ciaccio⁵, A. Di Domenico^{133a,133b}, C. Di Donato^{103a,103b}, A. Di Girolamo³⁰, B. Di Girolamo³⁰, A. Di Mattia¹⁵³, B. Di Micco^{135a,135b}, R. Di Nardo⁴⁷, A. Di Simone⁴⁸, R. Di Sipio^{20a,20b}, D. Di Valentino²⁹, F.A. Dias⁴⁶, M.A. Diaz^{32a}, E.B. Diehl⁸⁸, J. Dietrich⁴², T.A. Dietzsch^{58a}, S. Diglio⁸⁴, A. Dimitrievska^{13a}, J. Dingfelder²¹, C. Dionisi^{133a,133b}, P. Dita^{26a}, S. Dita^{26a}, F. Dittus³⁰, F. Djama⁸⁴, T. Djobava^{51b}, M.A.B. do Vale^{24c}, A. Do Valle Wemans^{125a,125g}, T.K.O. Doan⁵, D. Dobos³⁰, C. Doglioni⁴⁹, T. Doherty⁵³, T. Dohmae¹⁵⁶, J. Dolejsi¹²⁸, Z. Dolezal¹²⁸, B.A. Dolgoshein^{97,*}, M. Donadelli^{24d}, S. Donati^{123a,123b}, P. Dondero^{120a,120b}, J. Donini³⁴, J. Dopke¹³⁰, A. Doria^{103a}, M.T. Dova⁷⁰, A.T. Doyle⁵³, M. Dris¹⁰, J. Dubbert⁸⁸, S. Dube¹⁵, E. Dubreuil³⁴, E. Duchovni¹⁷³, G. Duckeck⁹⁹, O.A. Ducu^{26a}, D. Duda¹⁷⁶, A. Dudarev³⁰, F. Dudziak⁶³, L. Duflo¹¹⁶, L. Duguid⁷⁶, M. Dührssen³⁰, M. Dunford^{58a}, H. Duran Yildiz^{4a}, M. Düren⁵², A. Durglishvili^{51b}, M. Dwuznik^{38a}, M. Dyndal^{38a}, J. Ebke⁹⁹, W. Edson², N.C. Edwards⁴⁶, W. Ehrenfeld²¹, T. Eifert¹⁴⁴, G. Eigen¹⁴, K. Einsweiler¹⁵, T. Ekelof¹⁶⁷, M. El Kacimi^{136c}, M. Ellert¹⁶⁷, S. Elles⁵, F. Ellinghaus⁸², N. Ellis³⁰, J. Elmsheuser⁹⁹, M. Elsing³⁰, D. Emelianov¹³⁰, Y. Enari¹⁵⁶, O.C. Ender⁸², M. Endo¹¹⁷, R. Engelmann¹⁴⁹, J. Erdmann¹⁷⁷, A. Ereditato¹⁷, D. Eriksson^{147a}, G. Ernis¹⁷⁶, J. Ernst², M. Ernst²⁵, J. Ernwein¹³⁷, D. Errede¹⁶⁶, S. Errede¹⁶⁶, E. Ertel⁸², M. Escalier¹¹⁶, H. Esch⁴³, C. Escobar¹²⁴, B. Esposito⁴⁷, A.I. Etienne¹³⁷, E. Etzion¹⁵⁴, H. Evans⁶⁰, A. Ezhilov¹²², L. Fabbri^{20a,20b}, G. Facini³¹, R.M. Fakhruddinov¹²⁹, S. Falciano^{133a}, R.J. Falla⁷⁷, J. Faltova¹²⁸, Y. Fang^{33a}, M. Fanti^{90a,90b}, A. Farbin⁸, A. Farilla^{135a}, T. Farooque¹², S. Farrell¹⁵, S.M. Farrington¹⁷¹, P. Farthouat³⁰, F. Fassi^{136e}, P. Fassnacht³⁰, D. Fassouliotis⁹, A. Favareto^{50a,50b}, L. Fayard¹¹⁶, P. Federic^{145a}, O.L. Fedin^{122,j}, W. Fedorko¹⁶⁹, M. Fehling-Kaschek⁴⁸, S. Feigl³⁰, L. Felgioni⁸⁴, C. Feng^{33d}, E.J. Feng⁶, H. Feng⁸⁸, A.B. Fenyuk¹²⁹, S. Fernandez Perez³⁰, S. Ferrag⁵³, J. Ferrando⁵³, A. Ferrari¹⁶⁷, P. Ferrari¹⁰⁶, R. Ferrari^{120a}, D.E. Ferreira de Lima⁵³, A. Ferrer¹⁶⁸, D. Ferrere⁴⁹, C. Ferretti⁸⁸, A. Ferretto Parodi^{50a,50b}, M. Fiascaris³¹, F. Fiedler⁸², A. Filipčič⁷⁴, M. Filipuzzi⁴², F. Filthaut¹⁰⁵, M. Fincke-Keeler¹⁷⁰, K.D. Finelli¹⁵¹, M.C.N. Fiolhais^{125a,125c}, L. Fiorini¹⁶⁸, A. Firan⁴⁰, A. Fischer², J. Fischer¹⁷⁶, W.C. Fisher⁸⁹, E.A. Fitzgerald²³, M. Flechl⁴⁸, I. Fleck¹⁴², P. Fleischmann⁸⁸, S. Fleischmann¹⁷⁶, G.T. Fletcher¹⁴⁰, G. Fletcher⁷⁵, T. Flick¹⁷⁶, A. Floderus⁸⁰, L.R. Flores Castillo^{174,k}, A.C. Florez Bustos^{160b}, M.J. Flowerdew¹⁰⁰, A. Formica¹³⁷, A. Forti⁸³, D. Fortin^{160a}, D. Fournier¹¹⁶, H. Fox⁷¹, S. Fracchia¹², P. Francavilla⁷⁹, M. Franchini^{20a,20b}, S. Franchino³⁰, D. Francis³⁰, L. Franconi¹¹⁸, M. Franklin⁵⁷, S. Franz⁶¹, M. Fraternali^{120a,120b}, S.T. French²⁸, C. Friedrich⁴², F. Friedrich⁴⁴, D. Froidevaux³⁰, J.A. Frost²⁸, C. Fukunaga¹⁵⁷, E. Fullana Torregrosa⁸², B.G. Fulsom¹⁴⁴, J. Fuster¹⁶⁸, C. Gabaldon⁵⁵, O. Gabizon¹⁷³, A. Gabrielli^{20a,20b}, A. Gabrielli^{133a,133b}, S. Gadatsch¹⁰⁶, S. Gadomski⁴⁹, G. Gagliardi^{50a,50b}, P. Gagnon⁶⁰, C. Galea¹⁰⁵, B. Galhardo^{125a,125c}, E.J. Gallas¹¹⁹, V. Gallo¹⁷, B.J. Gallop¹³⁰, P. Gallus¹²⁷, G. Galster³⁶, K.K. Gan¹¹⁰, J. Gao^{33b,g}, Y.S. Gao^{144,e}, F.M. Garay Walls⁴⁶, F. Garbersson¹⁷⁷, C. García¹⁶⁸, J.E. García Navarro¹⁶⁸, M. Garcia-Sciveres¹⁵, R.W. Gardner³¹, N. Garelli¹⁴⁴, V. Garonne³⁰, C. Gatti⁴⁷, G. Gaudio^{120a}, B. Gaur¹⁴², L. Gauthier⁹⁴, P. Gauzzi^{133a,133b}, I.L. Gavrilenko⁹⁵, C. Gay¹⁶⁹, G. Gaycken²¹, E.N. Gazis¹⁰, P. Ge^{33d}, Z. Gece¹⁶⁹,

C.N.P. Gee¹³⁰, D.A.A. Geerts¹⁰⁶, Ch. Geich-Gimbel²¹, K. Gellerstedt^{147a,147b}, C. Gemme^{50a}, A. Gemmell⁵³, M.H. Genest⁵⁵, S. Gentile^{133a,133b}, M. George⁵⁴, S. George⁷⁶, D. Gerbaudo¹⁶⁴, A. Gershon¹⁵⁴, H. Ghazlane^{136b}, N. Ghodbane³⁴, B. Giacobbe^{20a}, S. Giagu^{133a,133b}, V. Giangiobbe¹², P. Giannetti^{123a,123b}, F. Gianotti³⁰, B. Gibbard²⁵, S.M. Gibson⁷⁶, M. Gilchriese¹⁵, T.P.S. Gillam²⁸, D. Gillberg³⁰, G. Gilles³⁴, D.M. Gingrich^{3,d}, N. Giokaris⁹, M.P. Giordani^{165a,165c}, R. Giordano^{103a,103b}, F.M. Giorgi^{20a}, F.M. Giorgi¹⁶, P.F. Giraud¹³⁷, D. Giugni^{90a}, C. Giuliani⁴⁸, M. Giulini^{58b}, B.K. Gjelsten¹¹⁸, S. Gkaitatzis¹⁵⁵, I. Gkialas^{155,7}, L.K. Gladilin⁹⁸, C. Glasman⁸¹, J. Glatzer³⁰, P.C.F. Glaysheer⁴⁶, A. Glazov⁴², G.L. Glonti⁶⁴, M. Goblirsch-Kolb¹⁰⁰, J.R. Goddard⁷⁵, J. Godfrey¹⁴³, J. Godlewski³⁰, C. Goeringer⁸², S. Goldfarb⁸⁸, T. Golling¹⁷⁷, D. Golubkov¹²⁹, A. Gomes^{125a,125b,125d}, L.S. Gomez Fajardo⁴², R. Gonçalo^{125a}, J. Goncalves Pinto Firmino Da Costa¹³⁷, L. Gonella²¹, S. González de la Hoz¹⁶⁸, G. Gonzalez Parra¹², S. Gonzalez-Sevilla⁴⁹, L. Goossens³⁰, P.A. Gorbounov⁹⁶, H.A. Gordon²⁵, I. Gorelov¹⁰⁴, B. Gorini³⁰, E. Gorini^{72a,72b}, A. Gorišek⁷⁴, E. Gornicki³⁹, A.T. Goshaw⁶, C. Gössling⁴³, M.I. Gostkin⁶⁴, M. Gouighri^{136a}, D. Goujdami^{136c}, M.P. Goulette⁴⁹, A.G. Goussiou¹³⁹, C. Goy⁵, S. Gozpinar²³, H.M.X. Grabas¹³⁷, L. Graber⁵⁴, I. Grabowska-Bold^{38a}, P. Grafström^{20a,20b}, K.-J. Grahn⁴², J. Gramling⁴⁹, E. Gramstad¹¹⁸, S. Grancagnolo¹⁶, V. Grassi¹⁴⁹, V. Gratchev¹²², H.M. Gray³⁰, E. Graziani^{135a}, O.G. Grebenyuk¹²², Z.D. Greenwood^{78,m}, K. Gregersen⁷⁷, I.M. Gregor⁴², P. Grenier¹⁴⁴, J. Griffiths⁸, A.A. Grillo¹³⁸, K. Grimm⁷¹, S. Grinstein^{12,n}, Ph. Gris³⁴, Y.V. Grishkevich⁹⁸, J.-F. Grivaz¹¹⁶, J.P. Grohs⁴⁴, A. Grohsjean⁴², E. Gross¹⁷³, J. Grosse-Knetter⁵⁴, G.C. Grossi^{134a,134b}, J. Groth-Jensen¹⁷³, Z.J. Grout¹⁵⁰, L. Guan^{33b}, F. Guescini⁴⁹, D. Guest¹⁷⁷, O. Gueta¹⁵⁴, C. Guicheney³⁴, E. Guido^{50a,50b}, T. Guillemin¹¹⁶, S. Guindon², U. Gul⁵³, C. Gumpert⁴⁴, J. Gunther¹²⁷, J. Guo³⁵, S. Gupta¹¹⁹, P. Gutierrez¹¹², N.G. Gutierrez Ortiz⁵³, C. Gutsche⁷⁷, N. Guttman¹⁵⁴, C. Guyot¹³⁷, C. Gwenlan¹¹⁹, C.B. Gwilliam⁷³, A. Haas¹⁰⁹, C. Haber¹⁵, H.K. Hadavand⁸, N. Haddad^{136e}, P. Haefner²¹, S. Hageböck²¹, Z. Hajduk³⁹, H. Hakobyan¹⁷⁸, M. Haleem⁴², D. Hall¹¹⁹, G. Halladjian⁸⁹, K. Hamacher¹⁷⁶, P. Hamal¹¹⁴, K. Hamano¹⁷⁰, M. Hamer⁵⁴, A. Hamilton^{146a}, S. Hamilton¹⁶², G.N. Hamity^{146c}, P.G. Hamnett⁴², L. Han^{33b}, K. Hanagaki¹¹⁷, K. Hanawa¹⁵⁶, M. Hance¹⁵, P. Hanke^{58a}, R. Hanna¹³⁷, J.B. Hansen³⁶, J.D. Hansen³⁶, P.H. Hansen³⁶, K. Hara¹⁶¹, A.S. Hard¹⁷⁴, T. Harenberg¹⁷⁶, F. Hariri¹¹⁶, S. Harkusha⁹¹, D. Harper⁸⁸, R.D. Harrington⁴⁶, O.M. Harris¹³⁹, P.F. Harrison¹⁷¹, F. Hartjes¹⁰⁶, M. Hasegawa⁶⁶, S. Hasegawa¹⁰², Y. Hasegawa¹⁴¹, A. Hasib¹¹², S. Hassani¹³⁷, S. Haug¹⁷, M. Hauschild³⁰, R. Hauser⁸⁹, M. Havranek¹²⁶, C.M. Hawkes¹⁸, R.J. Hawkings³⁰, A.D. Hawkins⁸⁰, T. Hayashi¹⁶¹, D. Hayden⁸⁹, C.P. Hays¹¹⁹, H.S. Hayward⁷³, S.J. Haywood¹³⁰, S.J. Head¹⁸, T. Heck⁸², V. Hedberg⁸⁰, L. Heelan⁸, S. Heim¹²¹, T. Heim¹⁷⁶, B. Heinemann¹⁵, L. Heinrich¹⁰⁹, J. Hejbal¹²⁶, L. Helary²², C. Heller⁹⁹, M. Heller³⁰, S. Hellman^{147a,147b}, D. Hellmich²¹, C. Helsen³⁰, J. Henderson¹¹⁹, R.C.W. Henderson⁷¹, Y. Heng¹⁷⁴, C. Hengler⁴², A. Henrichs¹⁷⁷, A.M. Henriques Correia³⁰, S. Henrot-Versille¹¹⁶, C. Hensel⁵⁴, G.H. Herbert¹⁶, Y. Hernández Jiménez¹⁶⁸, R. Herrberg-Schubert¹⁶, G. Herten⁴⁸, R. Hertenberger⁹⁹, L. Hervas³⁰, G.G. Hesketh⁷⁷, N.P. Hessey¹⁰⁶, R. Hickling⁷⁵, E. Higón-Rodríguez¹⁶⁸, E. Hill¹⁷⁰, J.C. Hill²⁸, K.H. Hiller⁴², S. Hillert²¹, S.J. Hillier¹⁸, I. Hinchliffe¹⁵, E. Hines¹²¹, M. Hirose¹⁵⁸, D. Hirschbuehl¹⁷⁶, J. Hobbs¹⁴⁹, N. Hod¹⁰⁶, M.C. Hodgkinson¹⁴⁰, P. Hodgson¹⁴⁰, A. Hoecker³⁰, M.R. Hoferkamp¹⁰⁴, F. Hoening⁹⁹, J. Hoffman⁴⁰, D. Hoffmann⁸⁴, J.I. Hofmann^{58a}, M. Hohlfield⁸², T.R. Holmes¹⁵, T.M. Hong¹²¹, L. Hooft van Huysduynen¹⁰⁹, Y. Horii¹⁰², J.-Y. Hostachy⁵⁵, S. Hou¹⁵², A. Hoummada^{136a}, J. Howard¹¹⁹, J. Howarth⁴², M. Hrabovsky¹¹⁴, I. Hristova¹⁶, J. Hrivnac¹¹⁶, T. Hryn'ova⁵, C. Hsu^{146c}, P.J. Hsu⁸², S.-C. Hsu¹³⁹, D. Hu³⁵, X. Hu²⁵, Y. Huang⁴², Z. Hubacek³⁰, F. Hubaut⁸⁴, F. Huegging²¹, T.B. Huffman¹¹⁹, E.W. Hughes³⁵, G. Hughes⁷¹, M. Huhtinen³⁰, T.A. Hülsing⁸², M. Hurwitz¹⁵, N. Huseynov^{64,b}, J. Huston⁸⁹, J. Huth⁵⁷, G. Iacobucci⁴⁹, G. Iakovidis¹⁰, I. Ibragimov¹⁴², L. Iconomidou-Fayard¹¹⁶, E. Ideal¹⁷⁷, P. Iengo^{103a}, O. Igonkina¹⁰⁶, T. Iizawa¹⁷², Y. Ikegami⁶⁵, K. Ikematsu¹⁴², M. Ikeno⁶⁵, Y. Ilchenko^{31,o}, D. Iliadis¹⁵⁵, N. Ilic¹⁵⁹, Y. Inamaru⁶⁶, T. Ince¹⁰⁰, P. Ioannou⁹, M. Iodice^{135a}, K. Iordanidou⁹, V. Ippolito⁵⁷, A. Irls Quiles¹⁶⁸, C. Isaksson¹⁶⁷, M. Ishino⁶⁷, M. Ishitsuka¹⁵⁸, R. Ishmukhametov¹¹⁰, C. Issever¹¹⁹, S. Istin^{19a}, J.M. Iturbe Ponce⁸³, R. Iuppa^{134a,134b}, J. Ivarsson⁸⁰, W. Iwanski³⁹, H. Iwasaki⁶⁵, J.M. Izen⁴¹, V. Izzo^{103a}, B. Jackson¹²¹, M. Jackson⁷³, P. Jackson¹, M.R. Jaekel³⁰, V. Jain², K. Jakobs⁴⁸, S. Jakobsen³⁰, T. Jakoubek¹²⁶, J. Jakubek¹²⁷, D.O. Jamin¹⁵², D.K. Jana⁷⁸, E. Jansen⁷⁷, H. Jansen³⁰, J. Janssen²¹, M. Janus¹⁷¹, G. Jarlskog⁸⁰, N. Javadov^{64,b}, T. Javůrek⁴⁸, L. Jeanty¹⁵, J. Jejelava^{51a,p}, G.-Y. Jeng¹⁵¹, D. Jennens⁸⁷, P. Jenni^{48,q}, J. Jentzsch⁴³, C. Jeske¹⁷¹, S. Jézéquel⁵, H. Ji¹⁷⁴, J. Jia¹⁴⁹, Y. Jiang^{33b}, M. Jimenez Belenguer⁴², S. Jin^{33a}, A. Jinaru^{26a}, O. Jinnouchi¹⁵⁸, M.D. Joergensen³⁶, K.E. Johansson^{147a,147b}, P. Johansson¹⁴⁰, K.A. Johns⁷, K. Jon-And^{147a,147b}, G. Jones¹⁷¹, R.W.L. Jones⁷¹, T.J. Jones⁷³, J. Jongmanns^{58a}, P.M. Jorge^{125a,125b}, K.D. Joshi⁸³, J. Jovicevic¹⁴⁸, X. Ju¹⁷⁴, C.A. Jung⁴³, R.M. Jungst³⁰, P. Jussel⁶¹, A. Juste Rozas^{12,n}, M. Kaci¹⁶⁸, A. Kaczmarek³⁹, M. Kado¹¹⁶, H. Kagan¹¹⁰, M. Kagan¹⁴⁴, E. Kajomovitz⁴⁵, C.W. Kalderon¹¹⁹, S. Kama⁴⁰, A. Kamenshchikov¹²⁹, N. Kanaya¹⁵⁶, M. Kaneda³⁰, S. Kaneti²⁸, V.A. Kantserov⁹⁷, J. Kanzaki⁶⁵, B. Kaplan¹⁰⁹, A. Kapliy³¹, D. Kar⁵³, K. Karakostas¹⁰, N. Karastathis¹⁰, M. Karnevskiy⁸², S.N. Karpov⁶⁴, Z.M. Karpova⁶⁴, K. Karthik¹⁰⁹, V. Kartvelishvili⁷¹, A.N. Karyukhin¹²⁹, L. Kashif¹⁷⁴, G. Kasieczka^{58b}, R.D. Kass¹¹⁰, A. Kastanas¹⁴, Y. Kataoka¹⁵⁶, A. Katre⁴⁹, J. Katzy⁴², V. Kaushik⁷, K. Kawagoe⁶⁹, T. Kawamoto¹⁵⁶, G. Kawamura⁵⁴, S. Kazama¹⁵⁶, V.F. Kazanin¹⁰⁸, M.Y. Kazarinov⁶⁴, R. Keeler¹⁷⁰, R. Kehoe⁴⁰, M. Keil⁵⁴, J.S. Keller⁴², J.J. Kempster⁷⁶, H. Keoshkerian⁵, O. Kepka¹²⁶, B.P. Kerševan⁷⁴, S. Kersten¹⁷⁶, K. Kessoku¹⁵⁶, J. Keung¹⁵⁹, F. Khalil-zada¹¹, H. Khandanyan^{147a,147b}, A. Khanov¹¹³, A. Khodinov⁹⁷, A. Khomich^{58a}, T.J. Khoo²⁸, G. Khorauli²¹, A. Khoroshilov¹⁷⁶, V. Khovanskij⁹⁶, E. Khramov⁶⁴, J. Khubua^{51b}, H.Y. Kim⁸, H. Kim^{147a,147b}, S.H. Kim¹⁶¹, N. Kimura¹⁷², O. Kind¹⁶, B.T. King⁷³, M. King¹⁶⁸, R.S.B. King¹¹⁹, S.B. King¹⁶⁹, J. Kirk¹³⁰, A.E. Kiryunin¹⁰⁰, T. Kishimoto⁶⁶, D. Kisielewska^{38a}, F. Kiss⁴⁸, T. Kittelmann¹²⁴, K. Kiuchi¹⁶¹, E. Kladiva^{145b}, M. Klein⁷³, U. Klein⁷³, K. Kleinknecht⁸², P. Klimek^{147a,147b}, A. Klimentov²⁵, R. Klingenberg⁴³, J.A. Klinger⁸³, T. Klioutchnikova³⁰, P.F. Klok¹⁰⁵, E.-E. Kluge^{58a}, P. Kluit¹⁰⁶, S. Kluth¹⁰⁰, E. Kneringer⁶¹, E.B.F.G. Knoop⁸⁴, A. Knue⁵³, D. Kobayashi¹⁵⁸, T. Kobayashi¹⁵⁶, M. Kobel⁴⁴,

M. Kocian¹⁴⁴, P. Kodys¹²⁸, P. Koevesarki²¹, T. Koffas²⁹, E. Koffeman¹⁰⁶, L.A. Kogan¹¹⁹, S. Kohlmann¹⁷⁶, Z. Kohout¹²⁷, T. Kohriki⁶⁵, T. Koi¹⁴⁴, H. Kolanoski¹⁶, I. Koletsou⁵, J. Koll⁸⁹, A.A. Komar^{95,*}, Y. Komori¹⁵⁶, T. Kondo⁶⁵, N. Kondrashova⁴², K. Köneke⁴⁸, A.C. König¹⁰⁵, S. König⁸², T. Kono^{65,r}, R. Konoplich^{109,s}, N. Konstantinidis⁷⁷, R. Kopeliansky¹⁵³, S. Koperny^{38a}, L. Köpke⁸², A.K. Kopp⁴⁸, K. Korcyl³⁹, K. Kordas¹⁵⁵, A. Korn⁷⁷, A.A. Korol^{108,t}, I. Korolkov¹², E.V. Korolkova¹⁴⁰, V.A. Korotkov¹²⁹, O. Kortner¹⁰⁰, S. Kortner¹⁰⁰, V.V. Kostyukhin²¹, V.M. Kotov⁶⁴, A. Kotwal⁴⁵, C. Kourkoumelis⁹, V. Kouskoura¹⁵⁵, A. Koutsman^{160a}, R. Kowalewski¹⁷⁰, T.Z. Kowalski^{38a}, W. Kozanecki¹³⁷, A.S. Kozhin¹²⁹, V. Kral¹²⁷, V.A. Kramarenko⁹⁸, G. Kramerberger⁷⁴, D. Krasnopevtsev⁹⁷, M.W. Krasny⁷⁹, A. Krasznahorkay³⁰, J.K. Kraus²¹, A. Kravchenko²⁵, S. Kreiss¹⁰⁹, M. Kretz^{58c}, J. Kretzschmar⁷³, K. Kreutzfeldt⁵², P. Krieger¹⁵⁹, K. Kroeninger⁵⁴, H. Kroha¹⁰⁰, J. Kroll¹²¹, J. Kroseberg²¹, J. Krstic^{13a}, U. Kruchonak⁶⁴, H. Krüger²¹, T. Kruker¹⁷, N. Krumnack⁶³, Z.V. Krumshiteyn⁶⁴, A. Kruse¹⁷⁴, M.C. Kruse⁴⁵, M. Kruskal²², T. Kubota⁸⁷, S. Kuday^{4a}, S. Kuehn⁴⁸, A. Kugel^{58c}, A. Kuhl¹³⁸, T. Kuhl⁴², V. Kukhtin⁶⁴, Y. Kulchitsky⁹¹, S. Kuleshov^{32b}, M. Kuna^{133a,133b}, J. Kunkle¹²¹, A. Kupco¹²⁶, H. Kurashige⁶⁶, Y.A. Kurochkin⁹¹, R. Kurumida⁶⁶, V. Kus¹²⁶, E.S. Kuwertz¹⁴⁸, M. Kuze¹⁵⁸, J. Kvita¹¹⁴, A. La Rosa⁴⁹, L. La Rotonda^{37a,37b}, C. Lacasta¹⁶⁸, F. Lacava^{133a,133b}, J. Lacey²⁹, H. Lacker¹⁶, D. Lacour⁷⁹, V.R. Lacuesta¹⁶⁸, E. Ladygin⁶⁴, R. Lafaye⁵, B. Laforge⁷⁹, T. Lagouri¹⁷⁷, S. Lai⁴⁸, H. Laier^{58a}, L. Lambourne⁷⁷, S. Lammers⁶⁰, C.L. Lampen⁷, W. Lampl⁷, E. Lançon¹³⁷, U. Landgraf⁴⁸, M.P.J. Landon⁷⁵, V.S. Lang^{58a}, A.J. Lankford¹⁶⁴, F. Lanni²⁵, K. Lantzsch³⁰, S. Laplace⁷⁹, C. Lapoire²¹, J.F. Laporte¹³⁷, T. Lari^{90a}, M. Lassnig³⁰, P. Laurelli⁴⁷, W. Lavrijsen¹⁵, A.T. Law¹³⁸, P. Laycock⁷³, O. Le Dortz⁷⁹, E. Le Guirriec⁸⁴, E. Le Menedeu¹², T. LeCompte⁶, F. Ledroit-Guillon⁵⁵, C.A. Lee¹⁵², H. Lee¹⁰⁶, J.S.H. Lee¹¹⁷, S.C. Lee¹⁵², L. Lee¹, G. Lefebvre⁷⁹, M. Lefebvre¹⁷⁰, F. Legger⁹⁹, C. Leggett¹⁵, A. Lehan⁷³, M. Lehmacher²¹, G. Lehmann Miotto³⁰, X. Lei⁷, W.A. Leight²⁹, A. Leisos¹⁵⁵, A.G. Leister¹⁷⁷, M.A.L. Leite^{24d}, R. Leitner¹²⁸, D. Lellouch¹⁷³, B. Lemmer⁵⁴, K.J.C. Leney⁷⁷, T. Lenz²¹, G. Lenzen¹⁷⁶, B. Lenzi³⁰, R. Leone⁷, S. Leone^{123a,123b}, K. Leonhardt⁴⁴, C. Leonidopoulos⁴⁶, S. Leontsinis¹⁰, C. Leroy⁹⁴, C.G. Lester²⁸, C.M. Lester¹²¹, M. Levchenko¹²², J. Levêque⁵, D. Levin⁸⁸, L.J. Levinson¹⁷³, M. Levy¹⁸, A. Lewis¹¹⁹, G.H. Lewis¹⁰⁹, A.M. Leyko²¹, M. Leyton⁴¹, B. Li^{33b,u}, B. Li⁸⁴, H. Li¹⁴⁹, H.L. Li³¹, L. Li⁴⁵, L. Li^{33e}, S. Li⁴⁵, Y. Li^{33c,v}, Z. Liang¹³⁸, H. Liao³⁴, B. Liberti^{134a}, P. Lichard³⁰, K. Lie¹⁶⁶, J. Liebal²¹, W. Liebig¹⁴, C. Limbach²¹, A. Limosani⁸⁷, S.C. Lin^{152,w}, T.H. Lin⁸², F. Linde¹⁰⁶, B.E. Lindquist¹⁴⁹, J.T. Linnemann⁸⁹, E. Lipeles¹²¹, A. Lipniacka¹⁴, M. Lisovyi⁴², T.M. Liss¹⁶⁶, D. Lissauer²⁵, A. Lister¹⁶⁹, A.M. Litke¹³⁸, B. Liu¹⁵², D. Liu¹⁵², J.B. Liu^{33b}, K. Liu^{33b,x}, L. Liu⁸⁸, M. Liu⁴⁵, M. Liu^{33b}, Y. Liu^{33b}, M. Livan^{120a,120b}, S.S.A. Livermore¹¹⁹, A. Lleres⁵⁵, J. Llorente Merino⁸¹, S.L. Lloyd⁷⁵, F. Lo Sterzo¹⁵², E. Lobodzinska⁴², P. Loch⁷, W.S. Lockman¹³⁸, T. Loddenkoetter²¹, F.K. Loebinger⁸³, A.E. Loevschall-Jensen³⁶, A. Loginov¹⁷⁷, T. Lohse¹⁶, K. Lohwasser⁴², M. Lokajicek¹²⁶, V.P. Lombardo⁵, B.A. Long²², J.D. Long⁸⁸, R.E. Long⁷¹, L. Lopes^{125a}, D. Lopez Mateos⁵⁷, B. Lopez Paredes¹⁴⁰, I. Lopez Paz¹², J. Lorenz⁹⁹, N. Lorenzo Martinez⁶⁰, M. Losada¹⁶³, P. Loscutoff¹⁵, X. Lou⁴¹, A. Lounis¹¹⁶, J. Love⁶, P.A. Love⁷¹, A.J. Lowe^{144,e}, F. Lu^{33a}, N. Lu⁸⁸, H.J. Lubatti¹³⁹, C. Luci^{133a,133b}, A. Lucotte⁵⁵, F. Luehring⁶⁰, W. Lukas⁶¹, L. Luminari^{133a}, O. Lundberg^{147a,147b}, B. Lund-Jensen¹⁴⁸, M. Lungwitz⁸², D. Lynn²⁵, R. Lysak¹²⁶, E. Lytken⁸⁰, H. Ma²⁵, L.L. Ma^{33d}, G. Maccarrone⁴⁷, A. Macchiolo¹⁰⁰, J. Machado Miguens^{125a,125b}, D. Macina³⁰, D. Madaffari⁸⁴, R. Madar⁴⁸, H.J. Maddocks⁷¹, W.F. Mader⁴⁴, A. Madsen¹⁶⁷, M. Maeno⁸, T. Maeno²⁵, E. Magradze⁵⁴, K. Mahboubi⁴⁸, J. Mahlstedt¹⁰⁶, S. Mahmoud⁷³, C. Maiani¹³⁷, C. Maidantchik^{24a}, A.A. Maier¹⁰⁰, A. Maio^{125a,125b,125d}, S. Majewski¹¹⁵, Y. Makida⁶⁵, N. Makovec¹¹⁶, P. Mal^{137,y}, B. Malaescu⁷⁹, Pa. Malecki³⁹, V.P. Maleev¹²², F. Malek⁵⁵, U. Mallik⁶², D. Malon⁶, C. Malone¹⁴⁴, S. Maltezos¹⁰, V.M. Malyshev¹⁰⁸, S. Malyukov³⁰, J. Mamuzic^{13b}, B. Mandelli³⁰, L. Mandelli^{90a}, I. Mandić⁷⁴, R. Mandrysch⁶², J. Maneira^{125a,125b}, A. Manfredini¹⁰⁰, L. Manhaes de Andrade Filho^{24b}, J.A. Manjarres Ramos^{160b}, A. Mann⁹⁹, P.M. Manning¹³⁸, A. Manousakis-Katsikakis⁹, B. Mansoulie¹³⁷, R. Mantifel⁸⁶, L. Mapelli³⁰, L. March¹⁶⁸, J.F. Marchand²⁹, G. Marchiori⁷⁹, M. Marcisovsky¹²⁶, C.P. Marino¹⁷⁰, M. Marjanovic^{13a}, C.N. Marques^{125a}, F. Marroquim^{24a}, S.P. Marsden⁸³, Z. Marshall¹⁵, L.F. Marti¹⁷, S. Marti-Garcia¹⁶⁸, B. Martin³⁰, B. Martin⁸⁹, T.A. Martin¹⁷¹, V.J. Martin⁴⁶, B. Martin dit Latour¹⁴, H. Martinez¹³⁷, M. Martinez^{12,n}, S. Martin-Haugh¹³⁰, A.C. Martyniuk⁷⁷, M. Marx¹³⁹, F. Marzano^{133a}, A. Marzin³⁰, L. Masetti⁸², T. Mashimo¹⁵⁶, R. Mashinistov⁹⁵, J. Masik⁸³, A.L. Maslennikov¹⁰⁸, I. Massa^{20a,20b}, L. Massa^{20a,20b}, N. Massol⁵, P. Mastrandrea¹⁴⁹, A. Mastroberardino^{37a,37b}, T. Masubuchi¹⁵⁶, P. Mättig¹⁷⁶, J. Mattmann⁸², J. Maurer^{26a}, S.J. Maxfield⁷³, D.A. Maximov^{108,t}, R. Mazini¹⁵², L. Mazzaferro^{134a,134b}, G. Mc Goldrick¹⁵⁹, S.P. Mc Kee⁸⁸, A. McCann⁸⁸, R.L. McCarthy¹⁴⁹, T.G. McCarthy²⁹, N.A. McCubbin¹³⁰, K.W. McFarlane^{56,*}, J.A. McFayden⁷⁷, G. Mchedlidze⁵⁴, S.J. McMahon¹³⁰, R.A. McPherson^{170,i}, A. Meade⁸⁵, J. Mechnich¹⁰⁶, M. Medinnis⁴², S. Meehan³¹, S. Mehlhase⁹⁹, A. Mehta⁷³, K. Meier^{58a}, C. Meineck⁹⁹, B. Meirose⁸⁰, C. Melachrinou³¹, B.R. Mellado Garcia^{146c}, F. Meloni¹⁷, A. Mengarelli^{20a,20b}, S. Menke¹⁰⁰, E. Meoni¹⁶², K.M. Mercurio⁵⁷, S. Mergelmeyer²¹, N. Meric¹³⁷, P. Mermod⁴⁹, L. Merola^{103a,103b}, C. Meroni^{90a}, F.S. Merritt³¹, H. Merritt¹¹⁰, A. Messina^{30,z}, J. Metcalfe²⁵, A.S. Mete¹⁶⁴, C. Meyer⁸², C. Meyer¹²¹, J.-P. Meyer¹³⁷, J. Meyer³⁰, R.P. Middleton¹³⁰, S. Migas⁷³, L. Mijović²¹, G. Mikenberg¹⁷³, M. Mikestikova¹²⁶, M. Mikuž⁷⁴, A. Milic³⁰, D.W. Miller³¹, C. Mills⁴⁶, A. Milov¹⁷³, D.A. Milstead^{147a,147b}, D. Milstein¹⁷³, A.A. Minaenko¹²⁹, I.A. Minashvili⁶⁴, A.I. Mincer¹⁰⁹, B. Mindur^{38a}, M. Mineev⁶⁴, Y. Ming¹⁷⁴, L.M. Mir¹², G. Mirabelli^{133a}, T. Mitani¹⁷², J. Mitrevski⁹⁹, V.A. Mitsou¹⁶⁸, S. Mitsui⁶⁵, A. Miucci⁴⁹, P.S. Miyagawa¹⁴⁰, J.U. Mjörnmark⁸⁰, T. Moa^{147a,147b}, K. Mochizuki⁸⁴, S. Mohapatra³⁵, W. Mohr⁴⁸, S. Molander^{147a,147b}, R. Moles-Valls¹⁶⁸, K. Mönig⁴², C. Monini⁵⁵, J. Monk³⁶, E. Monnier⁸⁴, J. Montejo Berlingen¹², F. Monticelli⁷⁰, S. Monzani^{133a,133b}, R.W. Moore³, N. Morange⁶², D. Moreno⁸², M. Moreno Llácer⁵⁴, P. Morettini^{50a}, M. Morgenstern⁴⁴, M. Morii⁵⁷, S. Moritz⁸², A.K. Morley¹⁴⁸, G. Mornacchi³⁰, J.D. Morris⁷⁵, L. Morvaj¹⁰², H.G. Moser¹⁰⁰, M. Mosidze^{51b}, J. Moss¹¹⁰, K. Motohashi¹⁵⁸, R. Mount¹⁴⁴, E. Mountricha²⁵, S.V. Mouraviev^{95,*}, E.J.W. Moyses⁸⁵,

S. Muanza⁸⁴, R.D. Mudd¹⁸, F. Mueller^{58a}, J. Mueller¹²⁴, K. Mueller²¹, T. Mueller²⁸, T. Mueller⁸², D. Muenstermann⁴⁹, Y. Munwes¹⁵⁴, J.A. Murillo Quijada¹⁸, W.J. Murray^{171,130}, H. Musheghyan⁵⁴, E. Musto¹⁵³, A.G. Myagkov^{129,aa}, M. Myska¹²⁷, O. Nackenhorst⁵⁴, J. Nadal⁵⁴, K. Nagai⁶¹, R. Nagai¹⁵⁸, Y. Nagai⁸⁴, K. Nagano⁶⁵, A. Nagarkar¹¹⁰, Y. Nagasaka⁵⁹, M. Nagel¹⁰⁰, A.M. Nairz³⁰, Y. Nakahama³⁰, K. Nakamura⁶⁵, T. Nakamura¹⁵⁶, I. Nakano¹¹¹, H. Namasivayam⁴¹, G. Nanava²¹, R. Narayan^{58b}, T. Nattermann²¹, T. Naumann⁴², G. Navarro¹⁶³, R. Nayyar⁷, H.A. Neal⁸⁸, P.Yu. Nechaeva⁹⁵, T.J. Neep⁸³, P.D. Nef¹⁴⁴, A. Negri^{120a,120b}, G. Negri³⁰, M. Negrini^{20a}, S. Nektarijevic⁴⁹, A. Nelson¹⁶⁴, T.K. Nelson¹⁴⁴, S. Nemecek¹²⁶, N. Nemethy¹⁰⁹, A.A. Nepomuceno^{24a}, M. Nessi^{30,ab}, M.S. Neubauer¹⁶⁶, M. Neumann¹⁷⁶, R.M. Neves¹⁰⁹, P. Nevski²⁵, P.R. Newman¹⁸, D.H. Nguyen⁶, R.B. Nickerson¹¹⁹, R. Nicolaidou¹³⁷, B. Nicquevert³⁰, J. Nielsen¹³⁸, N. Nikiforou³⁵, A. Nikiforov¹⁶, V. Nikolaenko^{129,aa}, I. Nikolic-Audit⁷⁹, K. Nikolics⁴⁹, K. Nikolopoulos¹⁸, P. Nilsson⁸, Y. Ninomiya¹⁵⁶, A. Nisati^{133a}, R. Nisius¹⁰⁰, T. Nobe¹⁵⁸, L. Nodulman⁶, M. Nomachi¹¹⁷, I. Nomidis²⁹, S. Norberg¹¹², M. Nordberg³⁰, O. Novgorodova⁴⁴, S. Nowak¹⁰⁰, M. Nozaki⁶⁵, L. Nozka¹¹⁴, K. Ntekas¹⁰, G. Nunes Hanninger⁸⁷, T. Nunnemann⁹⁹, E. Nurse⁷⁷, F. Nuti⁸⁷, B.J. O'Brien⁴⁶, F. O'grady⁷, D.C. O'Neil¹⁴³, V. O'Shea⁵³, F.G. Oakham^{29,d}, H. Oberlack¹⁰⁰, T. Obermann²¹, J. Ocariz⁷⁹, A. Ochi⁶⁶, M.I. Ochoa⁷⁷, S. Oda⁶⁹, S. Odaka⁶⁵, H. Ogren⁶⁰, A. Oh⁸³, S.H. Oh⁴⁵, C.C. Ohm¹⁵, H. Ohman¹⁶⁷, W. Okamura¹¹⁷, H. Okawa²⁵, Y. Okumura³¹, T. Okuyama¹⁵⁶, A. Olariu^{26a}, A.G. Olchevski⁶⁴, S.A. Olivares Pino⁴⁶, D. Oliveira Damazio²⁵, E. Oliver Garcia¹⁶⁸, A. Olszewski³⁹, J. Olszowska³⁹, A. Onofre^{125a,125e}, P.U.E. Onyisi^{31,o}, C.J. Oram^{160a}, M.J. Oreglia³¹, Y. Oren¹⁵⁴, D. Orestano^{135a,135b}, N. Orlando^{72a,72b}, C. Oropeza Barrera⁵³, R.S. Orr¹⁵⁹, B. Osculati^{50a,50b}, R. Ospanov¹²¹, G. Otero y Garzon²⁷, H. Otono⁶⁹, M. Ouchrif^{136d}, E.A. Ouellette¹⁷⁰, F. Ould-Saada¹¹⁸, A. Ouraou¹³⁷, K.P. Oussoren¹⁰⁶, Q. Ouyang^{33a}, A. Ovcharova¹⁵, M. Owen⁸³, V.E. Ozcan^{19a}, N. Ozturk⁸, K. Pachal¹¹⁹, A. Pacheco Pages¹², C. Padilla Aranda¹², M. Pagáčová⁴⁸, S. Pagan Griso¹⁵, E. Paganis¹⁴⁰, C. Pahl¹⁰⁰, F. Paige²⁵, P. Pais⁸⁵, K. Pajchel¹¹⁸, G. Palacino^{160b}, S. Palestini³⁰, M. Palka^{38b}, D. Pallin³⁴, A. Palma^{125a,125b}, J.D. Palmer¹⁸, Y.B. Pan¹⁷⁴, E. Panagiotopoulou¹⁰, J.G. Panduro Vazquez⁷⁶, P. Pani¹⁰⁶, N. Panikashvili⁸⁸, S. Panitkin²⁵, D. Pantea^{26a}, L. Paolozzi^{134a,134b}, Th.D. Papadopoulou¹⁰, K. Papageorgiou^{155,l}, A. Paramonov⁶, D. Paredes Hernandez³⁴, M.A. Parker²⁸, F. Parodi^{50a,50b}, J.A. Parsons³⁵, U. Parzefall⁴⁸, E. Pasqualucci^{133a}, S. Passaggio^{50a}, A. Passeri^{135a}, F. Pastore^{135a,135b,*}, Fr. Pastore⁷⁶, G. Pásztor²⁹, S. Patariaia¹⁷⁶, N.D. Patel¹⁵¹, J.R. Pater⁸³, S. Patricelli^{103a,103b}, T. Pauly³⁰, J. Pearce¹⁷⁰, M. Pedersen¹¹⁸, S. Pedraza Lopez¹⁶⁸, R. Pedro^{125a,125b}, S.V. Peleganchuk¹⁰⁸, D. Pelikan¹⁶⁷, H. Peng^{33b}, B. Penning³¹, J. Penwell⁶⁰, D.V. Perepelitsa²⁵, E. Perez Codina^{160a}, M.T. Pérez García-Estañ¹⁶⁸, V. Perez Reale³⁵, L. Perini^{90a,90b}, H. Pernegger³⁰, R. Perrino^{72a}, R. Peschke⁴², V.D. Peshekhonov⁶⁴, K. Peters³⁰, R.F.Y. Peters⁸³, B.A. Petersen³⁰, T.C. Petersen³⁶, E. Petit⁴², A. Petridis^{147a,147b}, C. Petridou¹⁵⁵, E. Petrolu^{133a}, F. Petrucci^{135a,135b}, N.E. Pettersson¹⁵⁸, R. Pezosa^{32b}, P.W. Phillips¹³⁰, G. Piacquadio¹⁴⁴, E. Pianori¹⁷¹, A. Picazio⁴⁹, E. Piccaro⁷⁵, M. Piccinini^{20a,20b}, R. Piegaia²⁷, D.T. Pignotti¹¹⁰, J.E. Pilcher³¹, A.D. Pilkington⁷⁷, J. Pina^{125a,125b,125d}, M. Pinamonti^{165a,165c,ac}, A. Pinder¹¹⁹, J.L. Pinfold³, A. Pingel³⁶, B. Pinto^{125a}, S. Pires⁷⁹, M. Pitt¹⁷³, C. Pizio^{90a,90b}, L. Plazak^{145a}, M.-A. Pleier²⁵, V. Pleskot¹²⁸, E. Plotnikova⁶⁴, P. Plucinski^{147a,147b}, S. Poddar^{58a}, F. Podlyski³⁴, R. Poettgen⁸², L. Poggioli¹¹⁶, D. Pohl²¹, M. Pohl⁴⁹, G. Polesello^{120a}, A. Policicchio^{37a,37b}, R. Polifka¹⁵⁹, A. Polini^{20a}, C.S. Pollard⁴⁵, V. Polychronakos²⁵, K. Pommès³⁰, L. Pontecorvo^{133a}, B.G. Pope⁸⁹, G.A. Popeneciu^{26b}, D.S. Popovic^{13a}, A. Poppleton³⁰, X. Portell Bueso¹², S. Pospisil¹²⁷, K. Potamianos¹⁵, I.N. Potrap⁶⁴, C.J. Potter¹⁵⁰, C.T. Potter¹¹⁵, G. Poulard³⁰, J. Poveda⁶⁰, V. Pozdnyakov⁶⁴, P. Pralavorio⁸⁴, A. Pranko¹⁵, S. Prasad³⁰, R. Pravahan⁸, S. Prell⁶³, D. Price⁸³, J. Price⁷³, L.E. Price⁶, D. Prieur¹²⁴, M. Primavera^{72a}, M. Proissl⁴⁶, K. Prokofiev⁴⁷, F. Prokoshin^{32b}, E. Protopapadaki¹³⁷, S. Protopopescu²⁵, J. Proudfoot⁶, M. Przybycien^{38a}, H. Przysiezniak⁵, E. Ptacek¹¹⁵, D. Puddu^{135a,135b}, E. Pueschel⁸⁵, D. Poldon¹⁴⁹, M. Purohit^{25,ad}, P. Puzo¹¹⁶, J. Qian⁸⁸, G. Qin⁵³, Y. Qin⁸³, A. Quadt⁵⁴, D.R. Quarrie¹⁵, W.B. Quayle^{165a,165b}, M. Queitsch-Maitland⁸³, D. Quilty⁵³, A. Qureshi^{160b}, V. Radeka²⁵, V. Radescu⁴², S.K. Radhakrishnan¹⁴⁹, P. Radloff¹¹⁵, P. Rados⁸⁷, F. Ragusa^{90a,90b}, G. Rahal¹⁷⁹, S. Rajagopalan²⁵, M. Rammensee³⁰, A.S. Randle-Conde⁴⁰, C. Rangel-Smith¹⁶⁷, K. Rao¹⁶⁴, F. Rauscher⁹⁹, T.C. Rave⁴⁸, T. Ravenscroft⁷³, M. Raymond³⁰, A.L. Read¹¹⁸, N.P. Readoff⁷³, D.M. Rebuzzi^{120a,120b}, A. Redelbach¹⁷⁵, G. Redlinger²⁵, R. Reece¹³⁸, K. Reeves⁴¹, L. Rehnisch¹⁶, H. Reisin²⁷, M. Relich¹⁶⁴, C. Rembser³⁰, H. Ren^{33a}, Z.L. Ren¹⁵², A. Renaud¹¹⁶, M. Rescigno^{133a}, S. Resconi^{90a}, O.L. Rezanova^{108,t}, P. Reznicek¹²⁸, R. Rezvani⁹⁴, R. Richter¹⁰⁰, M. Ridel⁷⁹, P. Rieck¹⁶, J. Rieger⁵⁴, M. Rijssenbeek¹⁴⁹, A. Rimoldi^{120a,120b}, L. Rinaldi^{20a}, E. Ritsch⁶¹, I. Riu¹², F. Rizatdinova¹¹³, E. Rizvi⁷⁵, S.H. Robertson^{86,i}, A. Robichaud-Veronneau⁸⁶, D. Robinson²⁸, J.E.M. Robinson⁸³, A. Robson⁵³, C. Roda^{123a,123b}, L. Rodrigues³⁰, S. Roe³⁰, O. Røhne¹¹⁸, S. Rolli¹⁶², A. Romaniouk⁹⁷, M. Romano^{20a,20b}, E. Romero Adam¹⁶⁸, N. Rompotis¹³⁹, M. Ronzani⁴⁸, L. Roos⁷⁹, E. Ros¹⁶⁸, S. Rosati^{133a}, K. Rosbach⁴⁹, M. Rose⁷⁶, P. Rose¹³⁸, P.L. Rosendahl¹⁴, O. Rosenthal¹⁴², V. Rossetti^{147a,147b}, E. Rossi^{103a,103b}, L.P. Rossi^{50a}, R. Rosten¹³⁹, M. Rotaru^{26a}, I. Roth¹⁷³, J. Rothberg¹³⁹, D. Rousseau¹¹⁶, C.R. Royon¹³⁷, A. Rozanov⁸⁴, Y. Rozen¹⁵³, X. Ruan^{146c}, F. Rubbo¹², I. Rubinskiy⁴², V.I. Rud⁹⁸, C. Rudolph⁴⁴, M.S. Rudolph¹⁵⁹, F. Rühr⁴⁸, A. Ruiz-Martinez³⁰, Z. Rurikova⁴⁸, N.A. Rusakovich⁶⁴, A. Ruschke⁹⁹, J.P. Rutherford⁷, N. Ruthmann⁴⁸, Y.F. Ryabov¹²², M. Rybar¹²⁸, G. Rybkin¹¹⁶, N.C. Ryder¹¹⁹, A.F. Saavedra¹⁵¹, S. Sacerdoti²⁷, A. Saddique³, I. Sadeh¹⁵⁴, H.F.-W. Sadrozinski¹³⁸, R. Sadykov⁶⁴, F. Safai Tehrani^{133a}, H. Sakamoto¹⁵⁶, Y. Sakurai¹⁷², G. Salamanna^{135a,135b}, A. Salamon^{134a}, M. Saleem¹¹², D. Salek¹⁰⁶, P.H. Sales De Bruin¹³⁹, D. Salihagic¹⁰⁰, A. Salkin¹⁴⁴, J. Salt¹⁶⁸, D. Salvatore^{37a,37b}, F. Salvatore¹⁵⁰, A. Salvucci¹⁰⁵, A. Salzburger³⁰, D. Sampsonidis¹⁵⁵, A. Sanchez^{103a,103b}, J. Sánchez¹⁶⁸, V. Sanchez Martinez¹⁶⁸, H. Sandaker¹⁴, R.L. Sandbach⁷⁵, H.G. Sander⁸², M.P. Sanders⁹⁹, M. Sandhoff¹⁷⁶, T. Sandoval²⁸, C. Sandoval¹⁶³, R. Sandstroem¹⁰⁰, D.P.C. Sankey¹³⁰, A. Sansoni⁴⁷, C. Santoni³⁴, R. Santonico^{134a,134b}, H. Santos^{125a}, I. Santoyo Castillo¹⁵⁰, K. Sapp¹²⁴, A. Saponov⁶⁴, J.G. Saraiva^{125a,125d}, B. Sarrazin²¹, G. Sartisoehn¹⁷⁶, O. Sasaki⁶⁵, Y. Sasaki¹⁵⁶, G. Sauvage^{5,*}

E. Sauvan⁵, P. Savard^{159,d}, D.O. Savu³⁰, C. Sawyer¹¹⁹, L. Sawyer^{78,m}, D.H. Saxon⁵³, J. Saxon¹²¹, C. Sbarra^{20a}, A. Sbrizzi³, T. Scanlon⁷⁷, D.A. Scannicchio¹⁶⁴, M. Scarcella¹⁵¹, V. Scarfone^{37a,37b}, J. Schaarschmidt¹⁷³, P. Schacht¹⁰⁰, D. Schaefer³⁰, R. Schaefer⁴², S. Schaepe²¹, S. Schaezel^{58b}, U. Schäfer⁸², A.C. Schaffer¹¹⁶, D. Schaile⁹⁹, R.D. Schamberger¹⁴⁹, V. Scharf^{58a}, V.A. Schegelsky¹²², D. Scheirich¹²⁸, M. Schernau¹⁶⁴, M.I. Scherzer³⁵, C. Schiavi^{50a,50b}, J. Schieck⁹⁹, C. Schillo⁴⁸, M. Schioppa^{37a,37b}, S. Schlenker³⁰, E. Schmidt⁴⁸, K. Schmieden³⁰, C. Schmitt⁸², S. Schmitt^{58b}, B. Schneider¹⁷, Y.J. Schnellbach⁷³, U. Schnoor⁴⁴, L. Schoeffel¹³⁷, A. Schoening^{58b}, B.D. Schoenrock⁸⁹, A.L.S. Schorlemmer⁵⁴, M. Schott⁸², D. Schouten^{160a}, J. Schovancova²⁵, S. Schramm¹⁵⁹, M. Schreyer¹⁷⁵, C. Schroeder⁸², N. Schuh⁸², M.J. Schultens²¹, H.-C. Schultz-Coulon^{58a}, H. Schulz¹⁶, M. Schumacher⁴⁸, B.A. Schumm¹³⁸, Ph. Schune¹³⁷, C. Schwanenberger⁸³, A. Schwartzman¹⁴⁴, Ph. Schwegler¹⁰⁰, Ph. Schwemling¹³⁷, R. Schwienhorst⁸⁹, J. Schwindling¹³⁷, T. Schwindt²¹, M. Schwoerer⁵, F.G. Sciacca¹⁷, E. Scifo¹¹⁶, G. Sciolla²³, W.G. Scott¹³⁰, F. Scuri^{123a,123b}, F. Scutti²¹, J. Searcy⁸⁸, G. Sedov⁴², E. Sedykh¹²², S.C. Seidel¹⁰⁴, A. Seiden¹³⁸, F. Seifert¹²⁷, J.M. Seixas^{24a}, G. Sekhniaidze^{103a}, S.J. Sekula⁴⁰, K.E. Selbach⁴⁶, D.M. Seliverstov^{122,*}, G. Sellers⁷³, N. Semprini-Cesari^{20a,20b}, C. Serfon³⁰, L. Serin¹¹⁶, L. Serkin⁵⁴, T. Serre⁸⁴, R. Seuster^{160a}, H. Severini¹¹², T. Sfiligoi⁷⁴, F. Sforza¹⁰⁰, A. Sfyrila³⁰, E. Shabalina⁵⁴, M. Shamim¹¹⁵, L.Y. Shan^{33a}, R. Shang¹⁶⁶, J.T. Shank²², M. Shapiro¹⁵, P.B. Shatalov⁹⁶, K. Shaw^{165a,165b}, C.Y. Shehu¹⁵⁰, P. Sherwood⁷⁷, L. Shi^{152,ae}, S. Shimizu⁶⁶, C.O. Shimmin¹⁶⁴, M. Shimojima¹⁰¹, M. Shiyakova⁶⁴, A. Shmeleva⁹⁵, M.J. Shochet³¹, D. Short¹¹⁹, S. Shrestha⁶³, E. Shulga⁹⁷, M.A. Shupe⁷, S. Shushkevich⁴², P. Sicho¹²⁶, O. Sidiropoulou¹⁵⁵, D. Sidorov¹¹³, A. Sidoti^{133a}, F. Siegert⁴⁴, Dj. Sijacki^{13a}, J. Silva^{125a,125d}, Y. Silver¹⁵⁴, D. Silverstein¹⁴⁴, S.B. Silverstein^{147a}, V. Simak¹²⁷, O. Simard⁵, Lj. Simic^{13a}, S. Simion¹¹⁶, E. Simioni⁸², B. Simmons⁷⁷, R. Simoniello^{90a,90b}, M. Simonyan³⁶, P. Sinervo¹⁵⁹, N.B. Sinev¹¹⁵, V. Sipica¹⁴², G. Siragusa¹⁷⁵, A. Sircar⁷⁸, A.N. Sisakyan^{64,*}, S.Yu. Sivoklov⁹⁸, J. Sjölín^{147a,147b}, T.B. Sjurson¹⁴, H.P. Skottowe⁵⁷, K.Yu. Skovpen¹⁰⁸, P. Skubic¹¹², M. Slater¹⁸, T. Slavicek¹²⁷, K. Sliwa¹⁶², V. Smakhtin¹⁷³, B.H. Smart⁴⁶, L. Smestad¹⁴, S.Yu. Smirnov⁹⁷, Y. Smirnov⁹⁷, L.N. Smirnova^{98,af}, O. Smirnova⁸⁰, K.M. Smith⁵³, M. Smizanska⁷¹, K. Smolek¹²⁷, A.A. Snesarev⁹⁵, G. Snidero⁷⁵, S. Snyder²⁵, R. Sobie^{170,i}, F. Socher⁴⁴, A. Soffer¹⁵⁴, D.A. Soh^{152,ae}, C.A. Solans³⁰, M. Solar¹²⁷, J. Solc¹²⁷, E.Yu. Soldatov⁹⁷, U. Soldevila¹⁶⁸, A.A. Solodkov¹²⁹, A. Soloshenko⁶⁴, O.V. Solovyanov¹²⁹, V. Solovye¹²², P. Sommer⁴⁸, H.Y. Song^{33b}, N. Soni¹, A. Sood¹⁵, A. Sopczak¹²⁷, B. Sopko¹²⁷, V. Sopko¹²⁷, V. Sorin¹², M. Sosebee⁸, R. Soualah^{165a,165c}, P. Soueid⁹⁴, A.M. Soukharev¹⁰⁸, D. South⁴², S. Spagnolo^{72a,72b}, F. Spanò⁷⁶, W.R. Spearman⁵⁷, F. Spettel¹⁰⁰, R. Spighi^{20a}, G. Spigo³⁰, L.A. Spiller⁸⁷, M. Spousta¹²⁸, T. Spreitzer¹⁵⁹, B. Spurlock⁸, R.D. St. Denis^{53,*}, S. Staerz⁴⁴, J. Stahlman¹²¹, R. Stamen^{58a}, S. Stamm¹⁶, E. Stanecka³⁹, R.W. Staneck⁶, C. Stanescu^{135a}, M. Stanescu-Bellu⁴², M.M. Stanitzki⁴², S. Stapnes¹¹⁸, E.A. Starchenko¹²⁹, J. Stark⁵⁵, P. Staroba¹²⁶, P. Starovoitov⁴², R. Staszewski³⁹, P. Stavina^{145a,*}, P. Steinberg²⁵, B. Stelzer¹⁴³, H.J. Stelzer³⁰, O. Stelzer-Chilton^{160a}, H. Stenzel⁵², S. Stern¹⁰⁰, G.A. Stewart⁵³, J.A. Stillings²¹, M.C. Stockton⁸⁶, M. Stoebe⁸⁶, G. Stoicica^{26a}, P. Stolte⁵⁴, S. Stonjek¹⁰⁰, A.R. Stradling⁸, A. Straessner⁴⁴, M.E. Stramaglia¹⁷, J. Strandberg¹⁴⁸, S. Strandberg^{147a,147b}, A. Strandlie¹¹⁸, E. Strauss¹⁴⁴, M. Strauss¹¹², P. Strizeneč^{145b}, R. Ströhmer¹⁷⁵, D.M. Strom¹¹⁵, R. Stroynowski⁴⁰, A. Struebig¹⁰⁵, S.A. Stucci¹⁷, B. Stugu¹⁴, N.A. Styles⁴², D. Su¹⁴⁴, J. Su¹²⁴, R. Subramaniam⁷⁸, A. Succurro¹², Y. Sugaya¹¹⁷, C. Suhr¹⁰⁷, M. Suk¹²⁷, V.V. Sulin⁹⁵, S. Sultansoy^{4c}, T. Sumida⁶⁷, S. Sun⁵⁷, X. Sun^{33a}, J.E. Sundermann⁴⁸, K. Suruliz¹⁴⁰, G. Susinno^{37a,37b}, M.R. Sutton¹⁵⁰, Y. Suzuki⁶⁵, M. Svatos¹²⁶, S. Swedish¹⁶⁹, M. Swiatlowski¹⁴⁴, I. Sykora^{145a}, T. Sykora¹²⁸, D. Ta⁸⁹, C. Taccini^{135a,135b}, K. Tackmann⁴², J. Taenzer¹⁵⁹, A. Taffard¹⁶⁴, R. Tafirout^{160a}, N. Taiblum¹⁵⁴, H. Takai²⁵, R. Takashima⁶⁸, H. Takeda⁶⁶, T. Takeshita¹⁴¹, Y. Takubo⁶⁵, M. Talby⁸⁴, A.A. Talyshv^{108,t}, J.Y.C. Tam¹⁷⁵, K.G. Tan⁸⁷, J. Tanaka¹⁵⁶, R. Tanaka¹¹⁶, S. Tanaka¹³², S. Tanaka⁶⁵, A.J. Tanasijczuk¹⁴³, B.B. Tannenwald¹¹⁰, N. Tannoury²¹, S. Tapprogge⁸², S. Tarem¹⁵³, F. Tarrade²⁹, G.F. Tartarelli^{90a}, P. Tas¹²⁸, M. Tasevsky¹²⁶, T. Tashiro⁶⁷, E. Tassi^{37a,37b}, A. Tavares Delgado^{125a,125b}, Y. Tayalati^{136d}, F.E. Taylor⁹³, G.N. Taylor⁸⁷, W. Taylor^{160b}, F.A. Teischinger³⁰, M. Teixeira Dias Castanheira⁷⁵, P. Teixeira-Dias⁷⁶, K.K. Temming⁴⁸, H. Ten Kate³⁰, P.K. Teng¹⁵², J.J. Teoh¹¹⁷, S. Terada⁶⁵, K. Terashi¹⁵⁶, J. Terron⁸¹, S. Terzo¹⁰⁰, M. Testa⁴⁷, R.J. Teuscher^{159,i}, J. Therhaag²¹, T. Thevenaux-Pelzer³⁴, J.P. Thomas¹⁸, J. Thomas-Wilsker⁷⁶, E.N. Thompson³⁵, P.D. Thompson¹⁸, P.D. Thompson¹⁵⁹, R.J. Thompson⁸³, A.S. Thompson⁵³, L.A. Thomsen³⁶, E. Thomson¹²¹, M. Thomson²⁸, W.M. Thong⁸⁷, R.P. Thun^{88,*}, F. Tian³⁵, M.J. Tibbetts¹⁵, V.O. Tikhomirov^{95,ag}, Yu.A. Tikhonov^{108,t}, S. Timoshenko⁹⁷, E. Tiouchichine⁸⁴, P. Tipton¹⁷⁷, S. Tisserant⁸⁴, T. Todorov⁵, S. Todorova-Nova¹²⁸, B. Toggerson⁷, J. Tojo⁶⁹, S. Tokár^{145a}, K. Tokushuku⁶⁵, K. Tollefson⁸⁹, L. Tomlinson⁸³, M. Tomoto¹⁰², L. Tompkins³¹, K. Toms¹⁰⁴, N.D. Topilin⁶⁴, E. Torrence¹¹⁵, H. Torres¹⁴³, E. Torrón Pastor¹⁶⁸, J. Toth^{84,ah}, F. Touchard⁸⁴, D.R. Tovey¹⁴⁰, H.L. Tran¹¹⁶, T. Trefzger¹⁷⁵, L. Tremblet³⁰, A. Tricoli³⁰, I.M. Trigger^{160a}, S. Trincaz-Duvoid⁷⁹, M.F. Tripiana¹², W. Trischuk¹⁵⁹, B. Trocme⁵⁵, C. Troncon^{90a}, M. Trottier-McDonald¹⁴³, M. Trovatelli^{135a,135b}, P. True⁸⁹, M. Trzebinski³⁹, A. Trzupek³⁹, C. Tsarouchas³⁰, J.C.L. Tseng¹¹⁹, P.V. Tsiarehka⁹¹, D. Tsionou¹³⁷, G. Tsipolitis¹⁰, N. Tsirintanis⁹, S. Tsiskaridze¹², V. Tsiskaridze⁴⁸, E.G. Tskhadadze^{51a}, I.I. Tsukerman⁹⁶, V. Tsulaia¹⁵, S. Tsuno⁶⁵, D. Tsybychev¹⁴⁹, A. Tudorache^{26a}, V. Tudorache^{26a}, A.N. Tuna¹²¹, S.A. Tupputi^{20a,20b}, S. Turchikhin^{98,af}, D. Turecek¹²⁷, I. Turk Cakir^{4d}, R. Turra^{90a,90b}, P.M. Tuts³⁵, A. Tykhonov⁴⁹, M. Tylmad^{147a,147b}, M. Tyndel¹³⁰, K. Uchida²¹, I. Ueda¹⁵⁶, R. Ueno²⁹, M. Ughetto⁸⁴, M. Uglan¹⁴, M. Uhlenbrock²¹, F. Ukegawa¹⁶¹, G. Unal³⁰, A. Undrus²⁵, G. Unel¹⁶⁴, F.C. Ungaro⁴⁸, Y. Unno⁶⁵, C. Unverdorben⁹⁹, D. Urbaniec³⁵, P. Urquijo⁸⁷, G. Usai⁸, A. Usanova⁶¹, L. Vacavant⁸⁴, V. Vacek¹²⁷, B. Vachon⁸⁶, N. Valencic¹⁰⁶, S. Valentineti^{20a,20b}, A. Valero¹⁶⁸, L. Valery³⁴, S. Valkar¹²⁸, E. Valladolid Gallego¹⁶⁸, S. Vallecorsa⁴⁹, J.A. Valls Ferrer¹⁶⁸, W. Van Den Wollenberg¹⁰⁶, P.C. Van Der Deijl¹⁰⁶, R. van der Geer¹⁰⁶, H. van der Graaf¹⁰⁶, R. Van Der Leeuw¹⁰⁶, D. van der Ster³⁰, N. van Eldik³⁰, P. van Gemmeren⁶, J. Van Nieuwkoop¹⁴³, I. van Vulpen¹⁰⁶, M.C. van Woerden³⁰, M. Vanadia^{133a,133b}, W. Vandelli³⁰, R. Vanguri¹²¹, A. Vaniachine⁶, P. Vankov⁴², F. Vannucci⁷⁹,

G. Vardanyan¹⁷⁸, R. Vari^{133a}, E.W. Varnes⁷, T. Varol⁸⁵, D. Varouchas⁷⁹, A. Vartapetian⁸, K.E. Varvell¹⁵¹, F. Vazeille³⁴, T. Vazquez Schroeder⁵⁴, J. Veatch⁷, F. Veloso^{125a,125c}, S. Veneziano^{133a}, A. Ventura^{72a,72b}, D. Ventura⁸⁵, M. Venturi¹⁷⁰, N. Venturi¹⁵⁹, A. Venturini²³, V. Vercesi^{120a}, M. Verducci^{133a,133b}, W. Verkerke¹⁰⁶, J.C. Vermeulen¹⁰⁶, A. Vest⁴⁴, M.C. Vetterli^{143,d}, O. Viazlo⁸⁰, I. Vichou¹⁶⁶, T. Vickey^{146c,ai}, O.E. Vickey Boeriu^{146c}, G.H.A. Viehhauser¹¹⁹, S. Viel¹⁶⁹, R. Vigne³⁰, M. Villa^{20a,20b}, M. Villaplana Perez^{90a,90b}, E. Vilucchi⁴⁷, M.G. Vinciter²⁹, V.B. Vinogradov⁶⁴, J. Virzi¹⁵, I. Vivarelli¹⁵⁰, F. Vives Vaque³, S. Vlachos¹⁰, D. Vladoiu⁹⁹, M. Vlasak¹²⁷, A. Vogel²¹, M. Vogel^{32a}, P. Vokac¹²⁷, G. Volpi^{123a,123b}, M. Volpi⁸⁷, H. von der Schmitt¹⁰⁰, H. von Radziewski⁴⁸, E. von Toerne²¹, V. Vorobel¹²⁸, K. Vorobev⁹⁷, M. Vos¹⁶⁸, R. Voss³⁰, J.H. Vosseveld⁷³, N. Vranjes¹³⁷, M. Vranjes Milosavljevic^{13a}, V. Vrba¹²⁶, M. Vreeswijk¹⁰⁶, T. Vu Anh⁴⁸, R. Vuillermet³⁰, I. Vukotic³¹, Z. Vykydal¹²⁷, P. Wagner²¹, W. Wagner¹⁷⁶, H. Wahlberg⁷⁰, S. Wahrmond⁴⁴, J. Wakabayashi¹⁰², J. Walder⁷¹, R. Walker⁹⁹, W. Walkowiak¹⁴², R. Wall¹⁷⁷, P. Waller⁷³, B. Walsh¹⁷⁷, C. Wang^{152,aj}, C. Wang⁴⁵, F. Wang¹⁷⁴, H. Wang¹⁵, H. Wang⁴⁰, J. Wang⁴², J. Wang^{33a}, K. Wang⁸⁶, R. Wang¹⁰⁴, S.M. Wang¹⁵², T. Wang²¹, X. Wang¹⁷⁷, C. Wanotayaroj¹¹⁵, A. Warburton⁸⁶, C.P. Ward²⁸, D.R. Wardrope⁷⁷, M. Warsinsky⁴⁸, A. Washbrook⁴⁶, C. Wasicki⁴², P.M. Watkins¹⁸, A.T. Watson¹⁸, I.J. Watson¹⁵¹, M.F. Watson¹⁸, G. Watts¹³⁹, S. Watts⁸³, B.M. Waugh⁷⁷, S. Webb⁸³, M.S. Weber¹⁷, S.W. Weber¹⁷⁵, J.S. Webster³¹, A.R. Weidberg¹¹⁹, P. Weigell¹⁰⁰, B. Weinert⁶⁰, J. Weingarten⁵⁴, C. Weiser⁴⁸, H. Weits¹⁰⁶, P.S. Wells³⁰, T. Wenaus²⁵, D. Wendland¹⁶, Z. Weng^{152,ae}, T. Wengler³⁰, S. Wenig³⁰, N. Wermes²¹, M. Werner⁴⁸, P. Werner³⁰, M. Wessels^{58a}, J. Wetter¹⁶², K. Whalen²⁹, A. White⁸, M.J. White¹, R. White^{32b}, S. White^{123a,123b}, D. Whiteson¹⁶⁴, D. Wicke¹⁷⁶, F.J. Wickens¹³⁰, W. Wiedenmann¹⁷⁴, M. Wielers¹³⁰, P. Wienemann²¹, C. Wiglesworth³⁶, L.A.M. Wiik-Fuchs²¹, P.A. Wijeratne⁷⁷, A. Wildauer¹⁰⁰, M.A. Wildt^{42,ak}, H.G. Wilkens³⁰, J.Z. Will⁹⁹, H.H. Williams¹²¹, S. Williams²⁸, C. Willis⁸⁹, S. Willocq⁸⁵, A. Wilson⁸⁸, J.A. Wilson¹⁸, I. Wingerter-Seez⁵, F. Winklmeier¹¹⁵, B.T. Winter²¹, M. Wittgen¹⁴⁴, T. Wittig⁴³, J. Wittkowski⁹⁹, S.J. Wollstadt⁸², M.W. Wolter³⁹, H. Wolters^{125a,125c}, B.K. Wosiek³⁹, J. Wotschack³⁰, M.J. Woudstra⁸³, K.W. Wozniak³⁹, M. Wright⁵³, M. Wu⁵⁵, S.L. Wu¹⁷⁴, X. Wu⁴⁹, Y. Wu⁸⁸, E. Wulf³⁵, T.R. Wyatt⁸³, B.M. Wynne⁴⁶, S. Xella³⁶, M. Xiao¹³⁷, D. Xu^{33a}, L. Xu^{33b,al}, B. Yabsley¹⁵¹, S. Yacoub^{146b,am}, R. Yakabe⁶⁶, M. Yamada⁶⁵, H. Yamaguchi¹⁵⁶, Y. Yamaguchi¹¹⁷, A. Yamamoto⁶⁵, K. Yamamoto⁶³, S. Yamamoto¹⁵⁶, T. Yamamura¹⁵⁶, T. Yamanaka¹⁵⁶, K. Yamauchi¹⁰², Y. Yamazaki⁶⁶, Z. Yan²², H. Yang^{33e}, H. Yang¹⁷⁴, U.K. Yang⁸³, Y. Yang¹¹⁰, S. Yanush⁹², L. Yao^{33a}, W-M. Yao¹⁵, Y. Yasu⁶⁵, E. Yatsenko⁴², K.H. Yau Wong²¹, J. Ye⁴⁰, S. Ye²⁵, I. Yeletsikh⁶⁴, A.L. Yen⁵⁷, E. Yildirim⁴², M. Yilmaz^{4b}, R. Yoosoofmiya¹²⁴, K. Yorita¹⁷², R. Yoshida⁶, K. Yoshihara¹⁵⁶, C. Young¹⁴⁴, C.J.S. Young³⁰, S. Youssef²², D.R. Yu¹⁵, J. Yu⁸, J.M. Yu⁸⁸, J. Yu¹¹³, L. Yuan⁶⁶, A. Yurkewicz¹⁰⁷, I. Yusuff^{28,an}, B. Zabinski³⁹, R. Zaidan⁶², A.M. Zaitsev^{129,aa}, A. Zaman¹⁴⁹, S. Zambito²³, L. Zanello^{133a,133b}, D. Zanzi¹⁰⁰, C. Zeitnitz¹⁷⁶, M. Zeman¹²⁷, A. Zemla^{38a}, K. Zengel²³, O. Zenin¹²⁹, T. Ženiš^{145a}, D. Zerwas¹¹⁶, G. Zevi della Porta⁵⁷, D. Zhang⁸⁸, F. Zhang¹⁷⁴, H. Zhang⁸⁹, J. Zhang⁶, L. Zhang¹⁵², X. Zhang^{33d}, Z. Zhang¹¹⁶, Z. Zhao^{33b}, A. Zhemchugov⁶⁴, J. Zhong¹¹⁹, B. Zhou⁸⁸, L. Zhou³⁵, N. Zhou¹⁶⁴, C.G. Zhu^{33d}, H. Zhu^{33a}, J. Zhu⁸⁸, Y. Zhu^{33b}, X. Zhuang^{33a}, K. Zhukov⁹⁵, A. Zibell¹⁷⁵, D. Zieminska⁶⁰, N.I. Zimine⁶⁴, C. Zimmermann⁸², R. Zimmermann²¹, S. Zimmermann²¹, S. Zimmermann⁴⁸, Z. Zinonos⁵⁴, M. Ziolkowski¹⁴², G. Zobernig¹⁷⁴, A. Zoccoli^{20a,20b}, M. zur Nedden¹⁶, G. Zurzolo^{103a,103b}, V. Zutshi¹⁰⁷, L. Zwalinski³⁰.

¹ Department of Physics, University of Adelaide, Adelaide, Australia

² Physics Department, SUNY Albany, Albany NY, United States of America

³ Department of Physics, University of Alberta, Edmonton AB, Canada

⁴ (a) Department of Physics, Ankara University, Ankara; (b) Department of Physics, Gazi University, Ankara; (c) Division of Physics, TOBB University of Economics and Technology, Ankara; (d) Turkish Atomic Energy Authority, Ankara, Turkey

⁵ LAPP, CNRS/IN2P3 and Université de Savoie, Annecy-le-Vieux, France

⁶ High Energy Physics Division, Argonne National Laboratory, Argonne IL, United States of America

⁷ Department of Physics, University of Arizona, Tucson AZ, United States of America

⁸ Department of Physics, The University of Texas at Arlington, Arlington TX, United States of America

⁹ Physics Department, University of Athens, Athens, Greece

¹⁰ Physics Department, National Technical University of Athens, Zografou, Greece

¹¹ Institute of Physics, Azerbaijan Academy of Sciences, Baku, Azerbaijan

¹² Institut de Física d'Altes Energies and Departament de Física de la Universitat Autònoma de Barcelona, Barcelona, Spain

¹³ (a) Institute of Physics, University of Belgrade, Belgrade; (b) Vinca Institute of Nuclear Sciences, University of Belgrade, Belgrade, Serbia

¹⁴ Department for Physics and Technology, University of Bergen, Bergen, Norway

¹⁵ Physics Division, Lawrence Berkeley National Laboratory and University of California, Berkeley CA, United States of America

¹⁶ Department of Physics, Humboldt University, Berlin, Germany

¹⁷ Albert Einstein Center for Fundamental Physics and Laboratory for High Energy Physics, University of Bern, Bern, Switzerland

¹⁸ School of Physics and Astronomy, University of Birmingham, Birmingham, United Kingdom

¹⁹ (a) Department of Physics, Bogazici University, Istanbul; (b) Department of Physics, Dogus University, Istanbul; (c) Department of Physics Engineering, Gaziantep University, Gaziantep, Turkey

- 20 (a) INFN Sezione di Bologna; (b) Dipartimento di Fisica e Astronomia, Università di Bologna, Bologna, Italy
- 21 Physikalisches Institut, University of Bonn, Bonn, Germany
- 22 Department of Physics, Boston University, Boston MA, United States of America
- 23 Department of Physics, Brandeis University, Waltham MA, United States of America
- 24 (a) Universidade Federal do Rio De Janeiro COPPE/EE/IF, Rio de Janeiro; (b) Federal University of Juiz de Fora (UFJF), Juiz de Fora; (c) Federal University of Sao Joao del Rei (UFSJ), Sao Joao del Rei; (d) Instituto de Fisica, Universidade de Sao Paulo, Sao Paulo, Brazil
- 25 Physics Department, Brookhaven National Laboratory, Upton NY, United States of America
- 26 (a) National Institute of Physics and Nuclear Engineering, Bucharest; (b) National Institute for Research and Development of Isotopic and Molecular Technologies, Physics Department, Cluj Napoca; (c) University Politehnica Bucharest, Bucharest; (d) West University in Timisoara, Timisoara, Romania
- 27 Departamento de Física, Universidad de Buenos Aires, Buenos Aires, Argentina
- 28 Cavendish Laboratory, University of Cambridge, Cambridge, United Kingdom
- 29 Department of Physics, Carleton University, Ottawa ON, Canada
- 30 CERN, Geneva, Switzerland
- 31 Enrico Fermi Institute, University of Chicago, Chicago IL, United States of America
- 32 (a) Departamento de Física, Pontificia Universidad Católica de Chile, Santiago; (b) Departamento de Física, Universidad Técnica Federico Santa María, Valparaíso, Chile
- 33 (a) Institute of High Energy Physics, Chinese Academy of Sciences, Beijing; (b) Department of Modern Physics, University of Science and Technology of China, Anhui; (c) Department of Physics, Nanjing University, Jiangsu; (d) School of Physics, Shandong University, Shandong; (e) Physics Department, Shanghai Jiao Tong University, Shanghai, China
- 34 Laboratoire de Physique Corpusculaire, Clermont Université and Université Blaise Pascal and CNRS/IN2P3, Clermont-Ferrand, France
- 35 Nevis Laboratory, Columbia University, Irvington NY, United States of America
- 36 Niels Bohr Institute, University of Copenhagen, Kobenhavn, Denmark
- 37 (a) INFN Gruppo Collegato di Cosenza, Laboratori Nazionali di Frascati; (b) Dipartimento di Fisica, Università della Calabria, Rende, Italy
- 38 (a) AGH University of Science and Technology, Faculty of Physics and Applied Computer Science, Krakow; (b) Marian Smoluchowski Institute of Physics, Jagiellonian University, Krakow, Poland
- 39 The Henryk Niewodniczanski Institute of Nuclear Physics, Polish Academy of Sciences, Krakow, Poland
- 40 Physics Department, Southern Methodist University, Dallas TX, United States of America
- 41 Physics Department, University of Texas at Dallas, Richardson TX, United States of America
- 42 DESY, Hamburg and Zeuthen, Germany
- 43 Institut für Experimentelle Physik IV, Technische Universität Dortmund, Dortmund, Germany
- 44 Institut für Kern- und Teilchenphysik, Technische Universität Dresden, Dresden, Germany
- 45 Department of Physics, Duke University, Durham NC, United States of America
- 46 SUPA - School of Physics and Astronomy, University of Edinburgh, Edinburgh, United Kingdom
- 47 INFN Laboratori Nazionali di Frascati, Frascati, Italy
- 48 Fakultät für Mathematik und Physik, Albert-Ludwigs-Universität, Freiburg, Germany
- 49 Section de Physique, Université de Genève, Geneva, Switzerland
- 50 (a) INFN Sezione di Genova; (b) Dipartimento di Fisica, Università di Genova, Genova, Italy
- 51 (a) E. Andronikashvili Institute of Physics, Iv. Javakhishvili Tbilisi State University, Tbilisi; (b) High Energy Physics Institute, Tbilisi State University, Tbilisi, Georgia
- 52 II Physikalisches Institut, Justus-Liebig-Universität Giessen, Giessen, Germany
- 53 SUPA - School of Physics and Astronomy, University of Glasgow, Glasgow, United Kingdom
- 54 II Physikalisches Institut, Georg-August-Universität, Göttingen, Germany
- 55 Laboratoire de Physique Subatomique et de Cosmologie, Université Grenoble-Alpes, CNRS/IN2P3, Grenoble, France
- 56 Department of Physics, Hampton University, Hampton VA, United States of America
- 57 Laboratory for Particle Physics and Cosmology, Harvard University, Cambridge MA, United States of America
- 58 (a) Kirchhoff-Institut für Physik, Ruprecht-Karls-Universität Heidelberg, Heidelberg; (b) Physikalisches Institut, Ruprecht-Karls-Universität Heidelberg, Heidelberg; (c) ZITI Institut für technische Informatik, Ruprecht-Karls-Universität Heidelberg, Mannheim, Germany
- 59 Faculty of Applied Information Science, Hiroshima Institute of Technology, Hiroshima, Japan
- 60 Department of Physics, Indiana University, Bloomington IN, United States of America
- 61 Institut für Astro- und Teilchenphysik, Leopold-Franzens-Universität, Innsbruck, Austria
- 62 University of Iowa, Iowa City IA, United States of America
- 63 Department of Physics and Astronomy, Iowa State University, Ames IA, United States of America
- 64 Joint Institute for Nuclear Research, JINR Dubna, Dubna, Russia

- 65 KEK, High Energy Accelerator Research Organization, Tsukuba, Japan
- 66 Graduate School of Science, Kobe University, Kobe, Japan
- 67 Faculty of Science, Kyoto University, Kyoto, Japan
- 68 Kyoto University of Education, Kyoto, Japan
- 69 Department of Physics, Kyushu University, Fukuoka, Japan
- 70 Instituto de Física La Plata, Universidad Nacional de La Plata and CONICET, La Plata, Argentina
- 71 Physics Department, Lancaster University, Lancaster, United Kingdom
- 72 ^(a) INFN Sezione di Lecce; ^(b) Dipartimento di Matematica e Fisica, Università del Salento, Lecce, Italy
- 73 Oliver Lodge Laboratory, University of Liverpool, Liverpool, United Kingdom
- 74 Department of Physics, Jožef Stefan Institute and University of Ljubljana, Ljubljana, Slovenia
- 75 School of Physics and Astronomy, Queen Mary University of London, London, United Kingdom
- 76 Department of Physics, Royal Holloway University of London, Surrey, United Kingdom
- 77 Department of Physics and Astronomy, University College London, London, United Kingdom
- 78 Louisiana Tech University, Ruston LA, United States of America
- 79 Laboratoire de Physique Nucléaire et de Hautes Energies, UPMC and Université Paris-Diderot and CNRS/IN2P3, Paris, France
- 80 Fysiska institutionen, Lunds universitet, Lund, Sweden
- 81 Departamento de Física Teórica C-15, Universidad Autónoma de Madrid, Madrid, Spain
- 82 Institut für Physik, Universität Mainz, Mainz, Germany
- 83 School of Physics and Astronomy, University of Manchester, Manchester, United Kingdom
- 84 CPPM, Aix-Marseille Université and CNRS/IN2P3, Marseille, France
- 85 Department of Physics, University of Massachusetts, Amherst MA, United States of America
- 86 Department of Physics, McGill University, Montreal QC, Canada
- 87 School of Physics, University of Melbourne, Victoria, Australia
- 88 Department of Physics, The University of Michigan, Ann Arbor MI, United States of America
- 89 Department of Physics and Astronomy, Michigan State University, East Lansing MI, United States of America
- 90 ^(a) INFN Sezione di Milano; ^(b) Dipartimento di Fisica, Università di Milano, Milano, Italy
- 91 B.I. Stepanov Institute of Physics, National Academy of Sciences of Belarus, Minsk, Republic of Belarus
- 92 National Scientific and Educational Centre for Particle and High Energy Physics, Minsk, Republic of Belarus
- 93 Department of Physics, Massachusetts Institute of Technology, Cambridge MA, United States of America
- 94 Group of Particle Physics, University of Montreal, Montreal QC, Canada
- 95 P.N. Lebedev Institute of Physics, Academy of Sciences, Moscow, Russia
- 96 Institute for Theoretical and Experimental Physics (ITEP), Moscow, Russia
- 97 Moscow Engineering and Physics Institute (MEPhI), Moscow, Russia
- 98 D.V.Skobel'tsyn Institute of Nuclear Physics, M.V.Lomonosov Moscow State University, Moscow, Russia
- 99 Fakultät für Physik, Ludwig-Maximilians-Universität München, München, Germany
- 100 Max-Planck-Institut für Physik (Werner-Heisenberg-Institut), München, Germany
- 101 Nagasaki Institute of Applied Science, Nagasaki, Japan
- 102 Graduate School of Science and Kobayashi-Maskawa Institute, Nagoya University, Nagoya, Japan
- 103 ^(a) INFN Sezione di Napoli; ^(b) Dipartimento di Fisica, Università di Napoli, Napoli, Italy
- 104 Department of Physics and Astronomy, University of New Mexico, Albuquerque NM, United States of America
- 105 Institute for Mathematics, Astrophysics and Particle Physics, Radboud University Nijmegen/Nikhef, Nijmegen, Netherlands
- 106 Nikhef National Institute for Subatomic Physics and University of Amsterdam, Amsterdam, Netherlands
- 107 Department of Physics, Northern Illinois University, DeKalb IL, United States of America
- 108 Budker Institute of Nuclear Physics, SB RAS, Novosibirsk, Russia
- 109 Department of Physics, New York University, New York NY, United States of America
- 110 Ohio State University, Columbus OH, United States of America
- 111 Faculty of Science, Okayama University, Okayama, Japan
- 112 Homer L. Dodge Department of Physics and Astronomy, University of Oklahoma, Norman OK, United States of America
- 113 Department of Physics, Oklahoma State University, Stillwater OK, United States of America
- 114 Palacký University, RCPTM, Olomouc, Czech Republic
- 115 Center for High Energy Physics, University of Oregon, Eugene OR, United States of America
- 116 LAL, Université Paris-Sud and CNRS/IN2P3, Orsay, France
- 117 Graduate School of Science, Osaka University, Osaka, Japan
- 118 Department of Physics, University of Oslo, Oslo, Norway
- 119 Department of Physics, Oxford University, Oxford, United Kingdom
- 120 ^(a) INFN Sezione di Pavia; ^(b) Dipartimento di Fisica, Università di Pavia, Pavia, Italy
- 121 Department of Physics, University of Pennsylvania, Philadelphia PA, United States of America

- 122 Petersburg Nuclear Physics Institute, Gatchina, Russia
- 123 (a) INFN Sezione di Pisa; (b) Dipartimento di Fisica E. Fermi, Università di Pisa, Pisa, Italy
- 124 Department of Physics and Astronomy, University of Pittsburgh, Pittsburgh PA, United States of America
- 125 (a) Laboratório de Instrumentação e Física Experimental de Partículas - LIP, Lisboa; (b) Faculdade de Ciências, Universidade de Lisboa, Lisboa; (c) Department of Physics, University of Coimbra, Coimbra; (d) Centro de Física Nuclear da Universidade de Lisboa, Lisboa; (e) Departamento de Física, Universidade do Minho, Braga; (f) Departamento de Física Teórica y del Cosmos and CAFPE, Universidad de Granada, Granada (Spain); (g) Dep Física and CEFITEC of Faculdade de Ciências e Tecnologia, Universidade Nova de Lisboa, Caparica, Portugal
- 126 Institute of Physics, Academy of Sciences of the Czech Republic, Praha, Czech Republic
- 127 Czech Technical University in Prague, Praha, Czech Republic
- 128 Faculty of Mathematics and Physics, Charles University in Prague, Praha, Czech Republic
- 129 State Research Center Institute for High Energy Physics, Protvino, Russia
- 130 Particle Physics Department, Rutherford Appleton Laboratory, Didcot, United Kingdom
- 131 Physics Department, University of Regina, Regina SK, Canada
- 132 Ritsumeikan University, Kusatsu, Shiga, Japan
- 133 (a) INFN Sezione di Roma; (b) Dipartimento di Fisica, Sapienza Università di Roma, Roma, Italy
- 134 (a) INFN Sezione di Roma Tor Vergata; (b) Dipartimento di Fisica, Università di Roma Tor Vergata, Roma, Italy
- 135 (a) INFN Sezione di Roma Tre; (b) Dipartimento di Matematica e Fisica, Università Roma Tre, Roma, Italy
- 136 (a) Faculté des Sciences Ain Chock, Réseau Universitaire de Physique des Hautes Energies - Université Hassan II, Casablanca; (b) Centre National de l'Energie des Sciences Techniques Nucleaires, Rabat; (c) Faculté des Sciences Semlalia, Université Cadi Ayyad, LPHEA-Marrakech; (d) Faculté des Sciences, Université Mohamed Premier and LPTPM, Oujda; (e) Faculté des sciences, Université Mohammed V-Agdal, Rabat, Morocco
- 137 DSM/IRFU (Institut de Recherches sur les Lois Fondamentales de l'Univers), CEA Saclay (Commissariat à l'Energie Atomique et aux Energies Alternatives), Gif-sur-Yvette, France
- 138 Santa Cruz Institute for Particle Physics, University of California Santa Cruz, Santa Cruz CA, United States of America
- 139 Department of Physics, University of Washington, Seattle WA, United States of America
- 140 Department of Physics and Astronomy, University of Sheffield, Sheffield, United Kingdom
- 141 Department of Physics, Shinshu University, Nagano, Japan
- 142 Fachbereich Physik, Universität Siegen, Siegen, Germany
- 143 Department of Physics, Simon Fraser University, Burnaby BC, Canada
- 144 SLAC National Accelerator Laboratory, Stanford CA, United States of America
- 145 (a) Faculty of Mathematics, Physics & Informatics, Comenius University, Bratislava; (b) Department of Subnuclear Physics, Institute of Experimental Physics of the Slovak Academy of Sciences, Kosice, Slovak Republic
- 146 (a) Department of Physics, University of Cape Town, Cape Town; (b) Department of Physics, University of Johannesburg, Johannesburg; (c) School of Physics, University of the Witwatersrand, Johannesburg, South Africa
- 147 (a) Department of Physics, Stockholm University; (b) The Oskar Klein Centre, Stockholm, Sweden
- 148 Physics Department, Royal Institute of Technology, Stockholm, Sweden
- 149 Departments of Physics & Astronomy and Chemistry, Stony Brook University, Stony Brook NY, United States of America
- 150 Department of Physics and Astronomy, University of Sussex, Brighton, United Kingdom
- 151 School of Physics, University of Sydney, Sydney, Australia
- 152 Institute of Physics, Academia Sinica, Taipei, Taiwan
- 153 Department of Physics, Technion: Israel Institute of Technology, Haifa, Israel
- 154 Raymond and Beverly Sackler School of Physics and Astronomy, Tel Aviv University, Tel Aviv, Israel
- 155 Department of Physics, Aristotle University of Thessaloniki, Thessaloniki, Greece
- 156 International Center for Elementary Particle Physics and Department of Physics, The University of Tokyo, Tokyo, Japan
- 157 Graduate School of Science and Technology, Tokyo Metropolitan University, Tokyo, Japan
- 158 Department of Physics, Tokyo Institute of Technology, Tokyo, Japan
- 159 Department of Physics, University of Toronto, Toronto ON, Canada
- 160 (a) TRIUMF, Vancouver BC; (b) Department of Physics and Astronomy, York University, Toronto ON, Canada
- 161 Faculty of Pure and Applied Sciences, University of Tsukuba, Tsukuba, Japan
- 162 Department of Physics and Astronomy, Tufts University, Medford MA, United States of America
- 163 Centro de Investigaciones, Universidad Antonio Narino, Bogota, Colombia
- 164 Department of Physics and Astronomy, University of California Irvine, Irvine CA, United States of America
- 165 (a) INFN Gruppo Collegato di Udine, Sezione di Trieste, Udine; (b) ICTP, Trieste; (c) Dipartimento di Chimica, Fisica e Ambiente, Università di Udine, Udine, Italy
- 166 Department of Physics, University of Illinois, Urbana IL, United States of America
- 167 Department of Physics and Astronomy, University of Uppsala, Uppsala, Sweden
- 168 Instituto de Física Corpuscular (IFIC) and Departamento de Física Atómica, Molecular y Nuclear and Departamento de

- Ingeniería Electrónica and Instituto de Microelectrónica de Barcelona (IMB-CNM), University of Valencia and CSIC, Valencia, Spain
- ¹⁶⁹ Department of Physics, University of British Columbia, Vancouver BC, Canada
- ¹⁷⁰ Department of Physics and Astronomy, University of Victoria, Victoria BC, Canada
- ¹⁷¹ Department of Physics, University of Warwick, Coventry, United Kingdom
- ¹⁷² Waseda University, Tokyo, Japan
- ¹⁷³ Department of Particle Physics, The Weizmann Institute of Science, Rehovot, Israel
- ¹⁷⁴ Department of Physics, University of Wisconsin, Madison WI, United States of America
- ¹⁷⁵ Fakultät für Physik und Astronomie, Julius-Maximilians-Universität, Würzburg, Germany
- ¹⁷⁶ Fachbereich C Physik, Bergische Universität Wuppertal, Wuppertal, Germany
- ¹⁷⁷ Department of Physics, Yale University, New Haven CT, United States of America
- ¹⁷⁸ Yerevan Physics Institute, Yerevan, Armenia
- ¹⁷⁹ Centre de Calcul de l'Institut National de Physique Nucléaire et de Physique des Particules (IN2P3), Villeurbanne, France
- ^a Also at Department of Physics, King's College London, London, United Kingdom
- ^b Also at Institute of Physics, Azerbaijan Academy of Sciences, Baku, Azerbaijan
- ^c Also at Particle Physics Department, Rutherford Appleton Laboratory, Didcot, United Kingdom
- ^d Also at TRIUMF, Vancouver BC, Canada
- ^e Also at Department of Physics, California State University, Fresno CA, United States of America
- ^f Also at Tomsk State University, Tomsk, Russia
- ^g Also at CPPM, Aix-Marseille Université and CNRS/IN2P3, Marseille, France
- ^h Also at Università di Napoli Parthenope, Napoli, Italy
- ⁱ Also at Institute of Particle Physics (IPP), Canada
- ^j Also at Department of Physics, St. Petersburg State Polytechnical University, St. Petersburg, Russia
- ^k Also at Chinese University of Hong Kong, China
- ^l Also at Department of Financial and Management Engineering, University of the Aegean, Chios, Greece
- ^m Also at Louisiana Tech University, Ruston LA, United States of America
- ⁿ Also at Institutio Catalana de Recerca i Estudis Avancats, ICREA, Barcelona, Spain
- ^o Also at Department of Physics, The University of Texas at Austin, Austin TX, United States of America
- ^p Also at Institute of Theoretical Physics, Iliia State University, Tbilisi, Georgia
- ^q Also at CERN, Geneva, Switzerland
- ^r Also at Ochadai Academic Production, Ochanomizu University, Tokyo, Japan
- ^s Also at Manhattan College, New York NY, United States of America
- ^t Also at Novosibirsk State University, Novosibirsk, Russia
- ^u Also at Institute of Physics, Academia Sinica, Taipei, Taiwan
- ^v Also at LAL, Université Paris-Sud and CNRS/IN2P3, Orsay, France
- ^w Also at Academia Sinica Grid Computing, Institute of Physics, Academia Sinica, Taipei, Taiwan
- ^x Also at Laboratoire de Physique Nucléaire et de Hautes Energies, UPMC and Université Paris-Diderot and CNRS/IN2P3, Paris, France
- ^y Also at School of Physical Sciences, National Institute of Science Education and Research, Bhubaneswar, India
- ^z Also at Dipartimento di Fisica, Sapienza Università di Roma, Roma, Italy
- ^{aa} Also at Moscow Institute of Physics and Technology State University, Dolgoprudny, Russia
- ^{ab} Also at Section de Physique, Université de Genève, Geneva, Switzerland
- ^{ac} Also at International School for Advanced Studies (SISSA), Trieste, Italy
- ^{ad} Also at Department of Physics and Astronomy, University of South Carolina, Columbia SC, United States of America
- ^{ae} Also at School of Physics and Engineering, Sun Yat-sen University, Guangzhou, China
- ^{af} Also at Faculty of Physics, M.V.Lomonosov Moscow State University, Moscow, Russia
- ^{ag} Also at Moscow Engineering and Physics Institute (MEPhI), Moscow, Russia
- ^{ah} Also at Institute for Particle and Nuclear Physics, Wigner Research Centre for Physics, Budapest, Hungary
- ^{ai} Also at Department of Physics, Oxford University, Oxford, United Kingdom
- ^{aj} Also at Department of Physics, Nanjing University, Jiangsu, China
- ^{ak} Also at Institut für Experimentalphysik, Universität Hamburg, Hamburg, Germany
- ^{al} Also at Department of Physics, The University of Michigan, Ann Arbor MI, United States of America
- ^{am} Also at Discipline of Physics, University of KwaZulu-Natal, Durban, South Africa
- ^{an} Also at University of Malaya, Department of Physics, Kuala Lumpur, Malaysia
- * Deceased